Helicopter Blade Parameter Extraction for Purposes of Radar Target Identification

Anria Cilliers

A thesis submitted to the Department of Electrical Engineering, University of Cape Town, in fulfilment of the requirements for the degree of

Master of Science in Engineering

at the

University of Cape Town

May 2010

Declaration

I declare that this dissertation is my own, unaided work. It is being submitted for the degree of Master of Science in Engineering in the University of Cape Town. It has not been submitted before for any degree or examination in any other university.

Signature of Author .....

Pretoria
24 May 2010

Abstract

The positive classification and identification of airborne targets beyond the visual range by using the reflected radar signal has become an increasingly valuable capability for the defence force of a country. The rotating structures on an airborne target cause additional Doppler modulation in the return signal which is known as the micro-Doppler effect. Information regarding the rotating structures can be extracted from this effect.

A technique based on time-frequency and tomographic analysis is introduced in this research to extract certain helicopter blade parameters which will aid in the identification of a helicopter. The proposed algorithm shows that (under certain conditions) it is possible to extract the number of main rotor blades, the blade length and the rotation rate of the helicopter's main rotor. These features can be used to determine the make and model of a particular helicopter.

The methodology followed in this research was a) to develop a point scatterer model to simulate the micro-Doppler effects from the helicopter and b) to develop a blade parameter extraction algorithm based on the simulation model. Finally this algorithm was validated by means of results obtained from measured radar data from several different military helicopters.

The algorithm was designed for a pulse-Doppler tracking radar, and the results achieved was encouraging in the sense that reliable results have been obtained for ranges up to 14 km.

Acknowledgements

I would like to express my sincere gratitude to the following persons and institutions for the support and assistance they provided during this study:

Prof Michael Inggs, my supervisor at UCT, for his guidance and support especially in the final stages of the study

Willie Nel, my supervisor at the CSIR, for his expert guidance, encouragement and unwavering support throughout the study

The South African Defence Force for funding this project

All the members of the Radar and EW team at DPSS that assisted during the helicopter trial, and supported me throughout the study

Regine Lord from UCT for the excellent language editing

Nicóle for proof reading the thesis and helping me to remember that this too shall pass

Berna and Paul for their encouragement, support and lovely visits on the farm

My dad and Elza for their continued encouragement and support during the study

My mom and Klem for their love, encouragement and unwavering support during the study

Izak, my loving husband, for his endless patience, support and wisdom in a very busy time.

To my Lord and Saviour Jesus Christ, who gave me His love throughout this study and the strength to finish it

Contents

List of Figures

List of Tables

List of Symbols

a	—	Left boundary of blade length distribution
A_r	—	Scale factor
b	—	Right boundary of blade length distribution
B	—	Bandwidth [Hz]
B_n	—	Noise bandwidth [Hz]
c	—	Speed of light [m/s]
D	—	Diameter of main rotor hub [m]
f_0	—	Centre frequency of receiver filters [Hz]
f_{bin}	—	Frequency in Doppler bins
f_c	—	Radar transmit frequency [Hz]
f_d	—	Maximum Doppler frequency [Hz]
$f_{d_{est}}$	—	Estimated Doppler frequency [Hz]
f_r	—	Angular frequency of the main rotor
$f(x, y)$	—	2-D function representing a 2-D object used in the Radon transform
Δf	—	Distance in frequency between sidebands [Hz]
Δf_{hub}	—	Maximum Doppler bandwidth of the rotor hub [Hz]
F_n	—	Noise figure of the receiver
G_r	—	Transmitter antenna gain [dB]
G_t	—	Receiver antenna gain [dB]
H	—	Height of a main rotor blade [m]
$H(f)$	—	Frequency response of receiver filters
k	—	Boltzmann's constant [J/deg]
L	—	Blade length [m]
L_{est}	—	Estimated blade length [m]

L_a	—	Antenna loss [dB]
L_r	—	Input RF loss [dB]
L_{min}	—	Distance between the hub centre and the blade [m]
L_{max}	—	Blade length [m]
N	—	Number of main rotor blades
N'	—	Number of sidebands in the return signal
N_{out}	—	Noise output from the receiver
N_{pulses}	—	Number of received pulses
$N_{rotations}$	—	Number of rotations in the simulation
P	—	Point scatterer
P_n	—	Thermal noise power [W]
P_s	—	Received signal power [W]
P_t	—	Transmit signal power [W]
$P(\alpha, r)$	—	1-D projections of the 2-D function in the Radon transform
Pr_σ	—	Probability of correct identification for a standard deviation
$\mathrm{Pr}_{correct}$	—	Probability of correct identification
r_{omega}	—	Rotation rate of the main rotor in RPM
R	—	Range from the radar to the centre of rotation on the main rotor hub [m]
R_0	—	Range from radar to the target [m]
$R(t)$	—	Time varying range to the blade tip of the helicopter [m]
R_k	—	Range as a function of the blade length in the point scatterer model
$s(t)$	—	Return signal from a point scatterer
s	—	Position of point scatterer in the simulation model
Sc	—	Scaling factor
S_{ret}	—	Return signal from point scatterer model
t	—	Time [s]
T_0	—	Reference temperature [K]
T_a	—	Temperature of the antenna [K]
T'_a	—	Atmospheric temperature [deg]
T_e	—	Receiver temperature [deg]
T_r	—	Temperature due to RF components [deg]
T_s	—	Input noise temperature [deg]
T_tr	—	Actual temperature of RF components [deg]
v	—	Radial velocity of the centre of rotation [m/s]
v_{tip}	—	Blade tip velocity [m/s]

$v_{tip_{est}}$	—	Estimated blade tip velocity [m/s]
v_h	—	Radial velocity of helicopter main rotor hub
$v_r(t)$	—	Theoretical return signal from a helicopter rotor blade
w_k	—	Windowing function
α	—	Constant amplitude for every scatterer in the model
ω_c	—	Angular frequency of the transmitted signal [rad/s]
ω_r	—	Angular velocity of the main rotor [rad/s]
ω_{est}	—	Estimated angular velocity of the main rotor [rad/s]
ω_h	—	Angular velocity of the main rotor hub [rad/s]
y	—	Normal distribution
X	—	Area between a and b
X_n	—	Output of the STFT
ϕ	—	Elevation angle [deg]
δ	—	Step size
$\Phi[r(t)]$	—	Phase of the return signal
θ_s	—	Incident angle [rad]
θ_{aspect}	—	Aspect angle [rad]
λ	—	Wavelength [m]
μ_n	—	Mean value of Gaussian distribution
σ	—	Standard deviation
σ^2	—	Variance
σ_{RCS}	—	RCS of a target [m^2]

Nomenclature

AS	—	Aerospatiale
ATS	—	Aviation Toward Success
CSIR	—	Council for Science and Industrial Research
dB	—	Decibel
DPSS	—	Defense, Peace, Safety and Security
EC	—	Eurocopter
EM	—	Electromagnetic
EW	—	Electronic Warfare
FFT	—	Fast Fourier Transform
GPS	—	Global Positioning System
HBM	—	Helicopter Blade Modulation
HPRF	—	High Pulse Repetition Frequency
HRR	—	High Range Resolution
IEEE	—	Institute of Electrical and Electronics Engineers
IFFT	—	Inverse Fast Fourier Transform
ILN	—	Improved L/N
IRT	—	Inverse Radon Transform
ISAR	—	Inverse Synthetic Aperture Radar
JR	—	Jet Ranger
LPRF	—	Low Pulse Repetition Frequency
LR	—	Long Ranger
MPRF	—	Medium Pulse Repetition Frequency
NCTR	—	Non-Cooperative Target Recognition
PRI	—	Pulse Repetition Interval
PRF	—	Pulse Repetition Frequency

RCS — Radar Cross Section
RF — Radio Frequency
RPM — Revolutions per Minute
SAAF — South African Air Force
SNR — Signal-to-noise Ratio
SPWV — Smooth Pseudo Wigner-Ville
STFT — Short-Time Fourier Transform
WVD — Wigner-Ville Distribution

Chapter 1

Introduction

1.1 Background

The problem of classifying and identifying airborne targets in a combat situation started during the First World War and has become increasingly important with the advances in airborne strike power (Tait [1]). This problem can be alleviated by a branch of engineering theory known as radar based Non-Cooperative Target Recognition (NCTR), which provides useful information on the features of the target at long range in order to obtain a positive identification of possible targets, especially where Identify Friend or Foe (IFF) systems are disabled or non-functional. Several different methods are used for the classification and identification process, each concentrating on different aspects of both the radar system and the target.

Both current and future military requirements can be addressed by an identification system where enemy targets such as aircraft or missiles could be identified beyond the visual range and with very little error. Tait [1] states that long range target identification functions are vital for future combat defence systems. Tait [1] further states that NCTR can also aid in minimizing the number of incidents where friendly aircraft have been destroyed because the IFF was malfunctioning, turned off, or jammed by enemy counter measure systems, or because of incorrect assessment from missile operators.

This problem can be alleviated, firstly by developing a system that correctly identifies the different aircraft in the South African Air Force (SAAF). In this way the solution would avoid a country's own aircraft being shot down. However, the identification of the

aircraft in the South African military fleet is only the first step. In addition, it is extremely important to identify local civilian aircraft correctly. It is furthermore just as important to identify both neutral and enemy aircraft correctly, by using radar information together with other sources of information to create situational awareness. This would make it possible to distinguish clearly among the aircraft in the South African military fleet, civilian, neutral or enemy aircraft.

Various different terms are used in the field of target recognition. To avoid confusion, the definitions used in this thesis, taken from the Institute of Electrical and Electronics Engineers (IEEE) standard radar definitions [2], are given here. The terms *target recognition* or *target classification* describe the radar's ability to separate targets into different classes, such as a helicopter, a jet aircraft, a propeller aircraft or a large sea vessel. According to the IEEE standard radar definition, *target identification* is the ability to identify a specific target, i.e. its make and model, the flight number of a commercial aircraft, an aircraft's side number, or the name painted on a ship. For this study, the definition is limited to refer only to the ability to discern the make and model of the target.

Figure 1.1 provides an overview of the different radar methods that can be used for NCTR. This particular breakdown of the methods that exist was defined by the Radar and Electronic Warfare (EW) research group at the Council for Science and Industrial Research (CSIR), and therefore the layout is not necessarily the same as in the literature. These methods are not used in isolation to solve the problem of target recognition, but are used in conjunction with other techniques to increase the probability of positive classification and/or identification of targets. There are three main areas into which radar NCTR techniques relating to airborne targets can be divided.

The first area is that of stationary (relative to the body) scattering recognition, where recognition systems are based on High Range Resolution (HRR) profiles and on Inverse Synthetic Aperture Radar (ISAR) measurements of targets. These methods aim to extract information based on the relative positions (and amplitudes) of fixed scattering centres on a target.

The second branch is that of rotating or moving scattering recognition. One of the characteristics of an aircraft that can be used to aid identification are the vibrating or rotating parts of the aircraft, such as the blades on the engine of a jet engine aircraft, the propeller(s) on a propeller aircraft or the rotor structure on a helicopter. When the electromagnetic (EM) wave is reflected from the vibrating or rotating structures on the

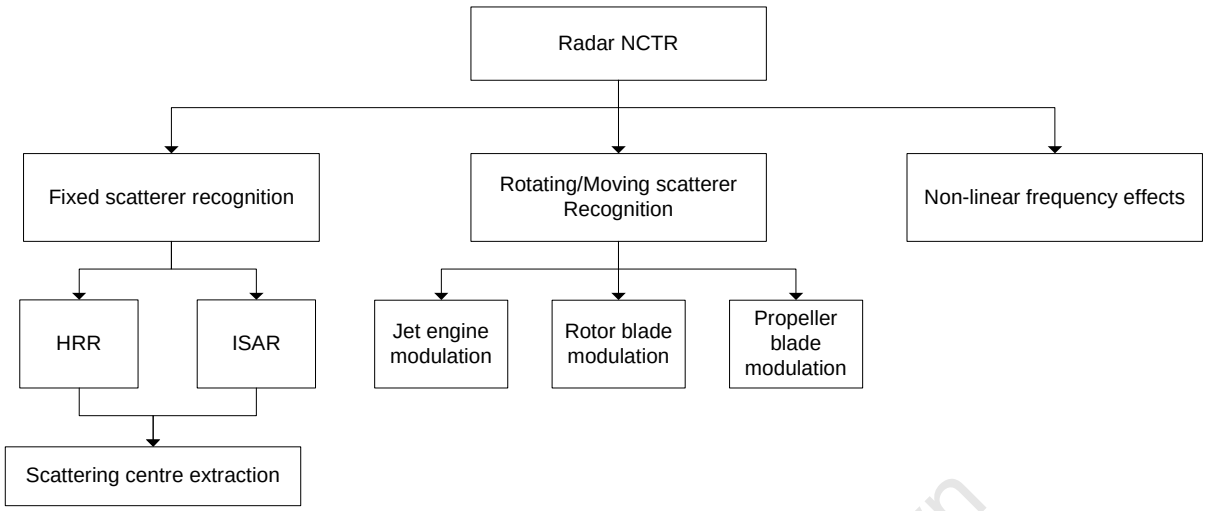

Figure 1.1: Different approaches and methods to the field of radar NCTR as defined by the Radar and EW research group at the CSIR.

target, Tait [1] states that additional frequency modulations are induced in the return signal and that additional sidebands around the mean Doppler frequency of the target can be observed. This phenomenon is known as the micro-Doppler effect, and it can greatly contribute to the classification of targets (Chen *et al.* [3]). Several research efforts have been published which use this modulation effect for classification purposes. This is a very active area of research and recent papers include Chen *et al.* [4], Yoon *et al.* [5], Martin and Mulgrew [6], Bullard and Dowdy [7], Pouliguen *et al.* [8], Bell [9] and Misiurewicz *et al.* [10].

The focus of this dissertation is on the helicopter rotor blade modulation aspect of NCTR. Figure 1.2 illustrates the importance of radar NCTR, for both military and civilian helicopters. The figure shows some of the different helicopters found around the world. It shows that there is a large variety of helicopters with different dimensions, functions and capabilities.

The question is whether the use of radar NCTR techniques would make it possible to identify the different helicopters, thus enabling a defence force to act appropriately upon detection of a hostile target. Identifying the target before any engagement through the use of radar NCTR could increase the available reaction time, specifically when compared with optical systems. There are two reasons for this. Firstly, radar NCTR could provide accurate detection and identification of the targets beyond the visual range and, secondly, it is independent of weather conditions and time of day. In other words, successful radar

Figure 1.2: Some of the different military and civilian helicopters that are used around the world.

target recognition can provide useful identification parameters sensed at long enough ranges to improve the response timeline of the defensive system regardless of weather conditions. The required ranges may vary, since it depends on the type of threat and type of defensive system.

1.2 Thesis Objectives

The problem of correctly identifying targets using only radar is rather complex and in many cases does not yet seem feasible. However, there is much information that the radar can extract to provide more information about a target. This research focuses on the extraction of helicopter blade parameters using radar and shows that this can benefit the world of radar target classification significantly. The main objectives of this dissertation are thus:

- To gain knowledge in the field of NCTR and to review the current work on blade modulation and the methods proposed in order to use this as an aid in identifying helicopters.
- To develop a database of military and civilian helicopters containing the key helicopter blade parameters that can be used for target identification.
- To develop a simulation model that demonstrates the micro-Doppler phenomenon and to use this to gain more insight into the problem.
- To develop a technique for extracting information from the micro-Doppler return, and to determine whether these estimates would contribute to the identification of a target. This method can be verified by using the data generated from the simulation model as input to the algorithm.
- To use measured radar data of helicopters to verify the simulation results and to test the algorithm, and thereafter to extend the processing method as necessary to gain as much information as possible from the recorded data.
- To perform a statistical analysis of all the measured data to gain insight into the conditions in which the proposed algorithm would work on its own, and when additional methods would be needed.
- To document the method that was used, clearly showing both its advantages and disadvantages.

1.3 Thesis Development

The outline of the thesis and the content of each chapter are discussed in this section.

1.3.1 Background theory

The background theory of micro-Doppler effects and the discussion of work addressing the problem of target recognition by using micro-Doppler effects presented in the literature are given in Chapter 2. In this chapter the theoretical return from a rotating object, such

as a helicopter rotor or the propeller of an engine, as presented by Martin and Mulgrew [6] is given and can be expressed as

$$\begin{aligned} v_r(t) &= \sum_{n=0}^{N-1} A_r(L) e^{j(\omega_c t - \frac{4\pi}{\lambda}(R+vt+\frac{L}{2}\cos(\theta)\sin(\omega_r t+\frac{2\pi n}{N})))} \\ &\quad \cdot \operatorname{sinc}(\frac{4\pi}{\lambda}\frac{L}{2}\cos(\theta)\sin(\omega_r t + \frac{2\pi n}{N})) \end{aligned} \tag{1.1}$$

If one analyses this expression, it is evident that the return of the target is based on three parameters, namely the number of blades, N, the blade length, L, and the angular velocity of the rotor or propeller, ω_r. By using the information in the return signal to extract these three parameters, it would therefore be possible to gain knowledge to identify the specific target.

The literature survey in Chapter 2 describes some of the work presented in the literature that proposes a solution to this problem by presenting various techniques and methods of extracting the rotor blade parameters that influence the modulation of the radar return signal. A particularly relevant work is the L/N technique created by Rotander and Von Sydow [11], where the quotient of the blade length and the number of blades is used for identification. Another technique was introduced by Yoon *et al.* [5], where the return signal is represented in the time-frequency domain: for high Signal-to-noise Ratio (SNR) conditions, the number of blades, the rotation rate and the rotor parity (viz. an odd or even number of blades) can be determined.

Other methods presented in the literature include the works conducted by Kulpa *et al.* [12], where the signal from the rotor hub of the helicopter is used for identification purposes. These papers as well as other techniques are discussed in detail in Chapter 2.

To validate the use of the three helicopter blade parameters (N, L and ω_r) a helicopter separability study was performed; the results of this are presented in the final section of Chapter 2. In this study, a database consisting of over one hundred military and civilian helicopters was generated, based on many sources from the internet. The database includes some of the key rotor blade parameters of the helicopters as well as other parameters such as the maximum velocity etc. This database was used to calculate the probability of correct identification, given a certain blade length and a rotation rate estimation error. This study was performed for the two cases: in the first scenario the helicopters had already been sorted according to the number of the main rotor blades, and in the second scenario, the number of blades was not known, and the probability of correct identification for the complete dataset was determined. The results from this

study give a good indication of how accurately the helicopter parameters need to be estimated in order to design a good identification technique. Figure 1.3 illustrates the probability of correct identification given a certain estimation error with regard to the estimated blade length (m).

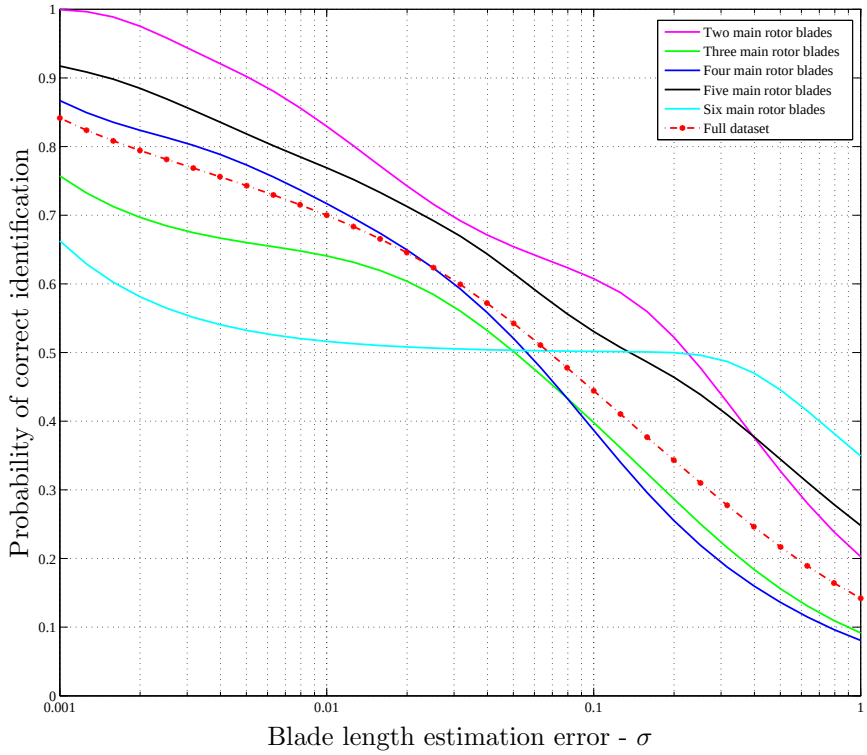

Figure 1.3: Probability of correct identification given the blade length estimation error in metres (m). The probability of correct identification within a class (number of main rotors) as well as the probability of correct identification over the complete data set is shown.

The results show that, in order to have a probability of correct identification of more than 70%, the blade length estimation error needs to be smaller than 1 cm. When the helicopters are, however, first separated according to number of blades, a higher estimation error will result in the same probability of correct identification. For instance, an estimation error of 3 cm will result in a probability of correct identification of 70% for helicopters with two main rotor blades. The graph shows the probability of correct identification for the different classes, as well as for the complete dataset, i.e. without separating the helicopters into classes according to the number of main rotor blades.

The chapter concludes with this separability analysis that indicates how accurately a target identification algorithm should estimate the various features.

1.3.2 Theoretical analysis

Chapter 3 gives a theoretical analysis of the proposed technique, and a detailed discussion of the simulation model that was developed to verify the method. The chapter gives the mathematical expression for a blade flash, which occurs when the rotor blade is perpendicular to the radar. The blade flash is a key characteristic of the return signal from a rotor blade. The simulation model that was developed shows the flash resulting from the blade at the instant when it is perpendicular to the radar. The radar cross section (RCS) of the blade is also discussed in this chapter: in this case, two models are used for the blade when it is perpendicular to the radar, i.e. when a flash occurs. The first model makes use of the RCS of a flat plate to model the blade. For this simplified model the curve on the leading edge of the blade was ignored. Therefore, a half cylindrical model which takes the curvature of the leading edge of the blade into account, is also presented in the chapter. The difference in RCS between these two models for a typical blade of 5 m is approximately 13 dBsm.

The equation giving the range from the radar to the tip of the rotating blade is also derived in Chapter 3, and is expressed as

$$R(t) = R_0 + L\cos\theta(t) \tag{1.2}$$

By taking the time derivative of this equation, the Doppler frequency at the tip of the blade can be expressed as

$$\begin{aligned} f_d(t) &= \frac{2v(t)}{\lambda} \\ &= -\frac{2L\omega}{\lambda} sin(\alpha(t)) \end{aligned} \tag{1.3}$$

The complete derivation for this equation is discussed in Chapter 3. The sinusoidal component in the time-varying Doppler frequency is visible in the time-frequency data of a helicopter. These sinusoids are a result of the tip scattering, and are thus discussed in detail in Chapter 3. Figure 1.4 gives the Doppler spectrum of simulated data showing both the blade flashes as well as the sinusoids resulting from the blade tips. These two important characteristics are used to estimate the blade parameters.

The simulation model is based on a simple point scatterer model as discussed by Chen *et al.* [3], where scatterers are placed at $1/4\lambda$ from each other on the blades. Although this model has some limitations, the two key characteristics of the micro-Doppler effect

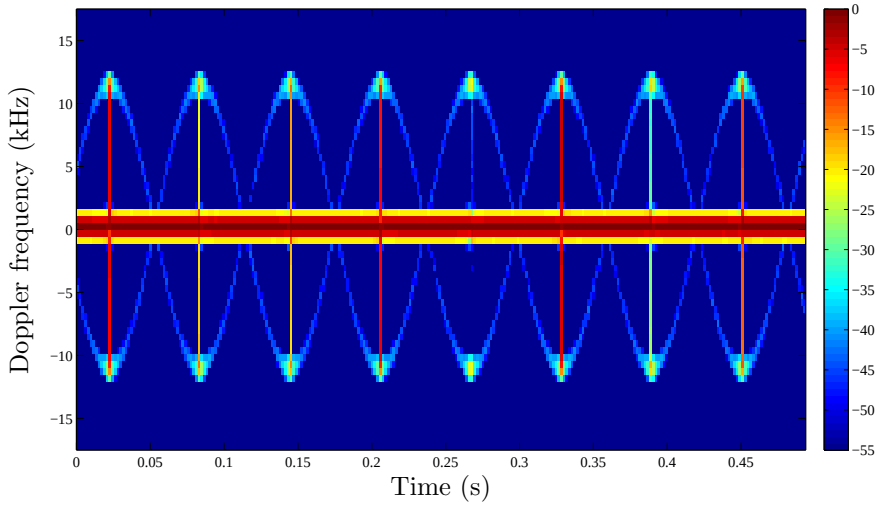

Figure 1.4: Doppler spectrum of simulated data for a main rotor with two blades. Both the blade flashes and the sinusoids resulting from the blade tip scattering are shown in the figure.

observed with helicopters are included. Figure 1.4 shows both the blade flash and the sinusoids from the blade tips. The number of blades for this target used in the simulation can be determined by counting the number of sinusoids in the Doppler spectrum, since there is a sinusoid for every blade tip. This method would, however, not be feasible in cases with low SNR. The simulation model for this research was also developed to include the effects of the tail rotor, as well as the return from the fuselage of the helicopter. The simulation model is discussed in detail in Chapter 3.

The Helicopter Blade Modulation (HBM) parameter extraction algorithm proposed in this work is presented in Chapter 3. Figure 1.5 shows a block diagram of the proposed method. Each of the different steps in the algorithm is discussed in detail in Chapter 3.

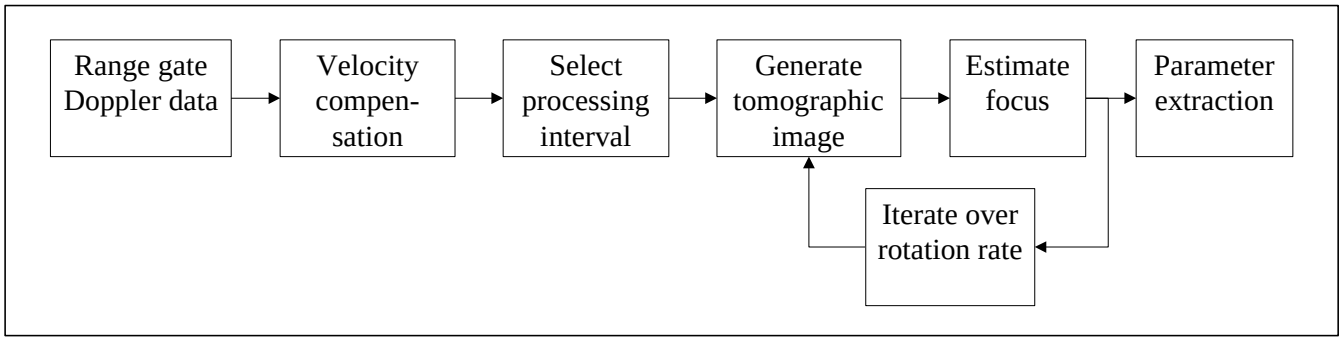

Figure 1.5: Block diagram of the HBM parameter extraction algortihm that was developed for this research.

The first three steps in the algorithm ensure that the data is in the correct format and that velocity compensation has been performed on the return from the helicopter fuselage. The length of the processing interval, which is used for the data that serves as the input to the tomographic imaging, has two main requirements. Firstly, it was experimentally determined that the algorithm would give the best results when the length of the interval is longer than one complete revolution of the main rotor: secondly, the best results were achieved when there was no decorrelation due to the variation of the phase of the helicopter blade tip sinusoids. The experimental results showed that the best imaging interval is more than one revolution and smaller than 400 ms.

The final part of the algorithm performs the blade parameter extraction. A tomographic imaging technique, namely the Inverse Radon Transform (IRT), is used to make a 2-D image of the helicopter blade tips. This technique is based on the Fourier slice theorem, which, according to Qureshi *et al.* [13], states that the 1-D Fourier transform of the projections of a function onto a line, at a certain angle, is equal to the slice of the 2-D Fourier transform of the function at the same angle. The Doppler spectrum data is used as input to the IRT, where the sinusoids can be seen as 1-D projections of a 2-D object at a certain angle. The image is therefore reconstructed by using the projected data at the correct angle, where the correct angle is determined from an estimation of the angular rate, ω of the main rotor. The rotation rate can be determined through an iterative process where an IRT image is constructed over a rotation rate search interval. A focused image of the blade tips is constructed for the rotation rate that is approximately equal to the actual rotor rotation rate. The maximum intensity and entropy of each image at a different rotation rate are taken to determine when the most focused image occurs and, in so doing, to determine the estimated rotation rate of the main rotor. Figure 1.6 shows a focused image of the blade tips for a helicopter with three main rotor blades by using the IRT.

The image is a Doppler-Doppler plot and therefore the maximum Doppler frequency at the tip of the blade can be estimated from the focused image, which can be related to the tip velocity of the blade. The blade length can further be determined from the estimated rotation rate (viz. the rate at which a focused image occurs) and the estimated blade tip velocity. Equation 1.4 shows how these parameters can be derived from the maximum Doppler frequency at the blade tip

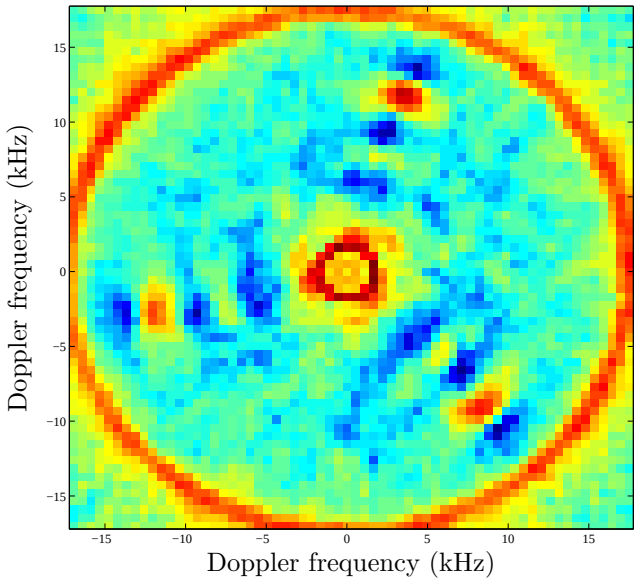

Figure 1.6: A focused image of three helicopter blade tips formed by the IRT process. The measured data showed in this figure is from a three-bladed helicopter.

$$\begin{aligned} v_{tip_{est}} &= \frac{f_{d_{est}}\lambda}{2} \\ L_{est} &= \frac{v_{tip_{est}}}{\omega_{est}} \end{aligned} \tag{1.4}$$

where λ is the wavelength of the transmitted signal and ω_{est} is determined from the focused IRT image. The radar range equation was also used to indicate the expected SNR for a helicopter with a typical blade length. The radar parameters that were used were chosen to correspond to one of the radars that was available for measurements for this research. Several other important factors are also discussed in Chapter 3, such as the compensation for the elevation angle error.

The conclusion of Chapter 3 is that the developed algorithm can indeed be helpful in the identification of helicopters, although actual measured radar data is required to validate this statement.

1.3.3 Experiment and results

The helicopter trial and the results from the measured data are discussed in Chapter 4. A measurement trial was conducted in Pretoria, during which nine different helicopters

as targets of opportunity, from three of the classes in the database (two, three and four main rotor blades respectively) were used. The aim of this trial was to gather data from helicopters that are in the same class (in terms of the number of blades) as well as from helicopters in different classes. The helicopters were also chosen such that there were targets with varying blade lengths, as well as targets with very similar blade parameters. Three flight profiles were performed, namely a racecourse profile (ranging from $3-12$ km), a turning hover profile and a desscent behind a hill. Two radars were used during the trial, namely, a monopulse tracking radar, working at X-band, and a RCS measurement radar, operating both in C and X-band. Most of the waveforms that were used had a high pulse repetition frequency (PRF) (viz. they were not ambiguous with regard to the maximum Doppler bandwidth of the target), but for some measurements medium PRF waveforms were used.

Chapter 4 further gives results from the various flight profiles of some of the helicopters. This validates the method for various helicopters, at various ranges and in the extreme cases of the experiment setup (ranges in the order of 12 km). Figures 1.6 and 1.7 show measured data for the AS 350B. These figures were generated from data measured during one of the inbound runs of the racecourse profile with the range to the target at approximately 6.5 km.

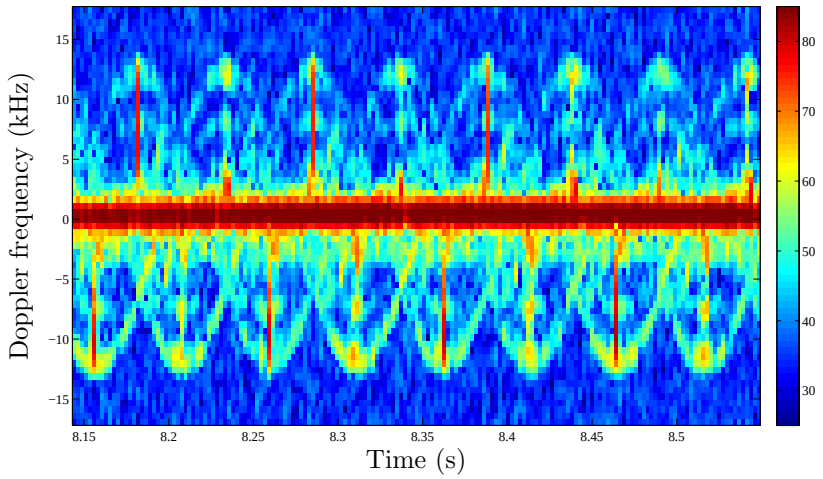

Figure 1.7: The Doppler spectrum of measured data for the AS 350B. This data was used as input to the IRT process.

The blade flashes and sinusoids resulting from the blade tip scattering can be seen in Figure 1.7. This data was used as input to the tomographic imaging process. The three blade tips can be seen from the focused IRT image (see Figure 1.6), from which the maximum Doppler frequency at the blade tips can be determined. The position of the

three blade tips is dependent on the start phase of the sinusoids in the Doppler spectrum data. Table 1.1 gives the estimated blade parameters for the interval of the data shown in the previous two figures.

Table 1.1: Estimated blade parameters for measured data of the AS350B. The ground truth data of the helicopter and the estimation error are also shown in the table.

Helicopter Parameters			**Estimated Parameters**			**Estimation error**	
N	**L (m)**	r_ω **(RPM)**	**N**	**L (m)**	r_ω **(RPM)**	**L (m)**	r_ω **(RPM)**
3	5.35	390	3	5.23	387	0.12 m	0.77%

This chapter further conducts a performance analysis of the algorithm, showing the estimated parameters for the different helicopters over range, for all the different flight profiles. The results are presented by showing the probability of correct identification over range for all the different helicopters and for the different flight profiles. The different methods that were used to estimate the rotation rate are also compared with each other, showing the results for both the entropy and the maximum intensity method. The chapter ends with an analysis of the measured data, which generated a number of new research questions.

1.3.4 Conclusion and future work

The final chapter of the thesis (Chapter 5) discusses the conclusions, the limitations of the current study, and the scope for future work. The new research questions and the limitations of the algorithm that were formulated during the performance analysis of the data in Chapter 4 are formally addressed, and first order solutions or explanations are given. Some of the questions raised and the new knowledge gained include:

- What is the actual processing gain achieved by using the IRT? This can be addressed by determining the SNR of the input data vs the SNR of the output data.
- The algorithm gives optimal results when the helicopter is flying in the horizontal plane. For manoeuvres where the target is making a teardrop turn, for example, this technique would not give reliable answers.
- The simulation model should be extended to include the polarization of the antenna as an input parameter to the system. Research by Pouliguen *et al.* [8] showed that by using horizontal polarization a higher SNR from the blade tip scattering can be achieved.

- How can the algorithm be extended to work for medium PRF waveforms?
- What other parameters of the helicopter can be used to aid in the identification process?

1.3.5 Summary

This research found that the use of the micro-Doppler signature analysis of helicopter rotor blades can play a significant role in the identification of airborne targets. The work presented in this thesis proposes a new method for estimating some of the helicopter blade parameters that are valuable features in the identification of helicopters. This method uses tomographic techniques to extract the blade parameters, and the results from both the simulation and the measured data show that the technique is feasible for a tracking radar, although there are certain limitations to the algorithm. The features extracted from the micro-Doppler return are the number of main rotor blades, the blade length (m) and finally the rotation rate of the main rotor.

A separability study performed on a database consisting of over 100 helicopters showed that, by using these parameters in a classification algorithm, the probability of correctly identifying a helicopter increases significantly. However, this is dependent on the accuracy of the estimations. Although this method cannot provide a complete solution to the problem of correctly identifying helicopters for radar NCTR, it makes a valuable contribution to address some of the underlying problems in the field of NCTR, especially for tracking radar applications. The work also shows that more features of the helicopter are required in order to estimate the make and model of the helicopter with a high probability of correct identification.

Chapter 2

Background theory and helicopter separability analysis

The background theory to helicopter blade modulation is discussed in this chapter, showing the equation given by Martin and Mulgrew [6], which describes the return from the rotating structures on a helicopter, and identifying the target parameters that influence the return signal. The second section of this chapter reviews the contributions made by the existing literature regarding the use of the micro-Doppler signature of rotating structures for the purposes of radar target identification. The various techniques proposed in the literature are discussed, including the main contributions made by the research as well as some of the advantages and disadvantages of using a particular method introduced in the literature.

The final section of this chapter is a separability analysis that was performed on helicopters from a database, which was specifically developed for this research. In this study the probability of correct identification is investigated, given the blade parameters that influence the micro-Doppler return signal. This study shows the required accuracy for a blade parameter extraction algorithm, given a certain probability of correct identification.

2.1 Blade modulation theory

The received radar signal from some airborne targets contains a modulation component resulting from the rotating parts of the target i.e. propeller blades, rotor blades or jet

engine blades. This frequency modulation, also known as the micro-Doppler effect (Chen *et al.* [3]), causes a number of sidebands about the centre frequency of the reflected signal. Work presented in the literature states that the information contained in the received micro-Doppler signals can be used as features in an identification process. Some of the research done in that area includes that of Chen *et al.* [4], Yoon *et al.* [5], Martin and Mulgrew [6], Bullard and Dowdy [7], Bell and Grubbs [9] and finally Misiurewicz *et al.* [10].

Martin and Mulgrew [6] give the theoretical return signal from the rotating parts of an airborne target. This model considers both propeller blades and helicopter rotor blades. Since the focus of this research is only on helicopters, the propeller blade case is not discussed. The model states that

$$\begin{aligned} S_r(t) &= \sum_{n=0}^{N-1} A_r(L) e^{j(\omega_c t - \frac{4\pi}{\lambda}(R+vt+\frac{L}{2}\cos(\theta)\sin(\omega_r t+\frac{2\pi n}{N})))} \\ &\quad \cdot \operatorname{sinc}(\frac{4\pi}{\lambda}\frac{L}{2}\cos(\theta)\sin(\omega_r t+\frac{2\pi n}{N})) \end{aligned} \tag{2.1}$$

where A_r is a scale factor, L is the distance from the centre of rotation to the blade tip, N is the number of main rotor blades, and R is the range from the centre of rotation to the radar. The time is indicated by t, v gives the radial velocity of the centre of rotation with respect to the radar, and the wavelength of the transmitted radar signal is indicated by λ. θ indicates the angle between the plane of rotation and the radar's line of sight to the centre of rotation. Finally ω_c is the radial frequency of the transmitted signal and ω_r is the angular velocity of the main rotor.

For the theoretical model above to hold true, several assumptions have been made by the authors. The rotor blades are firstly assumed to act as homogeneous, linear and rigid antennas. In reality, however, a real helicopter blade is an airfoil with a specific camber where parameters such as the blade pitch and angle of attack can influence the return signal for different aspect angles. The model further assumes that all the blades are always completely visible to the radar. This assumption will be true for most cases when investigating the main rotor blades. For the tail rotor of the helicopter, however, this will only be true for specific aspect angles, since the tail rotor is concealed by the body of the helicopter for some aspect angles to the radar. The final assumption that is made is that the target should be in the far field of the radar.

The influence of the micro-Doppler return on the spectrum of the total received signal is expressed by the following equations from Martin and Mulgrew [6], using the same

symbols as in Equation 2.1. Firstly, the number of significant sidebands resulting from the blade modulation can be expressed as

$$N' = \frac{8\pi L \cos(\theta)}{N\lambda} \tag{2.2}$$

The number of sidebands due to the blade modulation are therefore dependent on the blade length, the number of blades and the aspect angle of the centre of rotation with respect to the radar. The aspect angle is the only time-varying parameter, and therefore the position of the helicopter with respect to the radar will influence the number of sidebands in the return spectrum. The distance between each of the sidebands can be calculated as follows

$$\Delta f = N f_r \tag{2.3}$$

where f_r is the angular frequency of the helicopter rotor. Finally the bandwidth, B, of these sidebands is determined from using Equation 2.4.

$$B = \frac{8\pi f_r \cos(\theta)}{\lambda} \tag{2.4}$$

The theory described above shows that the blade modulation that occurs is dependent on five key parameters, namely, the number of blades, N, the blade length, L, the angular frequency f_r, the wavelength of the transmitted signal, λ and the aspect angle of the rotor, θ. Three of these parameters (N, L and f_r) are dependent on the specific target. The information in the spectrum regarding these parameters can therefore be used to aid in the identification of the helicopter. The separability of helicopters by using these three parameters is discussed later in this chapter (see Section 2.2).

2.1.1 Literature review

Different approaches have been followed in the literature to address the problem of radar target identification. This section discusses some of the techniques that have been proposed for the identification of targets with rotating blades, i.e. helicopters and propeller blades.

Rotander and von Sydow [11] in their paper on helicopter classification introduced an identification method that uses the three rotor parameters discussed above (L, N and f_r). The relation between these parameters can be expressed by means of two equations,

namely the time domain version of Equation 2.3 with $\tau = 1/\Delta f$, giving the period for the blade flashes in the time domain of the return, and

$$v_{tip} = 2\pi f_r L \tag{2.5}$$

to calculate the blade tip velocity. This tip velocity, v_{tip} is determined from the measured Doppler spectrum of the return signal. The authors use the ratio of the blade length (L) and the number of main rotor blades, N, for identification, since there are three unknowns and only two equations. This parameter can be expressed as

$$\frac{L}{N} = \frac{v_{tip}\tau}{2\pi} \tag{2.6}$$

This technique determines the L/N ratio and identifies the helicopter according to this value. The results presented in the paper show that the parity of the rotor, i.e. an odd or even number of blades, can also be used for identification by using symmetry in the Doppler spectrum. The authors state that for a helicopter with an even number of blades the return signal from the approaching and receding blades will occur simultaneously and the spectrum will be symmetrical. In the case of a target with odd parity, the returns of the approaching and receding blades will not occur at the same time instance. Rotander and von Sydow further state that the approaching rotor blades will have a positive Doppler frequency and the receding blades a negative Doppler frequency [11].

Although this method has been proven to work for some cases, further investigation has shown that this ratio is not very reliable, since the L/N values for some helicopters are very similar, and it would therefore be impossible to distinguish between certain targets. Table 2.1 shows a small selection of military and civilian helicopters that are used in South-Africa, indicating that this technique would fail for several cases. The L/N values for both the main and tail rotor blades are shown, since it might prove useful to look at the tail rotor parameters when the main rotor parameters are identical for two different helicopters.

The examples in Table 2.1 are taken from a database that was developed for this research, consisting of over 100 military and civilian helicopters.

Another constraint of the L/N ratio method is that a high SNR is required to determine the maximum tip velocity, v_{tip}, of the blade accurately. A high PRF waveform is another requirement that needs to be met, since aliasing of the blade flashes will prevent any accurate estimation of the tip velocity.

Table 2.1: Some of the civilian and military helicopters found in South Africa with their respective blade parameters. These include the number of blades (N), the blade length (L) and the L/N ratio introduced by Rotander and von Sydow [11] as a feature that can be used for helicopter identification.

	Main Rotor				**Tail Rotor**		
Helicopter	**N**	**L (m)**	**L/N**	**Parity**	**N**	**L (m)**	**L/N**
Bell 206	2	5.08	2.54	Even	2	-	
Alouette II	3	5.1	1.7	Odd	2	-	
Robinson R22	2	3.85	1.92	Even	2	0.53	0.27
Rooivalk	4	7.79	1.95	Even	5	1.52	0.3
Oryx	4	7.8	1.95	Even	5	1.57	0.3

Building on the work by Rotander and von Sydow [11], Tikkinen *et al.* [14] proposed an improved L/N (ILN) method, which makes use of both coherently and incoherently integrated time signals. The coherent time signal is used to determine the maximum tip velocity by using an improved edge detector; the time between blade flashes, τ, is determined from the incoherent time data given by a peak detector. Tikkinen's paper thus contributes with a method that gives a more accurate estimation for the tip velocity and the flash interval parameters.

The paper first discusses the radar waveform that is required to estimate the tip velocity from the coherent time signal. The trade-off between the PRF and coherent integration time is an important aspect that is discussed by using actual helicopter parameters from a database.

For low PRF (LPRF) waveforms the coherent integration time will be long enough to ensure that two main rotor blade flashes are seen. The trade-off lies in the fact that the micro-Doppler spectrum will be aliased with poor spectral resolution. The integration time for a medium PRF (MPRF) waveform will provide consecutive blade flashes for only some helicopters while the spectrum of the blade returns will still alias. Tikkinen [14] state that, in the case of a high PRF (HPRF) mode, the coherent integration time will decrease so significantly that consecutive blade flashes will not be captured. The micro-Doppler returns will, however, not be aliased in the case of HPRF, and a very good spectral resolution can be obtained. Although not explicitly stated in the paper, it is assumed that this work was developed for surveillance radar purposes, since the problem of missing the blade flash due to a short dwell time is not a factor at all in a tracking radar.

As stated earlier, the model proposed by Tikkinen [14] makes use of both a peak detector and an edge detector. The flash interval, τ, is estimated by implementing a peak detector on the incoherent integrated time signal, which allows a certain number of peaks to be detected in the signal according to certain rules. Given that only the peaks resulting from the main rotor blade flashes are detected,the time between flashes is estimated. As in the paper by Rotander and von Sydow [11], the edge detector is used to estimate the tip velocity, v_{tip}, from the coherently integrated data. The edge detector divides the time signal into small intervals in order to determine the mean value of each interval. Tikkinen [14] states that, by comparing the mean values of adjacent intervals, the edge can be defined. By using both the local mean and statistics over longer periods the return signal can be better characterized.

Tikkinen [14] concludes that the probability of correctly identifying of a helicopter is increased by using the improved edge detector especially in low SNR conditions, since a smaller estimation error is made for the tip velocity, v_{tip}. Although this method may prove to perform better in a classifier, the main underlying problem of the L/N method still persists.

Yoon *et al.* [5] in their paper on helicopter classification address the shortcomings of the L/N method by utilising a time-frequency analysis to estimate certain blade parameters. The Short-Time Fourier Transform (STFT) is used to determine both the parity and number of rotor blades of the helicopter.

The parity of the blades is determined by looking at the instances when the blades are perpendicular to the radar, i.e. when the blade flash occurs. For even parity, Yoon [5] states that the flashes of both the approaching and receding blades will occur simultaneously. For odd parity, the approaching and receding blades will not flash at the same time. The simulation model that was developed for the research and is presented in Chapter 3 of this thesis validates this statement.

Yoon [5] further shows that there are two methods to determine the number of main rotor blades (N). The first method determines the number of sinusoids seen in the time-frequency data that results from the blade tip scatterers. The Doppler spectrum of the data shows that each sinusoid represents the rotation of the tip of one of the rotor blades, and therefore the number of sinusoids is equal to the number of main rotor blades. Alternatively, the point where the sinusoids from the different blades cross one another, can be used to determine the number of blades (N) by taking the distance from zero

Doppler (or the reference frequency) to the cross point. For the case of two main rotor blades this point is at zero Doppler, for four main rotor blades it moves to $1/\sqrt{2}$ of the maximum Doppler frequency of the return signal.

For simulated data in high SNR conditions this method would prove sufficient. However, when considering measured helicopter data, where the reflection from the fuselage is very large, the cross points become increasingly difficult to see in the data, especially at longer ranges, due to the lower SNR. The method developed by Yoon [5] also makes use of the time domain data to determine the time between flashes, τ. The number, parity and angular frequency can therefore be determined by using this method for conditions with very high SNR, and where the return from the helicopter body does not obscure these cross points of the micro-Doppler effects.

The technique proposed by Yoon [5] has been verified by use of a simple point scatter method, which will be discussed in Chapter 3. The analysis showed that when the number of rotor blades becomes more than four, the counting of the sinusoids also becomes very difficult especially in low SNR conditions. Even for helicopters with three or four main rotor blades it is not always feasible to determine the number of blades by identifying the number of sinusoids in the Doppler spectrum of the generated data, given low SNR values. Therefore, although the work presented in this paper is a very good departure point for estimating some of the key helicopter parameters, it cannot be used in isolation since identification would fail for numerous cases and in various conditions.

In their paper on the micro-Doppler effect Chen *et al.* [3] discuss the different time-frequency analysis methods that can be used to investigate the micro-Doppler signals resulting from a rotating object. The need for analyzing the data in the time-frequency domain arises since the Fast Fourier Transform (FFT) of the data would not provide the complex time-varying frequency modulation components. Therefore Chen states that by using a high-resolution time-frequency transform these time-varying frequency modulation signals can be investigated [3].

According to Chen [3] there are several different time-frequency transforms that can be used. The most common method is the linear STFT, which divides the return signal into equally spaced blocks. A Fourier transform is performed on each block that is a function of a certain window function. From Allen [15] in his paper on short term spectral analysis the discrete STFT can be written as

$$X_n(e^{j\omega_k}) = \sum_{m=-\infty}^{\infty} w(n-m)x(m)e^{-j\omega_k m} \tag{2.7}$$

where w_k is the windowing function that determines which block of the signal, $x(m)$, is evaluated. The complex results are added to a matrix, where the amplitude and phase for each point in time and frequency are stored. By changing the length of the window function the resolution of both the frequency and time can be changed.

The resolution of the STFT is determined by the size of the time-limited window function. Allen [15] states that when designing the parameters for the STFT a trade-off exists between the time and frequency resolution. To obtain better time resolution in the data a smaller window is needed, which however results in poor frequency resolution. If the aim is to obtain very high frequency resolution, a larger window is needed, with the disadvantage of losing time resolution (Chen [3]).

Other time-frequency analysis techniques discussed by Chen [3] include bilinear transforms, which are listed below.

- Wigner-Ville Distribution (WVD)
- Cohen Class
- Choi Williams
- Pseudo Wigner
- Smooth Pseudo Wigner-Ville (SPWV)
- Cone Kernel

According to Chen [3] the advantage of using a bilinear transform is that the resolution of the time-frequency data is better than when using linear transforms; however, this method produces cross-term interference in the data. Another method used is an adaptive time-frequency transform, where the return signal is transformed into a series of basis functions, by using the Gabor function. This method gives a very high time-frequency resolution and can be used to separate the returns from the target according to the target's features (Chen [3]).

Although the bilinear and adaptive transforms have been proven to give better results, even the linear STFT would give adequate results depending on the requirements of the analysis, i.e. how good the resolution needs to be, and how little cross-term interference can be tolerated.

Chen [3] concludes that any time-frequency transform can be utilized to analyse the micro-Doppler modulation in the received signal. One of the key requirements for the transforms, however, is that high resolution in both the time and frequency domains and low cross-term interference should be achieved. The authors recommend that the pseudo Wigner-Ville distribution is one of the best options for this task. Even though the time-frequency resolution of this method is slightly less than that of some of the other transforms, the cross-term interference is largely reduced. The choice of transform is therefore a trade-off between resolution and the reduction in cross-term interference.

The approach used by Green [16] was to utilize the decametric waveband (3-30 MHz) for the transmitting radar signal, f_c. This implies that the wavelength of the transmitted signal is between 280 and 2800 times larger than X-band frequencies, which leads to a different scattering mechanism. Green [16] states that, due to the blade lengths of the helicopter (average of 5 m per blade), the scattering points are in the Rayleigh region. A resonating effect with the blade will be caused for frequencies of 30 MHz, since the wavelength of 9 m is in the same order as the helicopter blade length. In the paper by Green the rotor of the aircraft was modelled as a set of short circuited vee antennas, where the scatterers were assumed to induce a sinusoidal current distribution [16]. From measurements conducted in an anechoic chamber with models for two and three main rotor blade configurations, the Doppler spectrum has been obtained for the main rotor. The results showed that the spectrum contained a set of line pairs that were symmetric about the Doppler line with frequency intervals determined by the rotor frequency and number of blades. This indicates both AM and phase modulation of the backscattered signal from the blade tips.

Bullard and Dowdy [7] investigated the micro-Doppler effects by looking at recorded data of a S-55 Sikorsky helicopter. Their paper states that by using the correct Doppler feature extraction signal processing techniques the main rotor configuration, blade count, rotor parity, tail rotor blade count and configuration as well as the hub configuration can be determined. Their processing, however, does not show the estimates for all these parameters and it does not state how the configuration of the main hub, rotor and tail rotor can be determined.

The authors in [7] simply take a FFT of the recorded I/Q time domain data, and shift the return from the body of the helicopter to zero Doppler, i.e. compensation for the velocity of the helicopter body. After the velocity compensation the Inverse Fast-Fourier Transform (IFFT) is taken and the parameters are determined from the frequency filtered

time-domain data. Although the main and tail rotor flashes are visible in the time-domain data, the number of blades, their length and the configuration of the hub cannot be determined. It is also not stated in the paper how the authors propose to determine these parameters.

A useful contribution of Bullard and Dowdy's paper, however, is a table stating the tip velocities of both the main rotor and tail rotor blades for several military helicopters. This data was added to our database of helicopters.

Another approach to the problem of helicopter identification is to use the return signal from the main rotor hub of the helicopter. Research was conducted by a group of authors, which resulted in three papers, Misiurewicz *et al.* [10] and [17] and Kulpa *et al.* [12].

Misiurewicz [10] investigates the return signal from a helicopter by using a S-band surveillance radar with a range of up to 100 km with a PRF of 4 kHz, to record a Mi-2 Russian helicopter. Since a search radar was used, it proved difficult to record sufficient data during the short dwell times. After detection of the target the antenna was used to track the target, producing enough time to record more than one blade flash.

The recorded data was presented in both time and frequency domain graphs where flashes could be seen in the time data, and it was therefore possible to detect a hovering helicopter. The work that followed from this paper was presented by Misiurewicz *et al.* [17]. The authors claimed that in the previous study both the long range surveillance radars as well as the short range tracking radars experienced difficulty in detecting the rotor blades in a single scan, due the the short number of pulses on the target.

Misiurewicz [17] investigates the return from the hub of the main rotor. The hub of the helicopter rotor has a fairly complex structure, since there are various small parts, each with a very specific function (power transfer, blade attack angle steering and damping of blade vibrations - Misiurewicz [17]). All the different scatterers resulting from the different structures make the modeling of the return signal from the hub quite complex. To illustrate the complexity of these structures examples of helicopter rotor hubs are shown in Figure 2.1.

A simplified model of the main rotor hub was suggested by the authors, where the hub is modelled as a cylinder, with a large number of scatterers randomly distributed over the cylinder. By using this model the micro-Doppler effect caused by the hub was investigated by Misiurewicz [17]. To determine the Doppler distribution of the scatterers placed

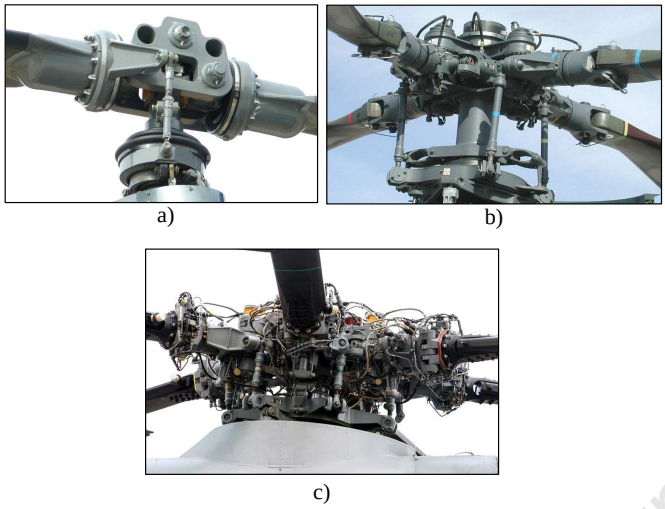

Figure 2.1: Main rotor hubs of the a) Robinson R-44, b) AS 330, and the c) Super Frelon helicopter.

around the hub, the velocity distribution of the scatterers was determined first. Equation 2.8 shows this velocity distribution density, where v_h is the radial velocity of the scatterers on the hub.

$$f_{v_h}(v_h) = \frac{2}{\pi D}\sqrt{(\omega_h D/2)^2 - v_h^2} \tag{2.8}$$

D denotes the diameter of the hub, and ω_h is the angular velocity of the hub. The paper states that one of the considerations that had to be taken into account in order to see the hub in the return data was, firstly, that the maximum linear speed of the hub with respect to the body of the helicopter is

$$v_h = \omega_h D/2 \tag{2.9}$$

which leads to the maximum Doppler bandwidth of the rotor hub

$$\Delta f_{hub} = \frac{\omega_r D}{\lambda} \tag{2.10}$$

It is very difficult to isolate the return of the rotor hub from the fuselage echo. Misiurewicz [17] states that the power spectrum estimation that is used should have a good enough resolution to show both strong and weak signals. An equation that needs to be met in order to detect the echo resulting from the hub is

$$N_{f_{hub}} = \frac{\Delta f_{hub}}{m}\Delta f \geq 4 \tag{2.11}$$

According to Misiurewicz [17], the fuselage echo occupies two Doppler resolution cells of width Δf, and the hub echo needs to occupy at least one more cell on either side of the fuselage echo in order to be detected. The authors state that, in order to see the return from the hub, a high resolution spectrum estimator is needed. The time on the target needs to be in the order of tens of milliseconds to achieve this high resolution. The same data that was used in the previous paper by Misiureiwcz [10] was presented once more, however, no further insight could be gained from the single graph shown in the paper.

Kulpa [12] used a parametric hub detection algorithm to produce better spectrum resolution, and therefore to detect the helicopter hub. The fuselage return is extracted from the data, leaving the return from the hub at low Doppler frequencies. The analysis of this method is only used with simulated data and, although promising results were obtained and the hub could be seen from the Monte-Carlo simulation results, this would not be so trivial for measured data. The reason is that, when the return from the fuselage is suppressed, information from the hub will be lost.

2.2 Helicopter separability analysis

In order to know how accurate the estimated helicopter blade parameters need to be for correct identification of a helicopter make and model, a helicopter separability analysis study was performed. A database of military, civilian and rescue helicopters was developed for this separability study, featuring more than 100 different helicopters, setting out the number of main rotor blades, the blade length and the main rotor rotation rate, as well as other features of each helicopter such as:

- Maximum velocity
- Average velocity
- Maximum altitude
- Number of tail rotor blades
- Blade length of tail rotor
- Rotation rate of the tail rotor
- Gear ratio

- Manufacturer
- Countries in which it is being used.

It was necessary to develop this database to obtain the various helicopter parameters for most of the helicopters found around the world, since such a database was not available in the open literature. The work on both the separability analysis and the helicopter database forms part of the unique contribution of this study to the research field.

This study was conducted to determine whether the use of the number of main rotor blades, the blade length and the main rotor rotation rate of a helicopter as features for an identification system would contribute to the positive identification of the target. The first feature that was used to divide the helicopters into different classes was the number of main rotor blades (N). This feature contributes greatly toward the identification of the target, and for the remainder of this dissertation the class that the helicopter belongs to will be an indication of the number of main rotor blades. Figure 2.2 shows the histogram for all the helicopters in the database, separated into various classes (according to the number of main rotor blades).

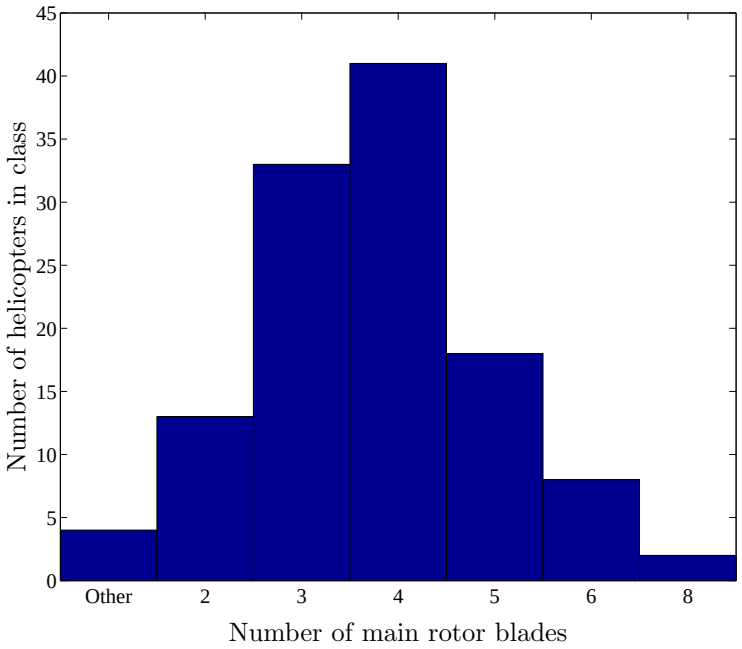

Figure 2.2: Distribution of the helicopters in the database according to the number of main rotor blades. The group "Other" refers to all the helicopters with more than one main rotor.

a) b) c)

Figure 2.3: Different configurations of helicopters with two counter-rotating main rotor blades. Three helicopters are shown with this configuration: a) Boeing Chinook, b) Kaman, and c) Kamov.

Figure 2.2 shows that 35% of the helicopters in the database have four main rotor blades, followed by 28% in the class of three-bladed helicopters. The five-bladed helicopter class has the third most entries with 15% of helicopters in the database. It is interesting to note that the two-bladed helicopters contribute to only 11% of the total number of helicopters. The class denoted as *other* on the graph represents that group of helicopters that have two main counter-rotating rotors. A variety of different helicopters that has this configuration, such as the Boeing Chinook, which has two main rotors, one at the front and one at the back of the helicopter. Another example is the Russian Kamov helicopter series. These helicopters have the second rotor directly above the first rotor. The third example of helicopters that fall into the class labeled *other* is the Kaman series, where the two rotors are tilted at an angle. Photographs of these three examples are shown in Figure 2.3.

Once the helicopters have been grouped by the number of main rotor blades, the blade length and rotation rate of the main rotor were used to separate the helicopters that fall within the same class. When using the blade length as a distinguishing feature, a distance measure was used to determine how far the helicopters were separated from one another, i.e. how much the blade lengths differed from one another and how accurate the blade length estimation had to be. Figure 2.4 shows the helicopters, separated by the number of main rotor blades (N) and plotted against the main rotor blade length (L).

For each class the minimum distance between the various blade lengths of the helicopters was determined. This parameter indicates the required accuracy of the algorithm estimating the blade length, hence what the maximum estimation error can be before the helicopter is wrongly identified. Table 2.2 shows this minimum distance for each of the different classes. The distance is a measure given in centimetres since the lengths of the blades in this case are used to measure the separation between helicopters. Table 2.2 shows the minimum distances between the blade lengths for all the different classes.

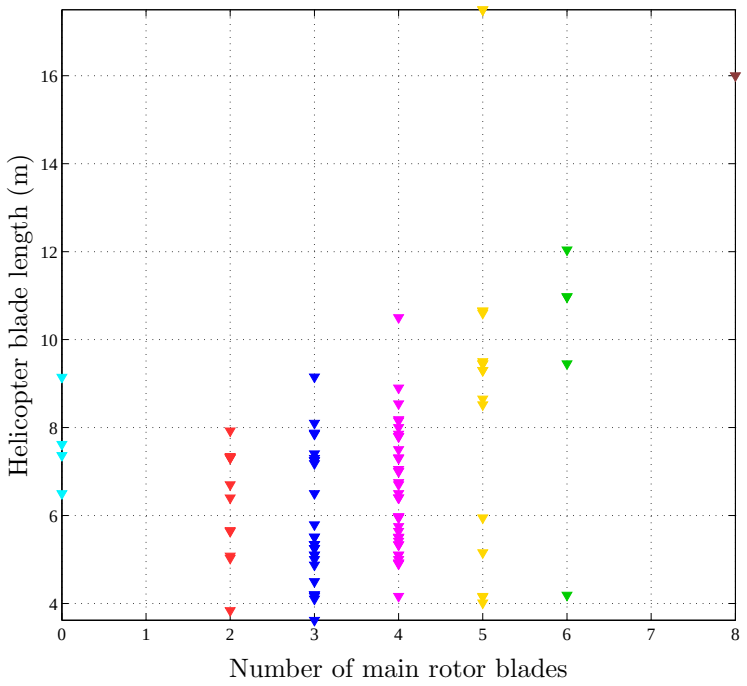

Figure 2.4: Helicopters from the database, divided into classes according to the number of main rotor blades, plotted against the main rotor blade length of each data sample. This figure shows how the blade lengths are distributed within a class.

The information given in Table 2.2 shows that, to identify a helicopter correctly without prior knowledge of the number of main rotor blades, the algorithm needs to be accurate within 0.5 cm of the ground truth blade length. There are, however, a number of helicopters with precisely the same blade lengths (different models from the same manufacturer). Therefore, by only using the blade length as an identifying feature, it would not be possible to separate these helicopters from one another, irrespective of the accuracy of the estimation algorithm.

To investigate the separability of the helicopters within a class further, the blade lengths of each helicopter were calculated, given a certain error in the blade length estimation. This would then indicate how the helicopters could be confused with each other given a certain error, especially when the blade lengths are very similar. The following set of figures shows the results for all the classes containing more than one helicopter. The results were calculated for blade length errors of 0.01 m, 0.1 m, 0.5 m and 1 m. Figure 2.5 shows the two-bladed helicopters from the database, with the ground truth blade length as the black dot for each helicopter, and the blade length estimation errors indicated by the error bars.

Table 2.2: Minimum distance between the blade lengths of the helicopters from each class (defined by the number of blade). These values indicate the required accuracy of the algorithm needed to separate the helicopters within a group.

Number of main rotor blades	**Minimum distance (cm)**
2	0.5
3	4
4	1
5	5
6	106.5
8	-
Other	26

Figure 2.5 shows that, although all the helicopters have a unique blade length (indicated by the black dot), the difference in these lengths is very small for some helicopters, such as the UH-1, Bell 212, the Super Cobra and the Bell 204.

For the three-bladed helicopters, there are three cases in the database where two helicopters have the exact same blade length. They are the Eurocopter AS350 and AS355, the Sikorsky S-55 and S-62 and finally the Kamov Ka-27 and Ka-29 Helix. For these cases other parameters, such as the rotation rate of the main rotor or the length of the tail rotor will have to be used to differentiate between these helicopters. However, for the three specific cases stated above, the rotation rate is also unknown; therefore, although the search space is significantly smaller, one will not be able to distinguish these helicopters from one another. The minimum distance shown in Table 2.2 for the three-bladed case is the first value that is bigger that 0, hence not taking the helicopters with the same blade lengths into account. Figure 2.6 shows the ground truth blade lengths for this class together with the estimated blade lengths, given a certain estimation error.

From Figure 2.6 there are more than four groups of helicopters that have very similar blade lengths. The first group can be identified for blade lengths of approximately 4 m. A big group of helicopters falls into the group that has blade lengths between 5 and 6. This indicates that the accuracy of the algorithm for helicopters with three blades needs to be very good, or other features such as the main rotor rotation rate have to be used as an additional identification feature.

In the class of the four-bladed main rotors there are two helicopters from different manufacturers that have the same blade length, the Mil Mi-4 and the Z-5 made by the Harbin Aircraft manufacturing company. As in the case of the class 3 helicopters, the main rotor rotation rates of these helicopters are also unknown, and thus other factors will have to

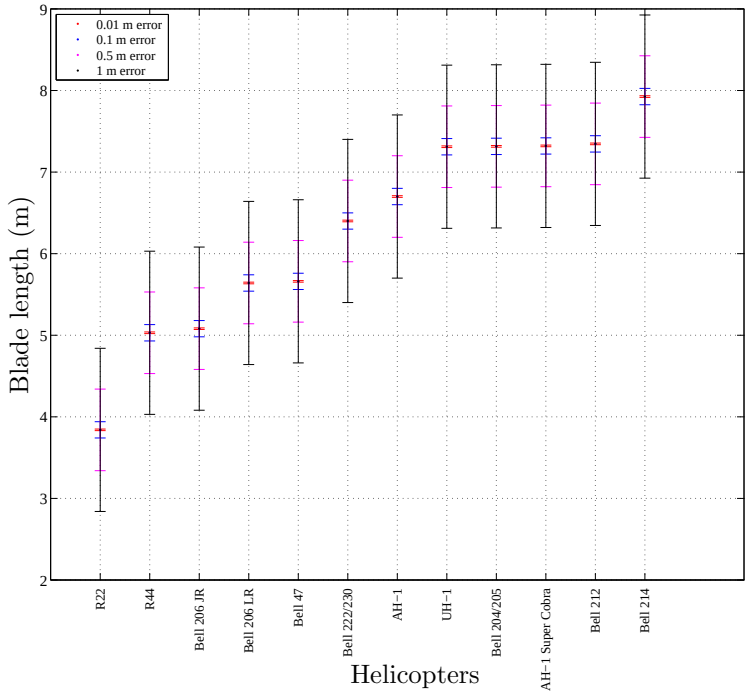

Figure 2.5: Separability of helicopters in the class of two main rotor blades. The figure shows how, given a certain blade length estimation error, one helicopter can be confused with another. For example, if an estimation error of 0.5 m is made, the Bell 206 JR will be wrongly identified as the Bell 206 LR.

be taken into consideration if positive identification is required. The distribution of and estimated blade lengths, given a certain error, for the case of helicopters with four main rotor blades, is shown in Figure 2.7.

Figure 2.7 shows that the helicopters are distributed over a large range of blade lengths, although there are still groups of helicopters that have very similar blade lengths. The same graph is showed for helicopters with five main rotor blades in Figure 2.8.

Although there are considerably fewer helicopters in class 5, the blade lengths of these helicopters are also very similar. The helicopters in the database with the longest blade lengths, the Mi-6 Hook and the Mi-10, are both in this class and both have a blade length of 17.5 m.

For the helicopters with six blades three of the entries have the same blade length, and the same rotation rate. These helicopters are all made by Sikorsky and are used in different military roles. The CH-53D Super Stallion, MH-53E Sea Dragon and MH-53J Pave Low III have the same parameters, although the CH-53D and the MH-53J are used inland, and the Sea Dragon is used for maritime related missions. Figure 2.9 gives the distribution

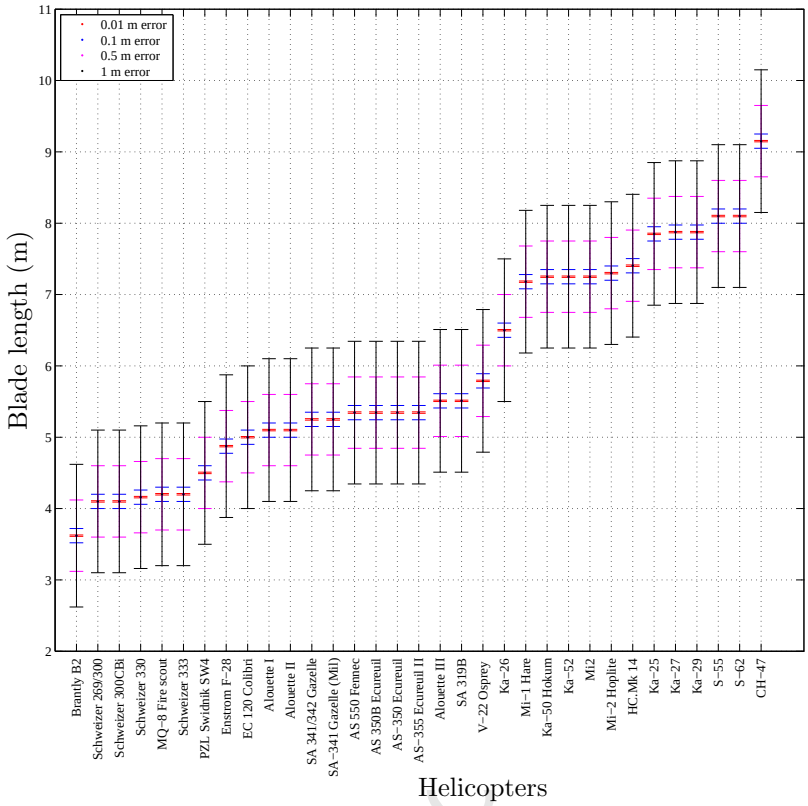

Figure 2.6: Separability of helicopters in the class of three main rotor blades. The figure shows how, given a certain blade length estimation error, one helicopter can be confused with another. There are a number of groups of helicopters within this class that have very similar blade lengths.

of blade lengths for helicopters with six main rotors, together with the estimated blade length errors.

2.2.1 Probability of correct helicopter identification based on Gaussian error distributions

A Gaussian error distribution was used to determine the probability of correctly identifying a helicopter within a certain class in the database. Figure 2.10 shows how the probability of correct identification was calculated for each sample in the database.

The normal distribution, indicated by a red line, shows the current sample, whereas the dashed curves show the two adjacent helicopters. The samples are sorted according to class, and within the class according to ascending blade lengths. The mean value, μ, for the normal distribution was taken as the ground truth blade length for each sample.

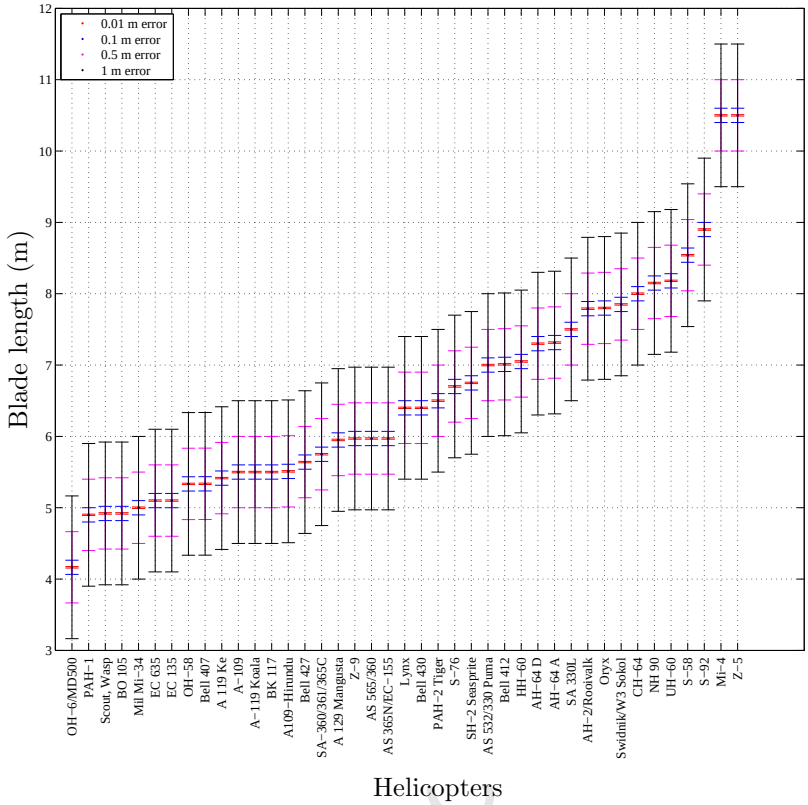

Figure 2.7: Separability of helicopters in the class of four main rotor blades. The figure shows how, given a certain blade length estimation error, one helicopter can be confused with another.

The variance, σ^2, for each sample was varied with a standard deviation ranging from a blade length estimation error of 0.001 m to 1 m. The boundary values, a and b, for each distribution, were chosen as the midpoints between two adjacent samples. Equation 2.12 shows how these parameters were calculated.

$$\begin{aligned} a &= \mu_{n-1} + \frac{(\mu_n - \mu_{n-1})}{2} \\ b &= \mu_n + \frac{(\mu_n - \mu_{n1})}{2} \end{aligned} \tag{2.12}$$

If the current sample is the first in the class, the left boundary, a, is chosen to be $\mu_n - 1$ m, and if the current sample is the last in the class, i.e. the sample with the longest blade length, the right boundary, b, is chosen to be $2\mu_n$. A step size, δ, was defined to calculate the area between the two boundaries for a certain σ, where

$$X = a : \delta : b \tag{2.13}$$

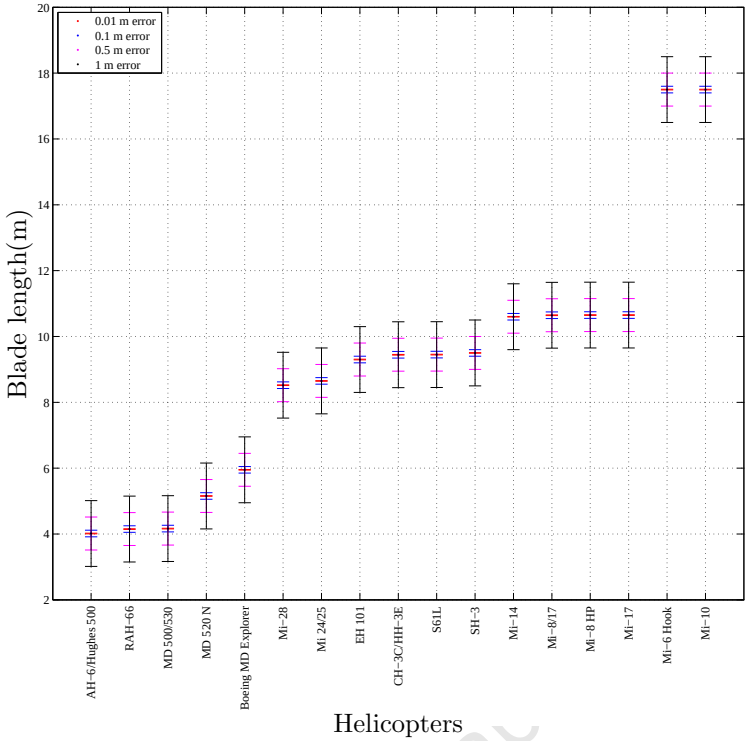

Figure 2.8: Separability of helicopters in the class of five main rotor blades. The figure shows how, given a certain blade length estimation error, one helicopter can be confused with another.

For a certain standard deviation the normal distribution was then calculated as

$$\begin{aligned} y &= f(x|\mu,\sigma) \\ &= \frac{1}{\sigma\sqrt{2\pi}} \exp \frac{-(x-\mu)^2}{2\sigma^2} \end{aligned} \tag{2.14}$$

To calculate the probability of correctly identifying a specific helicopter for a specific standard deviation, Equation 2.15 was used

$$\Pr_{\sigma} = \frac{\sum y\sigma}{N} \tag{2.15}$$

where the probability of correct identification is weighted by the number of samples, N, in the specific class. The probability of correct identification for a sample over all the standard deviation parameters was calculated as follows

$$\Pr_{correct} = \sum \Pr \tag{2.16}$$

This process was performed for all the different classes in the database, as well as for all the samples in the database, i.e. not taking into consideration the number of main

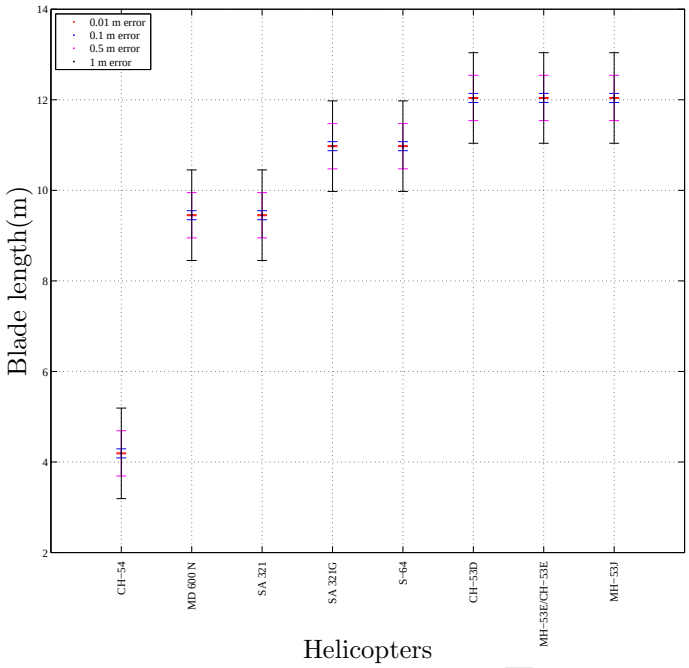

Figure 2.9: Separability of helicopters in the class of six main rotor blades. The figure shows how, given a certain blade length estimation error, one helicopter can be confused with another. In this class a number of helicopters have the same blade length.

rotor blades. The probability of correctly identifying a helicopter in a certain class given a certain blade length estimation error is shown in Figure 2.11.

This figure shows that, when only the blade length is taken into account and not the number of blades, the probability of correctly identifying the make and model of a helicopter is 70% for a blade length estimation error of only 1 cm (see the dotted red line on the graph). This shows that very accurate estimations are required when using only the blade length as a feature in the identification process. For some classes in the database a higher probability of correct identification is achieved for the same estimation error of 1 cm. Class 2 in the database will have a probability of correct identification of more than 80% for the same estimation error of 0.01 m. However, given the same σ the probability of correct identification for class 6 is approximately 50%.

The main rotor rotation rate in revolutions per minute (RPM) of the helicopters was used to determine whether this feature would aid in further separating the helicopters within a class. Figure 2.12 gives the different rotation rates for the helicopters in the database. The values that are given in the database represent the normal main rotor rotation rate. It should, however, be noted that helicopters are designed to have a varying rotation rate of approximately 20 RPM to either side of the normal value. The rotation rate for a

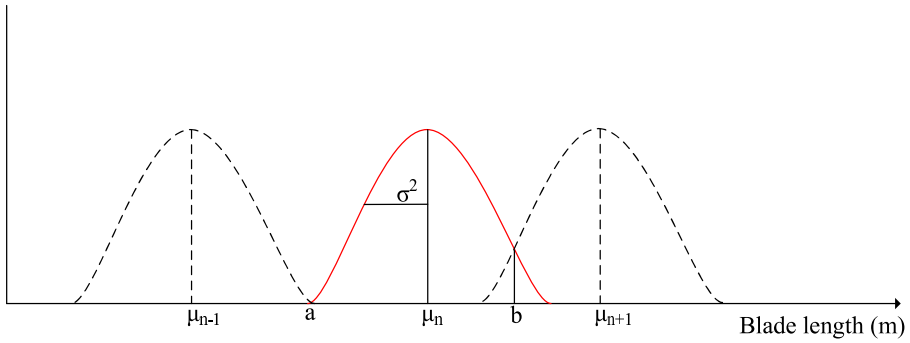

Figure 2.10: Representation of the method used to calculate the Gaussian error distribution of the blade lengths for the various helicopters in the database. The mean value, μ_n, gives the ground truth blade length for each data sample, and the variance, σ^2, indicates the blade length estimation error.

specific helicopter should therefore not be the only parameter that is used to distinguish helicopters from one another. It is also quite difficult to obtain this parameter since it is not a widely published feature, especially for the Russian manufactured helicopters. The rotation rates of only approximately 50% of the helicopters from the database could be found. To be able to show all the helicopters, even those with unknown rotation rates, a minimum value of 100 RPM was given to all the unknown entries. Figure 2.12 gives the main rotor rotation rates in RPM for the different classes in the database, where a class is again defined as the number of main rotor blades.

The same Gaussian error analysis that was performed on the blade lengths was performed on the rotation rates for the helicopters with known rotation rates. This analysis gives the probability of correct identification within a class, as well as over the complete data set of known rotation rates, when only this feature is taken into consideration. Figure 2.13 summarises the results from this analysis.

Figure 2.13 shows that, for the helicopters in the database with known rotation rate, the probability of correct identification given a rotation rate estimation error of 10 RPM is less than 50%. However, for some of the helicopter classes this probability is higher, given the same estimation error. For the class of five main rotor blades the probability is 72%, and for helicopter with two main rotor blades the probability of correct identification is 53%. The figure does, however, show that for the helicopters with three and four main rotor blades the probability of correct identification falls significantly for estimation errors of more than 3 RPM. To have an estimation error between 3 and 10 RPM is realistic, though since the main rotor of the helicopter is designed to have a varying rotation rate.

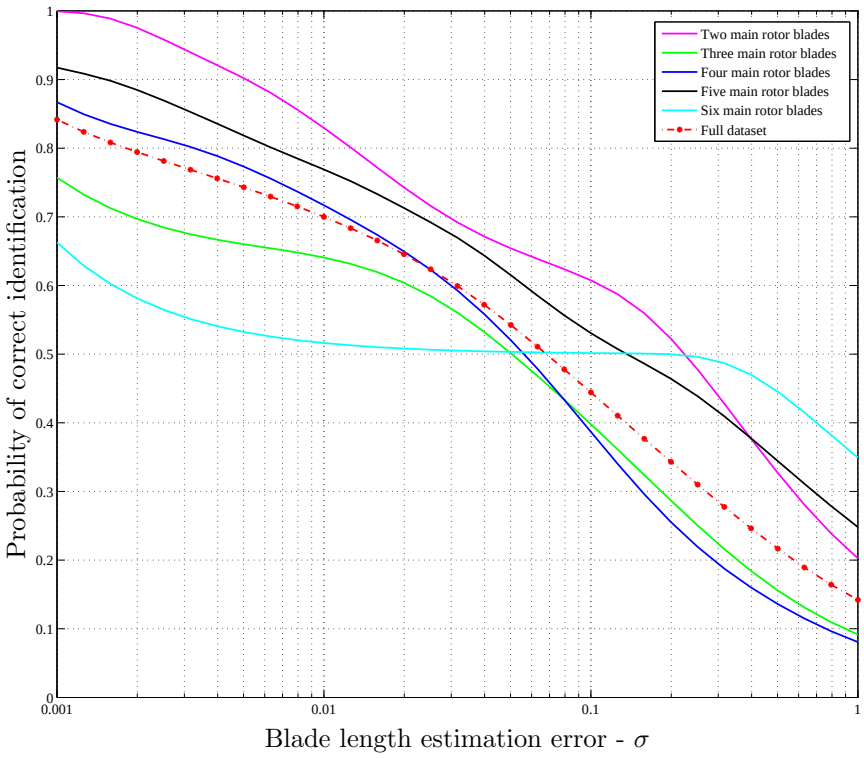

Figure 2.11: Probability of correct identification vs the blade length estimation error (σ) for the various classes in the database. The dotted red line shows the probability of correct identification over the complete set of samples in the database.

To have an even better understanding of the distribution of the helicopters in the different classes, Figure 2.14 gives the rotation rate of the helicopters' main rotor against the blade length. As expected the rotation rate decreases as the length of the blades increase. The legend on the graph shows the different colours that are used to represent the different classes. All the data points at 100 RPM indicate the helicopters with unknown rotation rates.

Other parameters, such as the number of tail rotors and the gear ratio of the helicopter, can also be used to distinguish further between helicopters of the same class. The analysis above shows that by using the number of blades, blade length and rotation rate of the main rotor as features, the data set from which an identification needs to be made is reduced significantly. A technique that estimates these three features would therefore be a very good start in the process of correctly identifying helicopter targets by make and model.

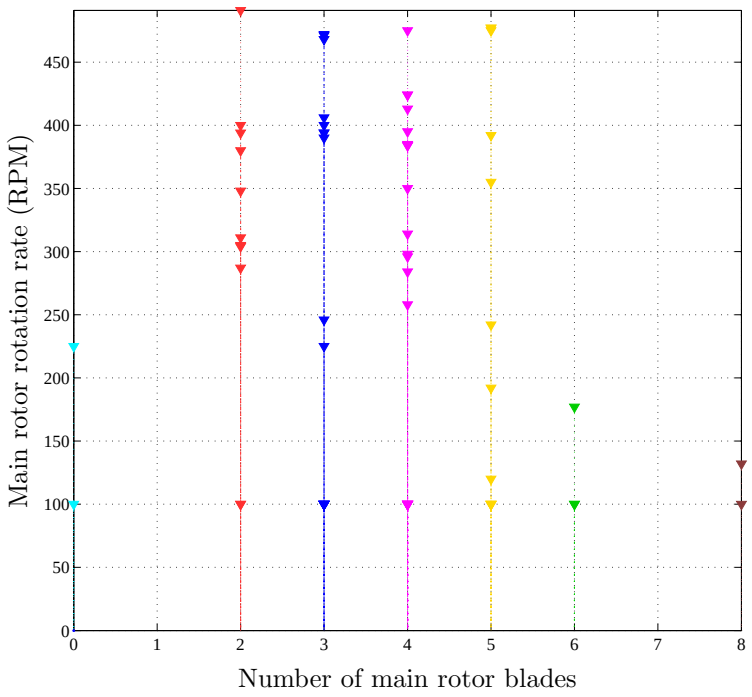

Figure 2.12: Main rotor rotation rates, r_ω, in RPM vs the number of main rotor blades (N) of helicopters with known and unknown rotation rates. For the helicopters with unknown rotation rates a minimum value of 100 RPM was chosen.

2.3 Summary

In this chapter the background theory to blade modulation is discussed by giving the equation from the paper by Martin and Mulgrew [6], which describes the theoretical micro-Doppler return signal and target parameters that influence this return signal. The analysis of this equation indicated that three important parameters of the rotating structure of the target influence the return signal. These parameters are the number of main rotor blades (N), the blade length (L) and the rotation rate or angular velocity of the main rotor (ω_r).

A review of the literature addressing the problem of using the micro-Doppler effect for helicopter identification was presented in the second section of the chapter, where the contribution of the various methods was discussed, and a critical review of the work was given.

The survey showed that there are several methods that can be used, such as the L/N quotient method introduced by Rotander and von Sydow [11], which was improved on by

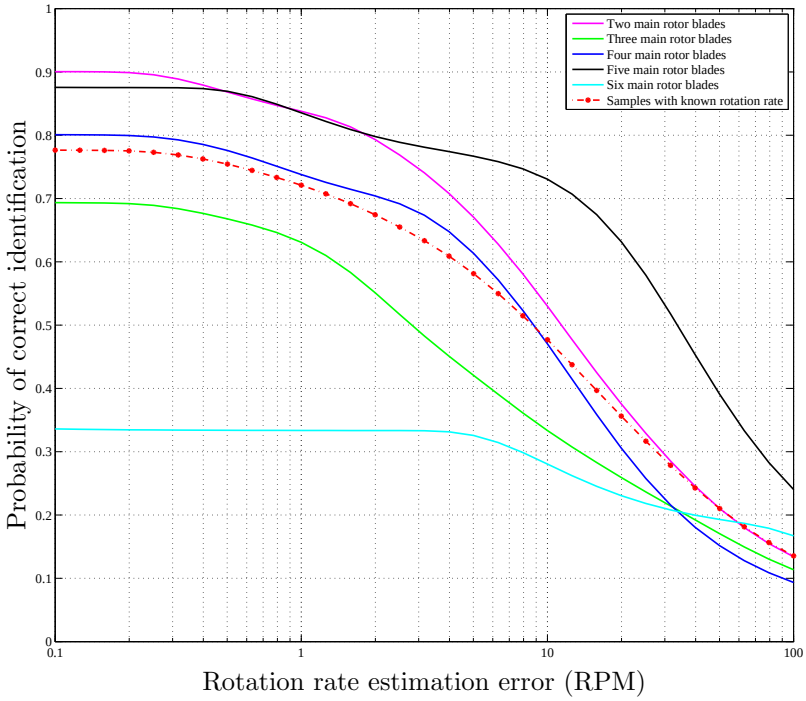

Figure 2.13: Probability of correct identification for helicopters with known rotation rate, given a certain rotation rate estimation error in RPM. The red dotted line on the graph shows the results for the complete dataset without prior knowledge of the class to which each data sample belongs.

Tikkinen [14]. The time-frequency analysis proposed by Yoon [5] shows that the number of blades and the rotation rate can be determined by only using the time-frequency domain data. Analysis of this method showed that the performance of this technique is greatly dependent on high signal to noise ratios (SNR).

A number of papers have been published on the return signal from the helicopter rotor hub. A very high Doppler resolution is required to obtain information from this structure though, and the papers proposing this method do not address all the problems of a real world scenario.

The final section of this chapter discussed the separability study that was performed on a dataset of 117 military and civilian helicopters. This study investigated the probability of correctly identifying a helicopter by make and model, if the number of main rotor blades and the blade length, or the number of blades and the rotation rate of the helicopter are known.

The use of the modulation due to the tail rotor return has not been addressed in either the literature survey or in the separability analysis. The effect of the tail rotor was left

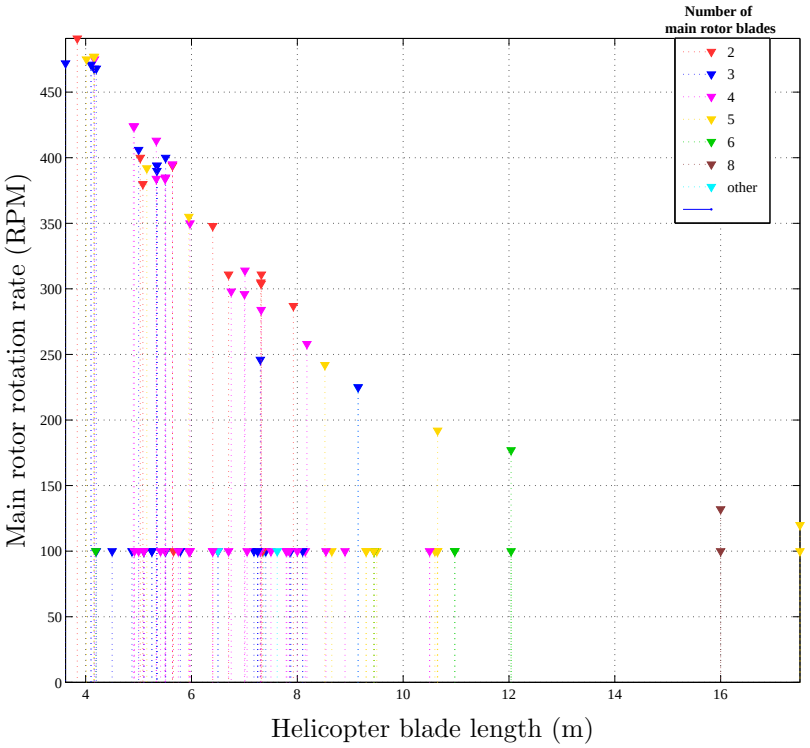

Figure 2.14: Blade length of each data sample against the main rotor rotation rate of the helicopter. The different colours on the graph indicate the various classes into which the helicopters have been sorted. The contour of the plot shows that, as the blade lengths increase, the rotation rate of the main rotor decreases, which can be derived intuitively.

out of the study for simplicity since other features are presented by tail rotor modulation such as rotation rate and the presence of a fenestron tail rotor (where the body of the helicopter shrouds the tail rotor for certain aspect angles). Future work should consider the addition of the tail rotor modulation for identification.

The following chapter gives the mathematical background behind blade modulation, which describes the mathematics of the blade flash and the Doppler effect, as an understanding of both these concepts is essential for the research on blade parameter extraction. The chapter also describes the simulation model that was developed and discusses the radar and target parameters used in the simulation, showing the results generated by the model.

The blade parameter extraction algorithm that is proposed in this work is described in detail and each of the important building blocks of the method is discussed. Some performance measures are also discussed, such as the gain in signal processing that is achieved by using this method. Measured data is shown for every function of the algo-

rithm. The chapter concludes with the proposed method, showing that theoretically and in simulation this technique seems to provide a feasible solution to part of the problem of helicopter identification for purposes of radar target identification.

Chapter 3

Mathematical analysis and Simulation model

Chapter 2 concluded with a separability analysis of the helicopters from the developed database. The results from this analysis showed that the probability of correctly identifying a certain helicopter will improve significantly when the number of main rotor blades, the length of these blades and the rotation rate of the main rotor are known and used as a feature set.

In this chapter a method is introduced to estimate these features from the return signal of a helicopter. The first section gives the mathematical analysis of blade flash detection and the Doppler effect. This is followed by a discussion of the point scatter model which was used to simulate the scatterers that are reflected from the rotating blades. The radar and target parameters that were chosen for the simulations as well as results from the simulation are shown, and the correlation between the mathematical analysis and the simulation results is presented.

The final section of the chapter gives a detailed description of the blade parameter estimation algorithm that was developed to extract the features as discussed in the separability analysis of Chapter 2. The various functions in the algorithm are discussed in detail, and the chapter ends by showing that, theoretically, it would be possible to estimate the number of blades, blade length and main rotor rotation rate of a helicopter. This hypothesis has also been confirmed by the results generated by the simulation model.

3.1 Blade flash detection

A simplified mathematical model of a rotor blade is used to illustrate the basic theory of helicopter blade detection. A very simple representation of the main rotor from Tait [1] is shown in Figure 3.1 to explain the mathematics of the blade flash resulting from the main rotor blade of the helicopter.

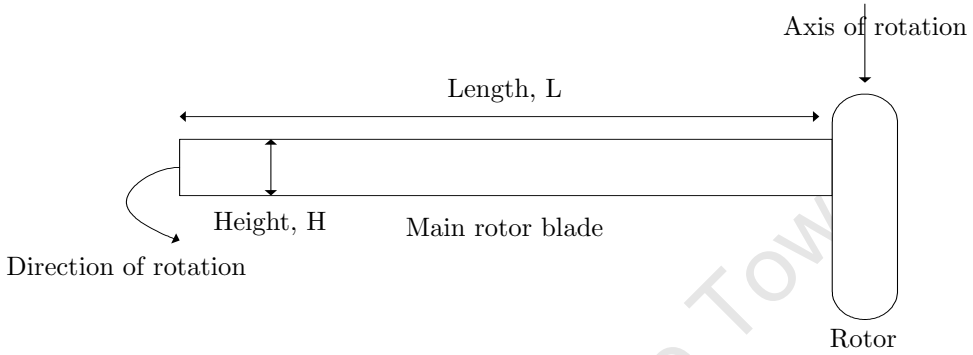

Figure 3.1: A simplified model of a helicopter rotor blade taken from Tait [1].

In Figure 3.1 the main rotor is represented as a rectangular plate with length L, and with height H. The first step is to determine the radar cross section (RCS) of the blade. The simplified model of the blade can be described as a flat plate and therefore the RCS of the blade can be determined by using the RCS of a flat plate. The RCS indicates the ability of a target to reflect the incident EM wave in the direction of the radar receiver. The RCS of a specific target is dependent on three factors, which are shown in Equation 3.1 and taken from Tait [1].

$$\sigma_{RCS} = (Projected\,cross\,section)(Reflectivity)(Directivity) \tag{3.1}$$

The projected cross section (geometric cross section of the target) is the projection of the target presented to the radar. Tait [1] further states that the target reflectivity is the ratio that indicates the energy of the incident EM wave that is reflected and not absorbed, and finally the target directivity is a measurement of the power that is scattered back in the direction of the radar since not all the reflected energy is in the direction of the radar antenna. The directivity is dimensionless and is a ratio of the backscattered power to the energy reflected by a point target. The RCS of a flat plate is given by Tait [1] as

$$\begin{aligned} \sigma_{RCS} &= 4\pi L^2 H^2/\lambda^2 \left(\frac{\sin\left((2\pi/\lambda)L\sin\theta\right)}{(2\pi/\lambda)L\sin\theta} \right)^2 \cos^2\theta \\ &= 4\pi L^2 H^2/\lambda^2 (\mathrm{sinc}((2\pi/\lambda)L\sin\theta))^2 \cos^2\theta \end{aligned} \tag{3.2}$$

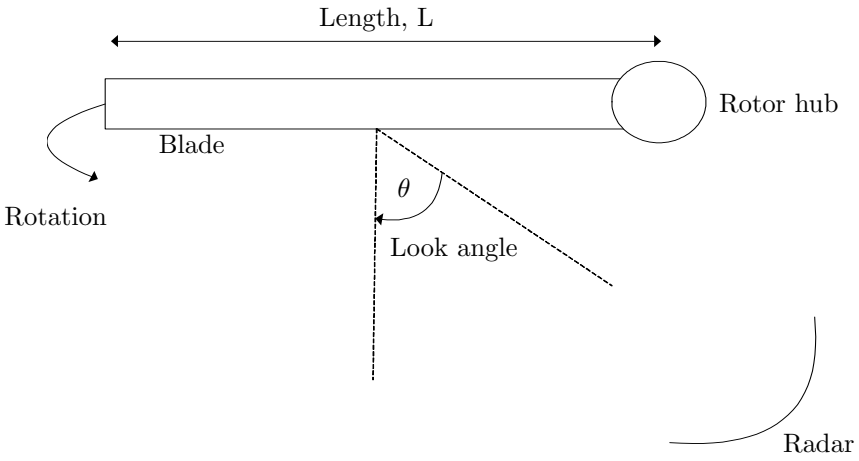

Figure 3.2: A model to determine the RCS of a rotor blade where the peak signal occurs when the blade is at a look angle of 0 degrees with respect to the radar.

where λ is the wavelength of the transmitted signal and θ is the incident angle from the radar to the target. Several assumptions were made for the model. Firstly, it is assumed that the radar is in the same plane as the vector, which is perpendicular to the plate or rotor blade, shown in Figure 3.2 as the dotted line. It was also assumed that the radar and the rotating blade were in the same plane.

The $\operatorname{sinc} x$ and $\cos^2 x$ terms in the model above represent the RCS in the horizontal plane, where the first term is due to the diffraction pattern that can be associated with an antenna aperture that is uniformly illuminated, and the second term is the projection of the aperture in the direction of θ. From these equations it can be deduced that for small look angles the RCS of a blade is large, and as the look angles increase, the RCS of the blade decreases.

The top graph in Figure 3.3 shows the RCS of a blade by implementing Equation 3.2. Here the angle θ is 0 degrees when the blade is perpendicular to the radar. The parameters used to generate this figure were taken from the database, and they use the helicopter with the shortest blade length, the Robinson R22, where L is 3.85 m, and a blade width of 0.10 m was used for the leading edge of the blade. The RF frequency, f_c is 8.5 GHz.

The edge of a helicopter blade is not flat however, and therefore it is believed that an improved model of the blade can be used to create a more accurate model of the RCS of a single helicopter blade. This was done by using a half cylindrical form for the blade since the leading edge of the blade is curved. Figure 3.4 shows a photo of a blade tip where the cylindrical form of the leading edge of the blade can be seen.

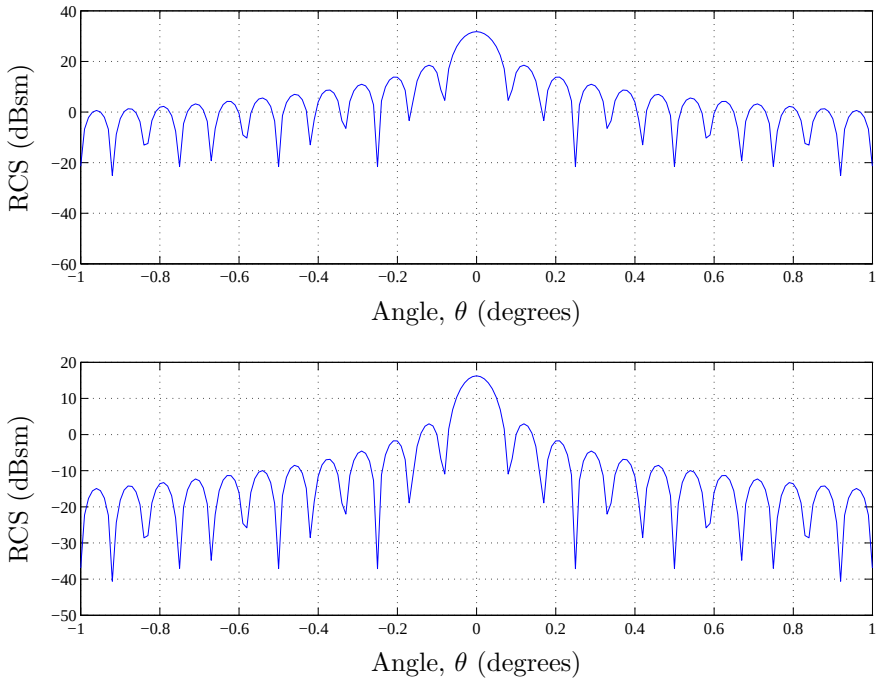

Figure 3.3: Theoretical RCS of a single blade with blade length, 3.85 m modelled as a) a flat plate and b) a half cylinder for a look angle ranging from −1 to 1 degrees.

To obtain a more accurate measure for the RCS of the blade, a different scaling factor was used by taking the maximum RCS equation for a circular cylinder as described by Tait [1]. The scaling factor, Sc, is given by Equation 3.3 as

$$Sc = \frac{2HL^2}{\lambda} \tag{3.3}$$

where H is the width of the leading edge of the blade, L is the blade length in metres and λ is the wavelength of the transmitted frequency, also in metres. The bottom graph in Figure 3.3 gives the RCS of the blade when modelled as a half cylinder. As expected, the RCS for the second model is smaller than that of the flat plate (approximately 13dBs smaller), since the curved area, from which the EM signal is reflected back to the radar is smaller.

The peak in RCS that occurs at 0 degrees can be clearly seen and the first side lobes occurs at approximately 0.08 degrees, 13 dBs smaller than the peak value at 0 degrees, which is the expected sidelobe level for a flat plate. The received signal has a peak in the RCS when the antenna is perpendicular to the blade, and the energy of the return reduces for approaching and receding blades by the $\operatorname{sinc} x$ function. Therefore a high

Figure 3.4: Tip of a helicopter blade. Due to this geometry of the blade, a half cylindrical form can been seen as a better approximation than a flat plate to determine the RCS of the blade.

peak can be expected for each blade flash when the look angle is 0 degrees, and for all the other angles low energy levels can be expected.

To show how the RCS of a blade changes when using a different blade length, the maximum blade length in the database was used to create the graph in Figure 3.5. The helicopter is the Mi-6 with a blade length of 17.5 m.

The blade flashes of helicopters with even parity will occur almost simultaneously since both the approaching and receding blades will be perpendicular to the radar at the same time instant. The frequency of the approaching blade will be at positive Doppler, and the opposite will be true for the receding blade, as stated by Rotander and Von Sydow [11]. For rotors with an odd blade parity, the approaching and receding flashes will not occur at the same time, since only one blade will be perpendicular to the antenna at a specific time.

3.2 Blade tip scattering

The rotating tip of a helicopter blade produces the maximum velocity, v_{max}, of the helicopter blade, (Yoon [5]), which also implies that the maximum Doppler frequency from the return signal is due to the blade tip scatterers. The return signal from these tip scatterers can therefore be used to extract information regarding the blade. The parameters that can be derived by using the scattering from the blade tips are discussed in more

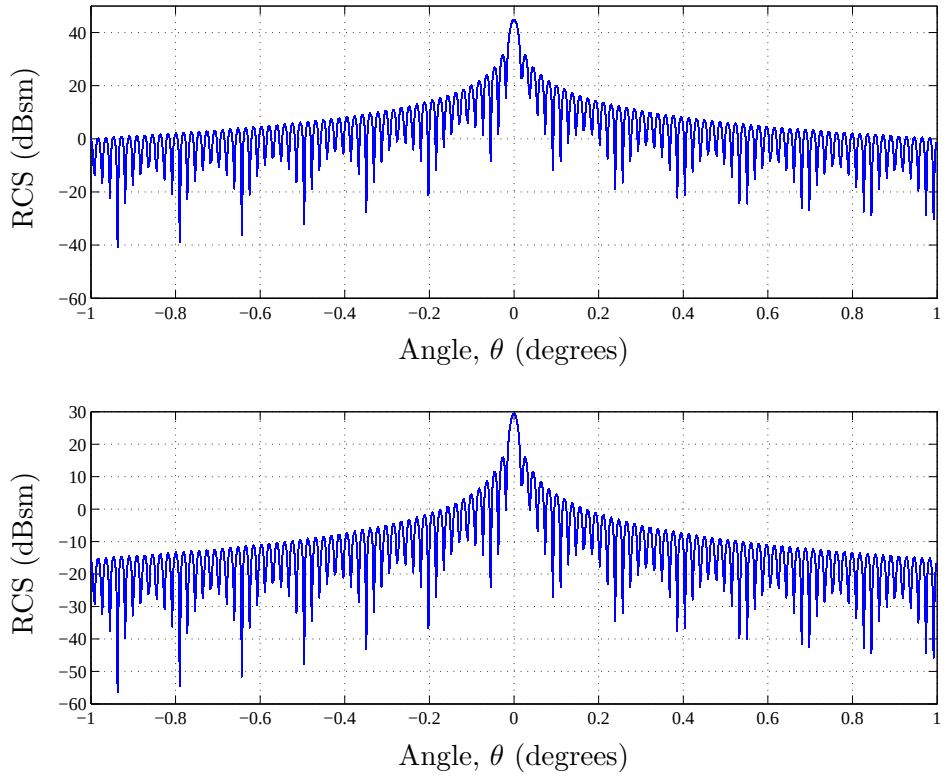

Figure 3.5: Theoretical RCS of a single blade with blade length, 17.5 m modelled as a) a flat plate and b) a half cylinder for a look angle ranging from −1 to 1 degrees.

detail later in the chapter. To gain a better understanding of the blade tip scattering, the range from the radar to the rotating main rotor blade tip is derived next. It is assumed that the main rotor blade is in the horizontal plane and that the helicopter is stationary. Figure 3.6 gives the scenario for deriving the range from the radar to the blade tip.

Equation 3.4 taken from Chen *et al.* [3] shows the range from the radar to the tip of the blade for the simple case where the elevation angle is zero as a function of time.

$$R(t) = \sqrt{R_0^2 + L^2 + 2R_0 L\cos\theta(t)} \tag{3.4}$$

R_0 is the range from the radar to the target (body of the helicopter), L is the blade length, where $L << R_0$ and θ is the time varying angle from the radar to the blade tip. The simplified form of Equation 3.4 is shown in Equation 3.9. To derive Equation 3.9 from Equation 3.4 first principles were used, since the derivation was not found in the literature. The derivation starts with the following equation

$$R(t) = R_0(1 + L^2/R_0^2 - 2L/R_0\cos\theta(t))^{1/2} \tag{3.5}$$

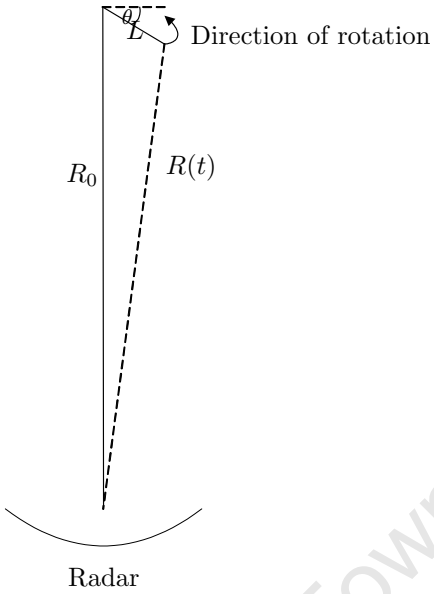

Figure 3.6: Geometry of a single main rotor blade of the helicopter with respect to the radar. The range from the radar to the target is indicated by R_0, and the time varying range to the blade tip is shown by $R(t)$, for the blade with length, L.

where $L^2/R_0^2 \approx 0$, which can be written as

$$R(t) = R_0(1 + 2k\cos\theta(t))^{1/2} \tag{3.6}$$

with $k = L/R_0$. Since $k^2 \approx 0$, the following term can be added under the square root.

$$R(t) = R_0(1 + 2k\cos\theta(t) + k^2\cos^2\theta(t))^{1/2} \tag{3.7}$$

By factorizing the term under the square root Equation 3.7 can be written as

$$\begin{aligned} R(t) &= R_0((1 + k\cos\theta(t))^2)^{1/2} \\ &= R_0(1 + k\cos\theta(t)) \\ &= R_0 + R_0 k\cos\theta(t) \end{aligned} \tag{3.8}$$

Finally by substituting k, the range from the radar to the tip of the blade can be expressed as (Chen [3])

$$R(t) = R_0 + L\cos\theta(t) \tag{3.9}$$

The range as a function of time from the radar to the tip of the main rotor blades can thus be seen as a constant with a sinusoidal component, due to the rotation of the blades.

The blade tip velocity as a function of time can be determined by taking the derivative of Equation 3.9. The time varying velocity of the blade tip can therefore be written as

$$\begin{aligned} \frac{dR}{dt} &= -L\sin\theta(t)\frac{d\theta(t)}{dt} \\ v(t) &= -L\omega\sin\theta(t) \end{aligned} \tag{3.10}$$

where ω_r is the rotation rate of the main rotor in rad/s. The blade tip velocity becomes a very important parameter, since this can be related to the length of the blade, which is one of the key features needed for identification. The relationship between the blade length and the blade tip velocity is

$$L = \frac{v_{tip}}{\omega_r} \tag{3.11}$$

The Doppler frequency at the tip of the blade as a function of time, which will also be the maximum Doppler frequency of the blade, can be used to estimate the tip velocity by using the expression

$$\begin{aligned} f_d(t) &= \frac{2v(t)_{tip}}{\lambda} \\ &= -\frac{2L\omega_r}{\lambda}sin\theta(t) \end{aligned} \tag{3.12}$$

where λ is the wavelength of the transmitted signal. Equation 3.12 shows that the Doppler frequency at the blade tip is also a function of time, therefore a time-frequency representation of the received scatterers would be a good method to investigate the estimation of the blade parameters. The angular rate of the main rotor is the other parameter that is required to determine the blade length L. The angular velocity of the main rotor is directly related to the rotation rate, r_ω (in RPM), by using Equation 3.13

$$r_\omega = \frac{60}{2\pi}\omega_r \tag{3.13}$$

The above equations give the mathematical analysis that is required for estimating the various parameters that form part of the feature set to identify a helicopter. It was also shown that, due to the rotating movement of the blades, the Doppler frequency and range toward the blade tip are time dependent and that a time-frequency analysis of helicopter data would provide useful insight into the problem.

3.3 Radar and target parameters

The radar and target parameters that were used in the simulation model closely resemble the parameters that one would expect in real world scenarios.

3.3.1 Radar parameters

The radar parameters chosen for the simulation were based on two of the CSIR's radar research facilities at the Pretoria campus of the CSIR. The two systems, Fynmeet and MECORT, are both coherent pulsed radars, where MECORT operates in the X-band and Fynmeet in both C- and X-band. Both medium and high PRF waveforms can be used for the two radars. Table 3.1 summarises some of the important radar parameters that were used to ensure that the simulation model closely resembled the properties of a real world measurement setup.

Table 3.1: Radar parameters used in the simulation model taken from the Fynmeet and MECORT systems. To ensure that realistic results were obtained from the simulation these parameters were used.

Parameter	**Parameter definition**	**Typical value**
c	Speed of light	2.988×10^8
f_c	Carrier frequency	$6.6 - 10$ GHz
λ	Wavelength of carrier frequency	$3.3 - 4.5$ cm
PRF	Sampling rate of the radar	$20 - 35$ kHz
θ_{aspect}	Aspect angle of the target	various

By using these parameters a realistic understanding could be formed of how well the technique would work in a real world scenario. There are some parameters that the model does not take into account though, such as the polarization of the radar antenna. The number of bursts and the pulses per burst are also parameters that can be controlled.

3.3.2 Target parameters

The helicopter parameters used for the model were also chosen to closely resemble those of an actual helicopter. Table 3.2 gives the boundaries that were chosen for the different

parameters used in the simulation. The variables used for the different parameters will be used throughout the chapter when discussing the simulation model.

Table 3.2: Helicopter rotor parameters used as input to the simulation model. These parameters are taken from the developed database to ensure that the simulation results of the micro-Doppler effect, caused by the rotor blades, are realistic.

Parameter	**Definition**	**Typical value**	
		Main rotor	Tail rotor
N	Number of rotor blades	$2-8$	$2-5$
L_{min}	Distance between hub centre and the blade	0.2 m	0.2 m
L_{max}	Blade length	$3.85-17.5$ m	$0.5-1$ m
r_ω	Rotation rate	$250-550$ RPM	$1250-2750$ RPM

The simulation model does not account for the Eurocopter helicopters with a fenestron tail rotor configuration. These tail rotors normally consist of between 8 and 13 blades, with a length of approximately 50 cm.

By using the parameters from Table 3.2 for the target the results from the simulation will be relevant and a better understanding of the problem can be achieved. There are, however, several factors that the simulation does not take into account, such as the pitch of the blades, and the fact that the rotation rate of the main rotor is not constant.

3.4 SNR estimates of blade flashes

According to Barton [18], the well-known radar range equation can be used to calculate the SNR of the return signal from a target, given certain radar parameters, the propagation path and the RCS of the target. The equation can therefore be used to determine the maximum range at which a target will be detected given certain radar parameters. This equation has been implemented to determine the relationship between the SNR and the range of the target from the radar for a blade flash. The outcome would therefore indicate the SNR for increasing range, and what the maximum distance is that a blade flash can still be observed in the data, given the radar parameters taken from the MECORT radar system. The radar range equation given by Barton [18] is expressed in Equation 3.4 which calculates the received signal power at the radar.

$$P_s = \frac{P_t G_t G_r \lambda^2 \sigma}{(4\pi)^3 R^4} \tag{3.14}$$

where P_s is the received signal power at the radar, P_t is the transmit power, G_t is the transmitting antenna gain and G_r indicates the receiving antenna gain. λ is the wavelength of the transmitted signal, and σ indicates the RCS of the target in m^2. The range from the radar to the target is R.

To determine the SNR of the received signal, the noise component in the received signal should also be calculated. Barton [18] states that there are two sources of noise: the first originates from within the radar, such as the wave guide, the duplexer noise and the receiver noise. The other source of noise comes from the environment, which includes factors such as solar or galactic noise, atmospheric noise and ground noise. The thermal noise power, generated by the radar receiver, is the effective input noise power and is defined by Skolnik [19] as

$$P_n = kT_sB_n \tag{3.15}$$

where k is Boltzmann's constant, 1.38×10^{-23} J/deg, T_s is the system input noise temperature in degrees, and B_n is the noise bandwidth of the receiver. For the detailed derivation of Equations and see Barton [18]. For the simulation all the relevant radar and target parameters were used in Equations 3.4 and 3.4 and the SNR of the received signal was calculated as

$$SNR = \frac{P_s}{P_n} \tag{3.16}$$

For the simulation the RCS of the blade based on the half-cylindrical form was used with a RCS of 71 m^2, and the range to the target was chosen from 2 - 70 km. The radar transmit frequency was 8.5 GHz. Due to confidentiality the other design parameters of the radar, such as the transmit power, antenna gain and noise figures, may not be disclosed.

Figure 3.7 shows the SNR over range for a blade flash, given specific radar parameters determined by using Equations 3.4 and 3.4.

This section showed that the detection of a blade flash, given the radar parameters of MECORT, is possible for ranges well beyond the visual range. The RCS of the blade is quite high, 71 m^2 for a 5 m blade, which is one of the reasons why a SNR of more than 20 dBs is achievable at a range of 70 km. The return from the blade tip scatterers however, are considerably smaller than that of the blade flash, and will be discussed again later

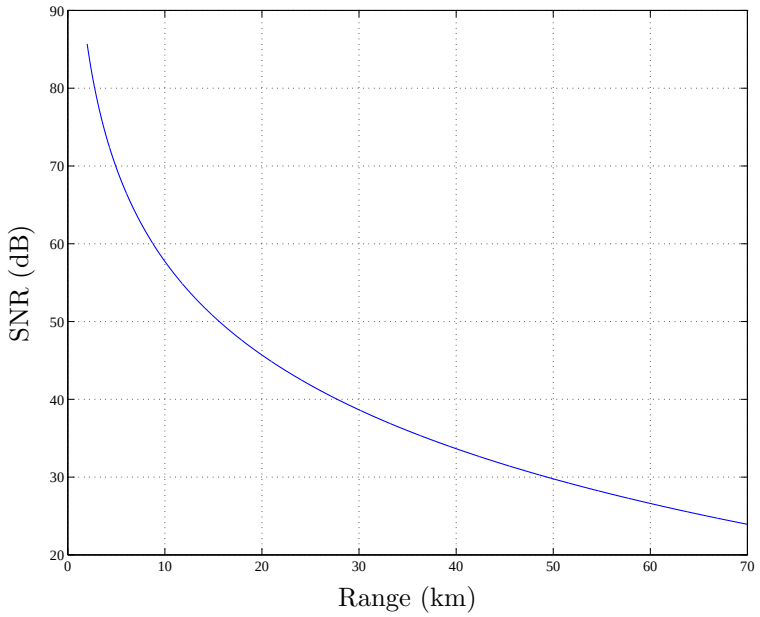

Figure 3.7: SNR of the received blade flash signal over increasing range. The blade has a length of 5 m and a RCS of 71 m^2, based on a half-cylindrical shape, with height 10 cm.

in this chapter. This analysis shows that it is possible to detect the blade flashes of a helicopter well beyond the visual range, for the given radar parameters.

3.5 Doppler effect

The proposed algorithm makes extensive use of the frequency domain for both processing and representing the data, which include the micro-Doppler component in the return signal. The Doppler effect is therefore a key concept in the development of the model, since the rotating rotor blades will cause both positive and negative Doppler sidebands around the Doppler frequency resulting from the helicopter body. It is well known that the Doppler effect occurs when the transmitted radar signal is reflected from a moving target at a range, R_0, from the radar, a radial velocity, v, and a certain aspect angle, θ. When the distance, R_0, between the antenna and the target decreases, the wavelength of the incident EM wave is in effect smaller, thus resulting in a higher frequency in the received signal compared to the transmitted signal. When the target is moving away from the radar, the exact opposite effect occurs. As the distance, R_0, between the target and the radar increases, the wavelength of the reflected signal also increases, thus resulting in a lower frequency since the wavelength is inversely proportional to the frequency ($\lambda = 1/f_c$).

The phase component of the transmitted and received signal is used to obtain the Doppler frequency of the target since the frequency, defined by Tait [1], is the rate of change of phase with time. The phase of the received signal will therefore differ from the start phase of the transmitted signal. A pulsed radar measures this phase difference from pulse to pulse and the Doppler frequency can be determined by taking the time derivative of the phase. Equation 3.17 from Tait [1] shows that when a radar transmits a sinusoidal waveform, with a carrier frequency f_c, the returned signal from a point scatterer, P, can be expressed as

$$\begin{aligned} s(t) &= \rho(x,y,z)\exp\left(j2\pi f\frac{2r(t)}{c}\right) \\ &= \rho(x,y,z)\exp\left(j\Phi[r(t)]\right) \end{aligned} \tag{3.17}$$

where $\rho(x,y,z)$ is the reflectivity function of the point scatterer, P is the local coordinates of the target, (x,y,z). c is the speed of the transmitted EM wave and $r(t)$ is the scalar, which represents both the distance and angle from the radar to the target. Tait [1] shows that the phase of the returned signal can be expressed as

$$\Phi[r(t)] = 2\pi f\frac{(2r(t))}{c} \tag{3.18}$$

The final step is to take the time derivative of the phase $\Phi[r(t)]$, which leads to the well known Doppler equation of

$$\begin{aligned} f_d &= \frac{2vf_c}{c} \\ &= \frac{2v}{\lambda} \end{aligned} \tag{3.19}$$

where v is the velocity of the target, and f_c is the transmitted frequency.

In a pulsed radar the Doppler frequency is also used to determine the maximum unambiguous velocity. The Doppler frequency can then be related to the pulse repetition frequency (PRF) of the radar, where f_d gives the maximum PRF required to avoid aliasing. Here, the PRF represents the sampling rate at which the radar samples the specific target.

3.6 Point scatterer model

A model was developed based on the mathematics of the previous section to simulate the micro-Doppler effects due to the HBM. A simple point scatterer method was used, similar

to the model proposed by Chen [3]. This model was designed to account for the two main characteristics of the micro-Doppler effect, namely the blade flashes (which occurs when the blade is perpendicular to the radar), and the sinusoidal returns resulting from the rotating blade tips.

The scatterers are placed at better than a $1/4\lambda$ to preserve the structure of the blade flash, and to prevent any grating lobes in the angular scattering pattern of the blades. The scattering from the tip of the main rotor blades is also included in the model, and the expected sinusoidal waveform can be seen in the time-frequency representation of the simulation data. The position of the scatterers, s, for both the main and tail rotor blades are determined by using the following equation

$$s = L_{min} : 1/4\lambda : L_{max} \tag{3.20}$$

where L_{min} and L_{max} were defined in Table 3.2. The return from the body of the helicopter is represented by a large amplitude scatterer located at the centre position. The simulation can also be performed by ignoring the fuselage return, especially when the question under investigation does not depend on the return from the body. The model uses the number of main rotor rotations, together with the main rotor rotation rate and the PRF of the waveform to calculate the number of pulses received from the target as shown in Equation 3.21.

$$N_{pulses} = \frac{PRF}{r_\omega/60} N_{rotations} \tag{3.21}$$

The resultant amplitude and phase of the blade returns are calculated by using the following equation

$$S_{ret} = \sum_{k=1}^{K} \alpha_k e^{-j2\pi R_k/\lambda} \tag{3.22}$$

where α is an assigned constant amplitude for every scatterer on the blade, and λ is the wavelength. R_k is a function of the minimum and maximum blade length (L_{min} and L_{max}), the spacing of the scatterers on the blade and lastly of the orientation of the main rotor blade relative to the radar at the time when the transmitted pulse interacts with the blade. In this model it is assumed that the blades are stationary at the measurement instant, after which the blades turn to a new position and the next measurement is taken. The blades therefore have a new position for every measurement. The total number of scatterers is given by K. Figure 3.8 shows a geometric representation of the point scatterer model where both the main and tail rotor blades can be seen.

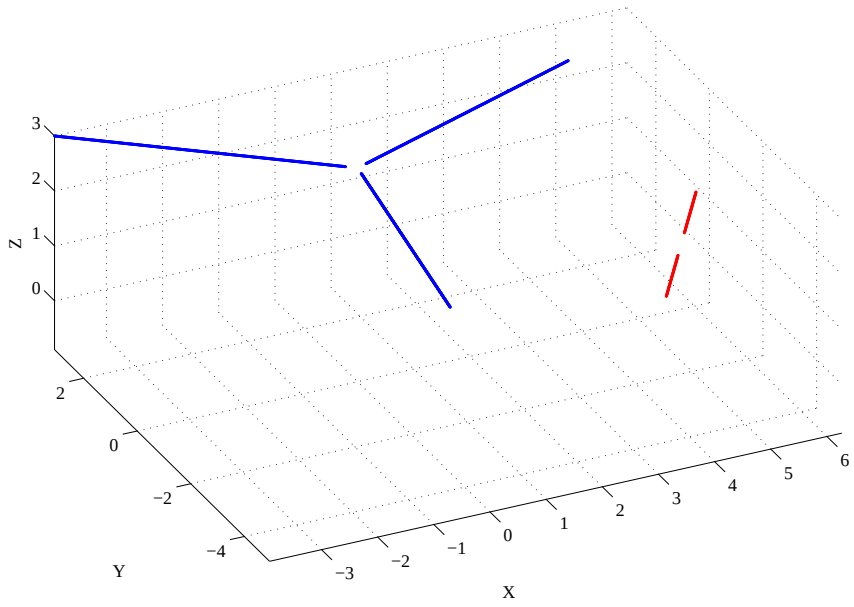

Figure 3.8: A geometric representation of the point scatterer model that generates the return signals from the rotating main and tail rotor blades of a helicopter. X, Y and Z are the reference coordinates of the model.

In the example shown in Figure 3.8 the main rotor has 3 blades with a tail rotor of 2 blades. This model was also extended to take the tail rotor into account where the same method was used to place the scatterers on the tail rotor. From the equations used in the model, the micro-Doppler effects are expected to be seen both in the time and time-frequency domain. In the time domain the blade flash returns are expected for both the main and tail rotor. Figure 3.9 shows the time domain data for one of the simulation results where the target was a two-bladed helicopter, the Robinson R22, with a blade length of 3.85 m and a rotation rate of 491 RPM. The transmitted frequency was 8.5 GHz, and a PRF of 35 kHz was used to avoid aliasing. Only the main rotor and the body of the helicopter were simulated in this case.

The blade flashes can be clearly seen from Figure 3.9. The time between flashes can also be determined, but unless the number of blades is known this measure would not aid in the estimation of the rotation rate of the rotor. The amplitude of the return signal in Figure 3.9 is in $dBscat$, since the amplitude of the signal is relative to a single scatterer with an amplitude of 1. One way to validate the point scatter model is to show the return of a single blade flash, which is shown in Figure 3.10. This can be compared to Figure 3.3, where the RCS of a single blade (with the same blade length) is shown, when approximated as a flat plate. The peak amplitude, of the two figures differ by almost 21

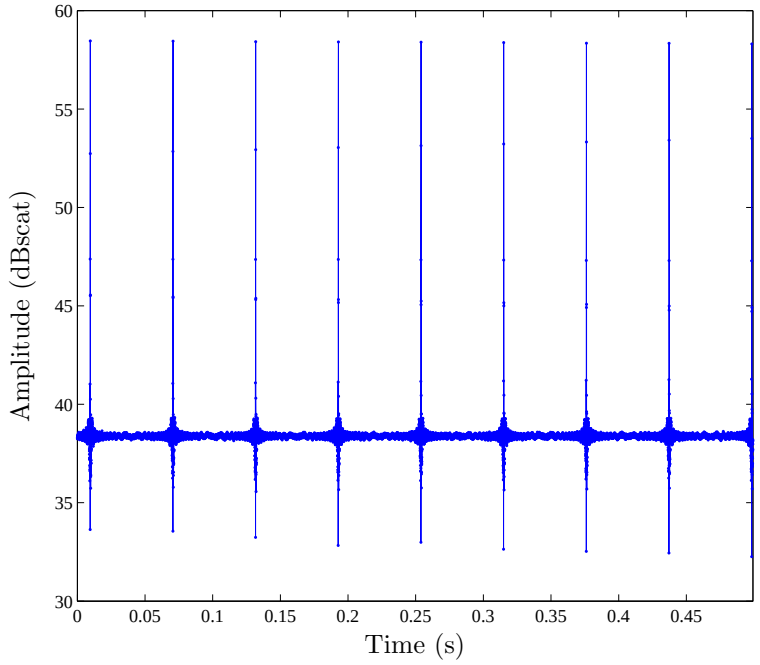

Figure 3.9: Time domain data of the return signal from a target with a blade length of 3.85 m, and rotation rate of 491 RPM.

dBs. This can be attributed to the fact that the point scatterer model does not convert the return signal to absolute RCS, and the return therefore needs to be multiplied by a conversion factor if the two peak amplitudes are to be compared. The two figures show that the sidelobes of the point scatterer model are 13 dBs less than the peak amplitude, which can be confirmed by the theoretical result shown in Figure 3.3.

3.6.1 Doppler-time response

To perform the time-frequency analysis a spectrogram of the return signal, S_{ret}, is obtained by using a M-point Blackman windowed STFT. Figure 3.11 gives the time-frequency domain representation of the simulated data shown in Figure 3.9, where M was chosen as 64 samples, with no overlap between adjacent FFTs.

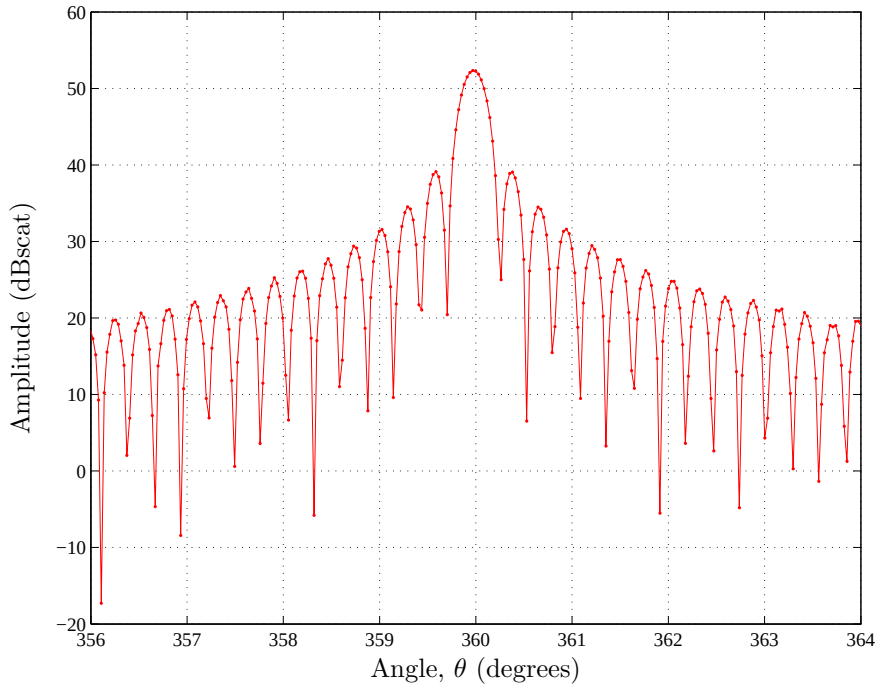

Figure 3.10: A single blade flash return generated by the point scatterer model, for a target with a blade length of 3.85 m. As with the RCS of a flat plate, the levels of the first sidelobes are 13 dBs less than the peak amplitude.

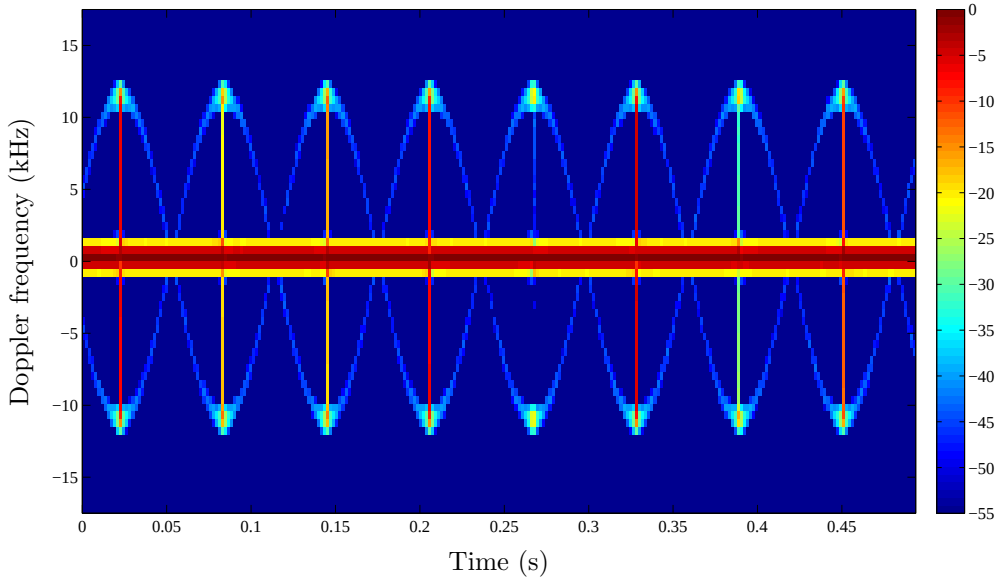

Figure 3.11: Doppler spectrum of the simulated return signals from the body and main rotor blades of a helicopter with blade length 3.85 m and an even number of blades. A PRF of 35 kHz was used to generate this data with the transmit frequency at 8.5 GHz.

From Figure 3.11 the approach of using a point scatterer model seems to be valid since the results from the simulated data can be confirmed by the mathematics. When a main rotor blade is perpendicular to the radar line of sight, a blade flash occurs that contains Doppler content dependent on L_{min}, L_{max} and the angular rate, ω, of the main rotor as well as the transmitted signal wavelength. By analysing the relative position (in time) of the approaching and receding blade flashes, the parity of N (odd or even) can be determined. The scattering from the helicopter blade tips can also be seen in Figure 3.11 from the sinusoidal Doppler pattern, due to the rotating helicopter blades. Note also that the return signal from the blade tips is significantly weaker than that of the body of the helicopter and of the blade flashes. From the simulated data the amplitude of the approaching and receding blade tips are equal. Analysis of measured data, however, showed that this is not true for all helicopters, since the approaching blade tip scatterers are stronger than the receding tip scatterers for some helicopters, and vice versa.

To illustrate the effect that the tail rotor has on both the time and time-frequency domain data, a simulation was performed with the helicopter and radar parameters shown in Table 3.3.

Table 3.3: Radar and target parameters used in the point scatterer simulation. The tail rotor parameters are included since the effect of the return from the tail rotor was investigated.

Parameter	**Value**
Main rotor: N	3
Main rotor: L	5.35 m
Main rotor: r_ω	365 RPM
Tail rotor: N	2
Tail rotor: L	1.86
Tail rotor: r_ω	2086 RPM
PRF	30 kHz
Range: R_0	5 km
f_c	8.5 GHz
Aspect angle	0 degrees

The helicopter parameters used for this simulation were taken from the database and represent the AS 550 Fennec, which is a military helicopter manufactured by Aerospatiale/Eurocopter. The aspect angle from the radar antenna to the nose of the helicopter was chosen at 0 degrees, since the Doppler frequency resulting from the tail rotor is a maximum at this angle. The tail rotor flashes would therefore be clearly visible. At 90

degrees aspect angle the tail rotor flashes will produce no Doppler since the radial velocity of the blades is 0 m/s with respect to the radar. Figure 3.12 shows the time domain data for this simulation, where both tail and main rotor flashes are visible.

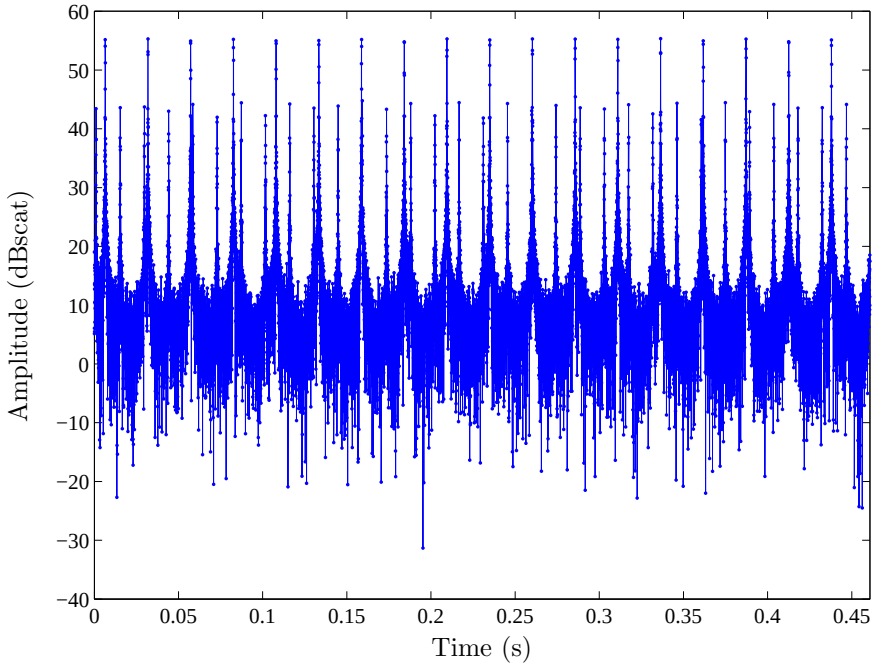

Figure 3.12: Simulated time domain data of the return signal from both the main and tail rotor blade. The main rotor blade length is 5.35 m, and the tail rotor blade length is 1.86 m. The transmit frequency is 8.5 GHz, with a PRF of 30 kHz. Both the tail and main rotor blade flashes are visible in the time domain data.

Even though the returns from the tail rotor are at a maximum due to the aspect angle, the amplitude of the main rotor blade flashes is still in the order of 10 dBs greater than that of the tail rotor, assuming that the main rotor blades are in the horizontal plane with 0 degree pitch or roll. This is confirmed by using both the flat plate and half cylindrical model, which were used to calculate the RCS of the helicopter blade to calculate the RCS of the tail rotor. Figure 3.13 shows the Doppler spectrum corresponding to this simulation, where the flashes due to the tail rotor are clearly visible. Note also that since this helicopter has an odd number of main rotors, the approaching and receding flashes do not occur at the same time.

The rotation rate of the tail rotor is approximately 5 times higher than that of the main rotor, which accounts for the tail rotor flashes that occur more frequently than the main rotor flashes.

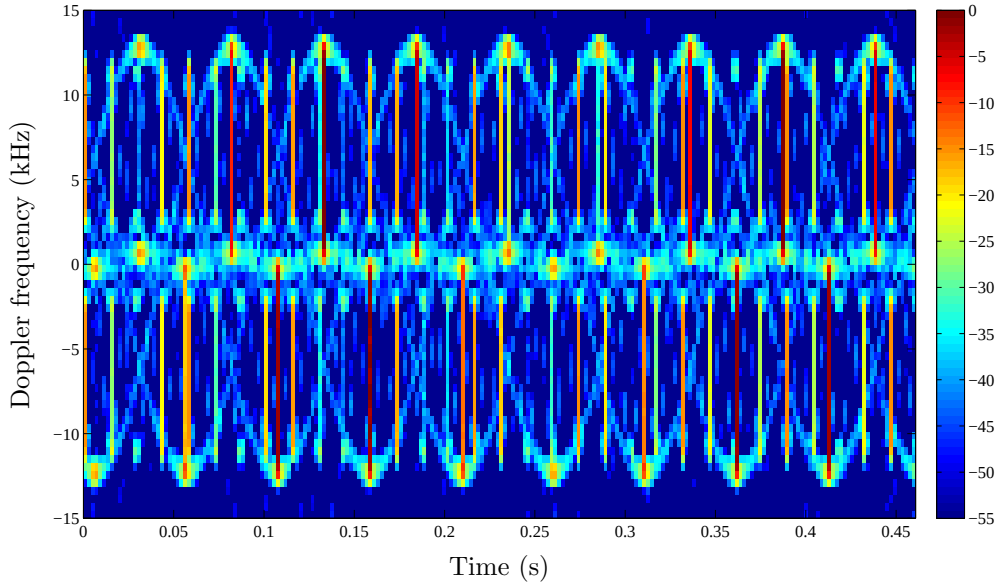

Figure 3.13: Doppler spectrum of the simulated return signal consisting of the main and tail rotor blade returns. The flashes from the tail rotor occur more frequent due to the higher rotation rate.

The gear ratio is the parameter that is used to describe this relationship between the main and tail rotor rotation rates provided that both the number of main and tail rotor blades are known.

The PRF of the transmitted waveform is a very important parameter when investigating the micro-Doppler effects due to helicopter blade modulation, especially when using the time-frequency data to aid in the estimation of the blade parameters. A high PRF is needed to avoid aliasing of the blade flashes and of the sinusoids at the blade tips. The minimum PRF required to ensure unambiguous velocity measurements is equal to the Doppler frequency at the tip of the blade. This can be calculated using Equation 3.19. Figure 3.14 shows the spectrogram for a simulation where the PRF is equal to the maximum Doppler frequency at the blade tip.

Therefore any PRF lower than this value will result in aliasing of the blade flashes in the time-frequency domain. In Figure 3.15 a PRF of 10% less than the minimum required PRF, in this case 24.7 kHz, was used, to simulate the return signal from the main rotor blades. Both the blade flashes and the sinusoids around the blade flash are folded over to the opposite Doppler frequency. High PRF waveforms are therefore very important when measuring helicopters, if the data is to be processed by using the time-frequency domain data.

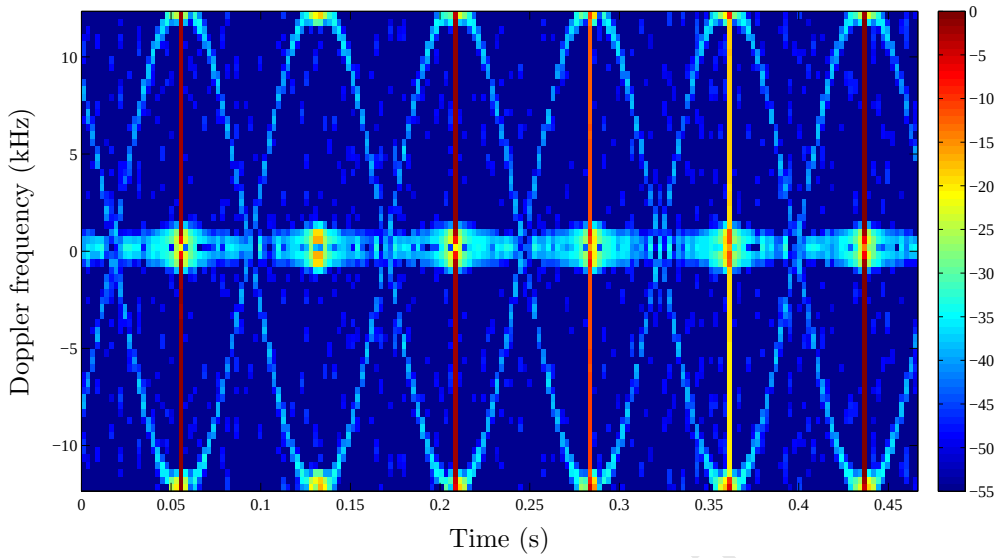

Figure 3.14: Doppler spectrum of the main rotor blades return signal simulated with a waveform where the minimum required PRF was used to avoid aliasing. This value is equal to the maximum Doppler frequency at the blade tip.

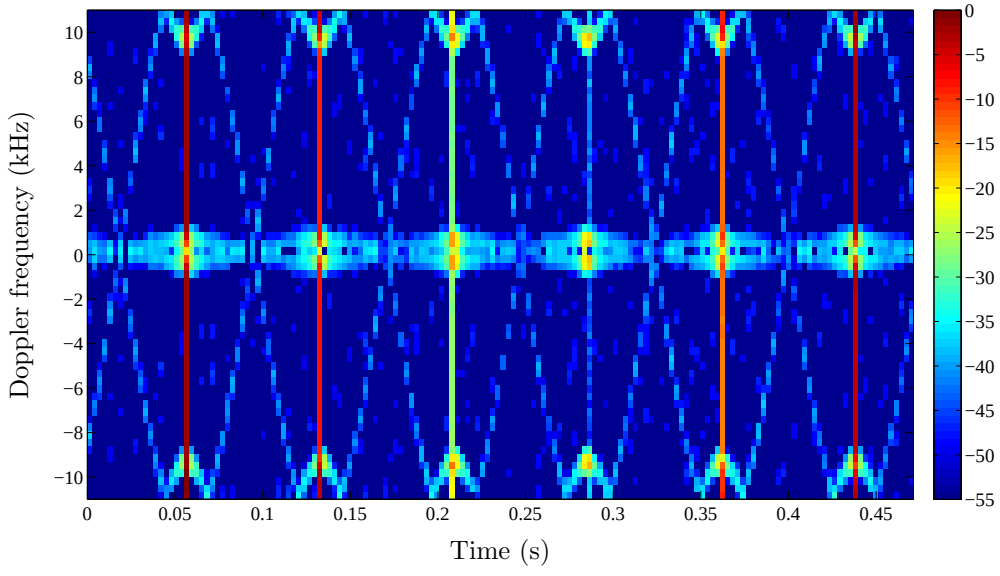

Figure 3.15: Doppler spectrum of the return signal from simulated main rotor data when using a waveform that has a PRF lower than the maximum Doppler frequency at the blade tip, which causes aliasing of the blade flash and the blade tip scatterers. This value, f_d is 24.7 kHz for this case, with a PRF of 10% lower than the required value.

3.7 Blade parameter estimation algorithm

In the previous section the model that was used to simulate return signals from the rotor blades of a helicopter was discussed, and by comparing the results from this model with the mathematics of the theoretical return from a rotating object, the point scatterer model proved to be a good representation of the return signal. This model was therefore used to provide simulated data with which the design of a blade parameter estimation algorithm could be developed. This section describes the proposed new algorithm and gives a detailed discussion of each of the key processing steps in the algorithm. For most of the steps the same process is used for both generated and measured data. However, some of the steps are only performed on the recorded helicopter data such as the velocity compensation for the body of the helicopter. Although the helicopter trial and the results from the trial are only discussed in the following chapter, the algorithm is discussed in this section. Some results from the trial measurements will be shown in this section to illustrate the functionality of certain steps in the algorithm.

The objective of this algorithm is to estimate the three key helicopter parameters that have been identified in the separability study. These three parameters are the:

- Number of main rotor blades (N)
- Main rotor blade length (L)
- Main rotor rotation rate (r_ω)

Figure 3.16 gives a block diagram of the key processing steps of the algorithm. Each of these steps will now be discussed in detail.

3.7.1 Doppler data

Most of the analysis of the data takes place in the time-frequency domain, where both the blade flashes and the sinusoids from the blade tips can be seen. The first step in the algorithm is therefore to convert the data to the time-frequency domain. Figure 3.11 shows an example of the simulated time-frequency data. A time-frequency plot for measured helicopter data, recorded by the MECORT radar facility, is shown in Figure 3.17.

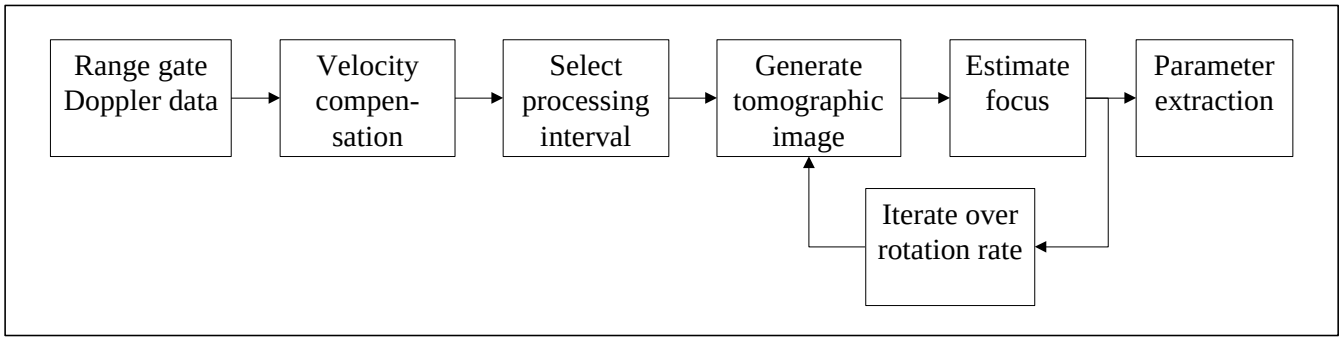

Figure 3.16: Block diagram showing the key processing steps of the helicopter blade parameter extraction algorithm. This algorithm can be performed on both simulated and measured data, although the simulated data does not use all the functions shown in the diagram.

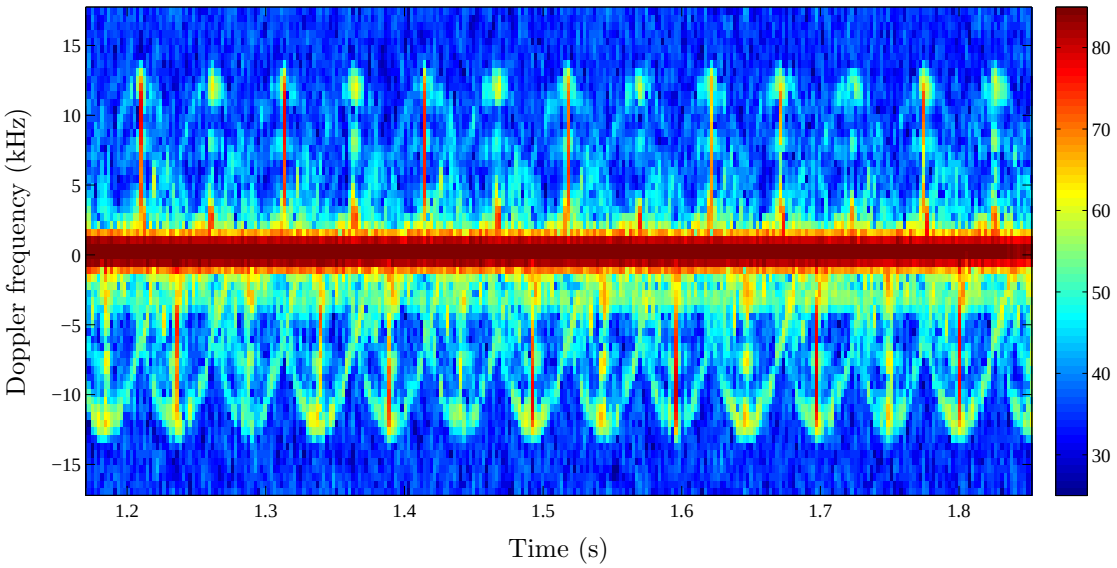

Figure 3.17: Doppler spectrum of measured helicopter data. Both the blade flash and the sinusoidal return from the blade tip can be observed in the data. The odd parity of the main rotor can be seen from the asymmetrical return of the approaching and receding blade flashes. The helicopter is an AS 350B, and was recorded with MECORT, with f_c equal to 8.5 GHz, and a PRF of 33 kHz.

In Figure 3.17 both the blade flashes and sinusoids resulting from the blade tip scattering can be seen. The PRF for this recording was 33 kHz, which is more than the maximum Doppler frequency at the tip of the blade. By looking at this figure this can be roughly determined as 28 kHz. By comparing Figure 3.17 and Figure 3.11 the point scatterer model can be validated, since the effects seen in the simulation results correspond to those of actual recorded data. The data was recorded with a pulsed-Doppler radar and with the correct setup, easily yields the time-frequency representation of the data, since this is directly measured by the radar. The Doppler is calculated as the Fourier transform of a burst of pulses (which in this case is 64), which relates to 64 Doppler bins, since the Doppler frequency is calculated from pulse to pulse.

Note that not all the blade flashes in Figure 3.11 have the same intensity in the returned energy, the reason being that the blade flash is not always sampled at the exact moment when it is perpendicular to the radar, which leads to lower energy levels in the return signal.

3.7.2 Doppler tracking and velocity compensation

To extract the helicopter blade parameters from the returned signal of a helicopter, the main focus falls on the Doppler return resulting from the blade tips. To estimate this accurately, the reference frequency (Doppler frequency resulting from the velocity of the fuselage) needs to be constant. A very important step therefore is to shift the Doppler return from the helicopter body to zero Doppler, which is termed velocity compensation. Figure 3.18 shows recorded data where the velocity of the fuselage causes the mean Doppler return to drift over time.

The first step in the process to compensate for the velocity of the helicopter is to implement a centroid tracking filter for the fuselage return. The Doppler tracking filter was only implemented over certain Doppler bins, which relate to the region in which the return from the helicopter body can be expected. From the database the maximum velocity over the complete dataset is 280 km/h. This was converted to Doppler frequency, given the transmitting frequency, f_c and then to Doppler bins to obtain the defined region of the tracking filter. From this velocity value it was determined that Doppler bins $22:42$ would be used for the Doppler tracking filter (given a waveform with 64 pulses), and the centroid was calculated for this area, where bin 32 represents zero Doppler. This defined region relates to a positive and negative Doppler frequency of 4.83 kHz.

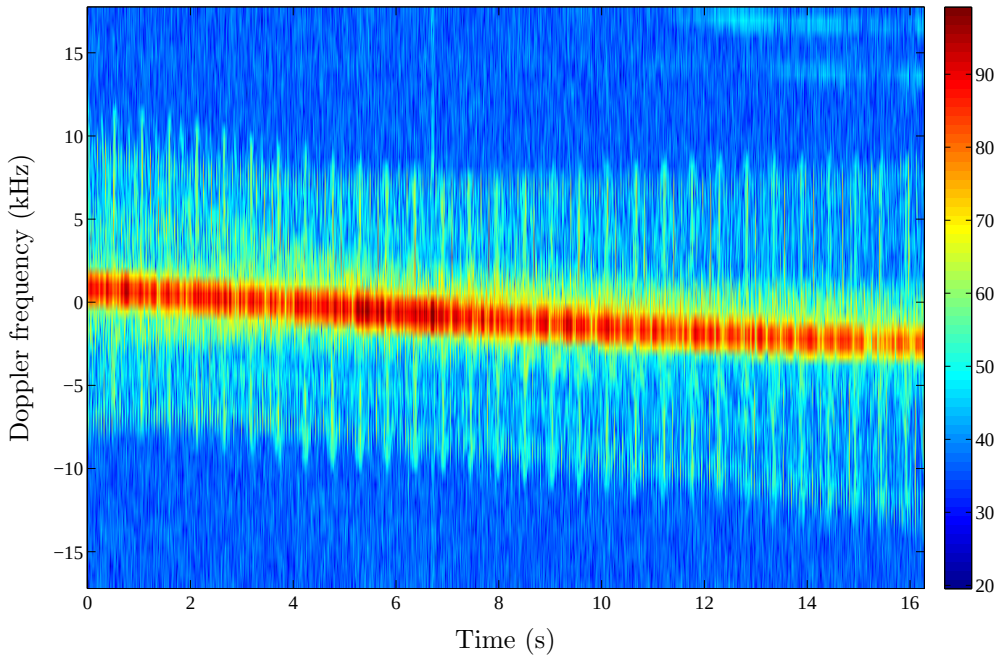

Figure 3.18: Doppler spectrum of recorded helicopter data before velocity compensation is performed to shift the velocity resulting from the fuselage to zero Doppler, to determine accurately the Doppler frequency at the blade tips.

A lowpass filter was used to remove all the high frequency components of the centroid. A fifth order Butterworth filter with a normalized cut-off frequency of 0.01 rad/s was implemented. The filter was given time to reach a steady state before it was used as an estimate of the centroid. Figure 3.19 shows the same measured data as in Figure 3.18, including both the trace of the calculated centroid (in magenta) and the trace of the centroid filter (in black).

The final step for the velocity compensation is to determine a phase correction factor, which is determined for each spectral estimate. An IFFT of the data is taken and the data is multiplied by this phase correction factor. This process is concluded by taking the FFT of this corrected data. Figure 3.20 shows the recorded data after the Doppler frequency of the fuselage has been shifted to zero Doppler.

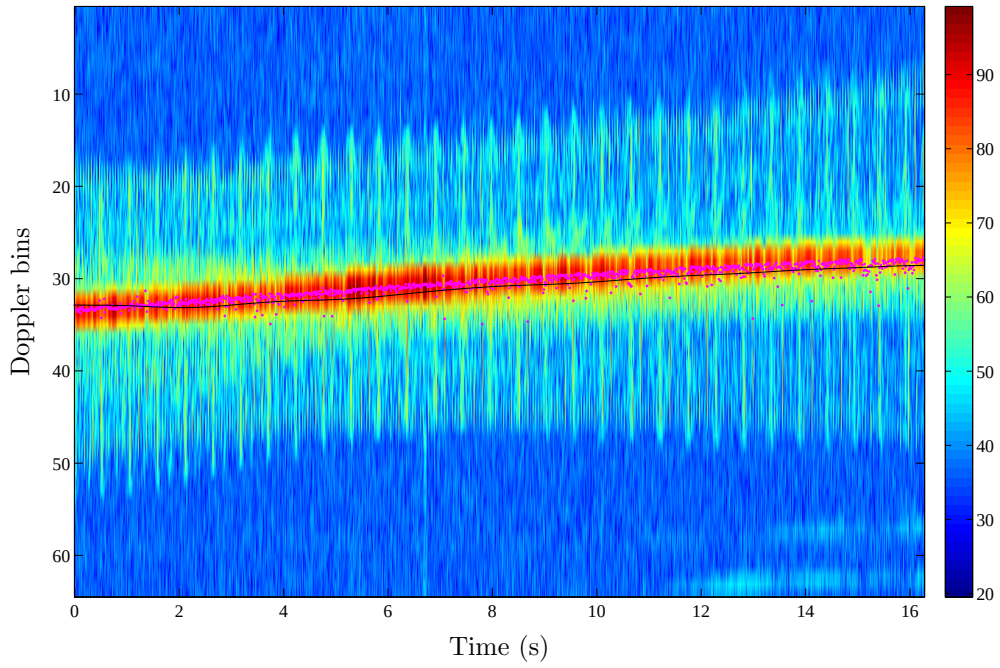

Figure 3.19: Doppler spectrum of measured helicopter data showing the centroid trace in magenta used for the Doppler tracking filter. The output of the lowpass centroid filter is indicated by the black line. The output of this filter is used to shift the velocity of the fuselage return to zero Doppler.

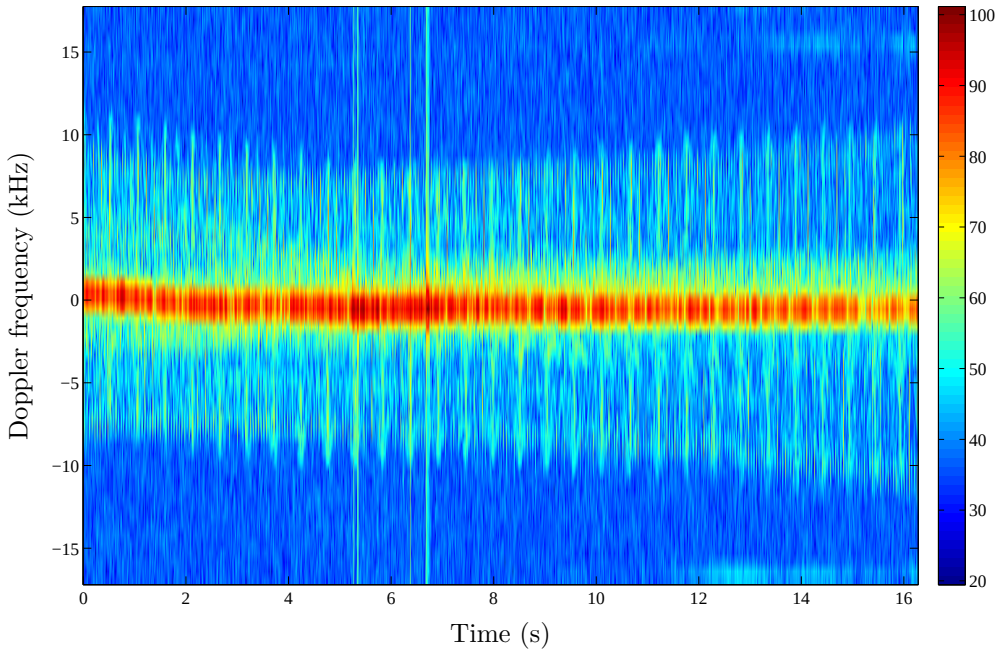

Figure 3.20: Doppler spectrum of measured helicopter data after velocity compensation has been performed. The return from the fuselage is now centred around zero Doppler, and the Doppler frequency of the blade tips can be determined from the zero Doppler reference.

3.7.3 Selection of processing interval

Once the body of the helicopter has been shifted to zero Doppler, the processing interval which will serve as the input to the tomographic imaging process has to be selected. The selection of this interval can either be performed automatically or the user can determine the section of data to be analysed by hand. It was found empirically that a processing interval of approximately 400 ms is required, firstly to ensure that at least one full rotation of the rotor was completed and secondly to ensure that the input data is coherent and that the rotation rate of the main rotor is constant during the processing interval. Figure 3.21 shows an example of measured data, after the user has specified the processing interval.

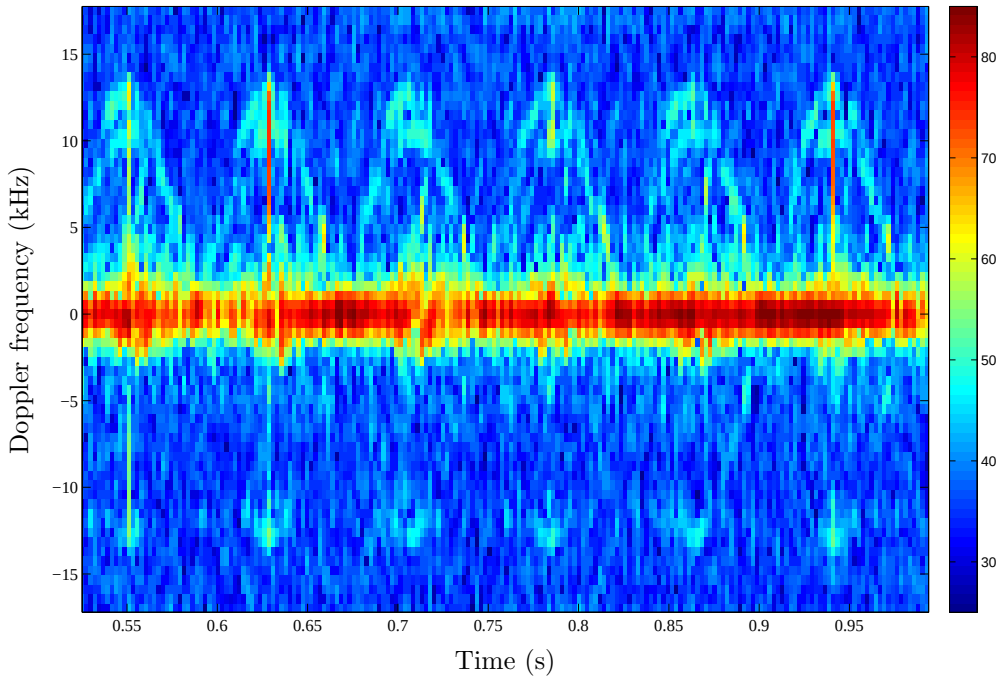

Figure 3.21: Doppler spectrum of measured helicopter data (two main rotor blades) after the processing interval has been selected. The data represents approximately 400 ms, which serves as the input to the tomographic imaging process. Note that the sinusoids and blade flashes for the approaching blade (positive Doppler) are more pronounced.

Figure 3.21 shows that the blade flashes and sinusoidal returns from the blade tips are more pronounced for the approaching blade (positive Doppler frequency) than the receding blade (negative Doppler frequency). The energy reflected from the leading edge of the blade is therefore more than that of the trailing edge of the blade, as expected and predicted in the paper by Pouliguen *et al.* [8]. The next step is to estimate the sinusoids in the data using a tomographic imaging technique. The velocity compensated data se-

lected in the processing interval is used as input to this technique, which is discussed in the next section.

3.7.4 Tomographic Imaging

The field of tomography is widely used for several different applications such as radio astronomy, seismology and medical imaging according to Chen *et al.* [20]. Chen states that an object can be reconstructed from the planar integrals of the data [20]. The Radon Transform (RT) is a technique that can be used to calculate a set of 1-D projections from a 2-D function, $f(x, y)$, and can be expressed as

$$P(\alpha, r) = \int\int f(x, y)\delta(x\cos\alpha + y\sin\alpha - r)dxdy \tag{3.23}$$

Figure 3.22 gives the scenario for which this equation holds true.

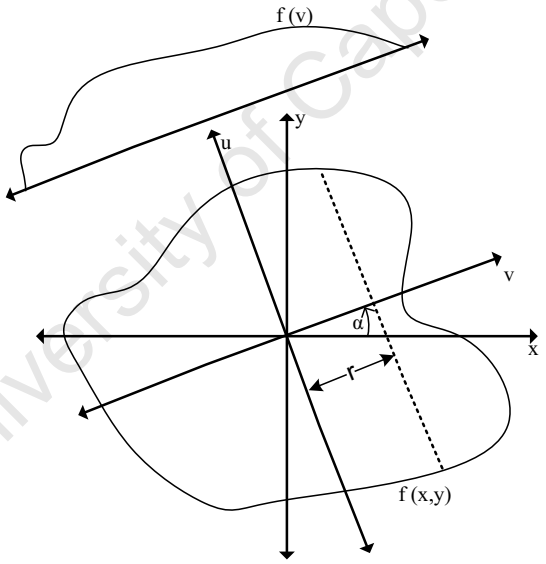

Figure 3.22: Geometry of a 2-D object, $f(x, y)$, and its 1-D projections, $f(v)$, that are used to define the Radon transform. α is the angle at which the projection is made, and r indicates the distance from the origin at which the line integral is taken to calculate the 1-D projection.

In this figure α is the angle of the line v. The projection is made on this line, and the r indicates the distance from the origin at which the line integral for a specific point of the projection is carried out. The complete set of 1-projections of the function $f(x, y)$ is the function $P(\alpha, r)$

The inverse function of the Radon transform can be used when a 2-D function has a set of projections at various angles, and it is required to reconstruct the 2-D function from the set of 1-D projections. Qureshi *et al.* [13] state that one of the methods used to perform this reconstruction of a 2-D image from its 1-D projections is the Fourier slice theorem. This theorem states that the 1-D Fourier transform of the projections of a function onto a line v at a specific angle α is equal to a slice of the 2-D Fourier transform of the function $f(x, y)$ at the same angle. This method defined by Equation 3.24 is known as the Inverse Radon Transform (IRT) and can be used to reconstruct the function $f(x, y)$ when a set of 1-D projections at various angles is given.

$$f(x,y) = \int_{-\infty}^{\infty}\int_{-\infty}^{\infty} P_\alpha(t) e^{j2\pi(ux+vy)} du dv \tag{3.24}$$

The 2-D Fourier transform of the function is first constructed from the projections and their known projection angles, and then an inverse 2-D Fourier transform is used to calculate the original 2-D function.

The sinusoids seen in the time-frequency helicopter data resulting from the scattering at the blade tips can be interpreted as a set of 1-D projections. This statement is made by using Equation 3.12, which shows that the Doppler frequency at the tip of the blade is a projection of the cross-range coordinate of the blade tip, with a scaling factor of $2\omega_r/\lambda$. A set of these projections is seen by looking at the Doppler spectrum of the data.

A focused 2-D image of the main rotor blade tips can therefore be formed by using the IRT, given that the angle of projection for each profile is known. Assuming that ω_r is constant, the angle of each projection can be estimated as a linear function vs time with unknown slope.

A linear search method is used to estimate the correct angular rate by using the IRT image focus as the fitness criteria. Two methods can be used to determine the search boundaries. The first approach estimates the period or rotation rate from the sinusoids in the Doppler spectrum data, and the search is performed by searching above and below this estimated value of ω_r. The other method makes use of the information in the helicopter database. The search space is defined by using the minimum and maximum rotation rates of all the helicopters in the database, which range from 200 to 550 RPM.

A focused image of the blade tips will form at the rotation rate that corresponds to the period of the sinusoids in the time-frequency data. To obtain a better dynamic range the body of the helicopter has been masked for this search process. Figure 3.23 shows

an example of a focused image, taken from measured data. The graph on the left shows the image where the body of the helicopter has been masked, and the graph on the right shows the focused 2D image, where the body of the helicopter can be seen as the small red circle in the middle of the graph, at 0 Doppler frequency.

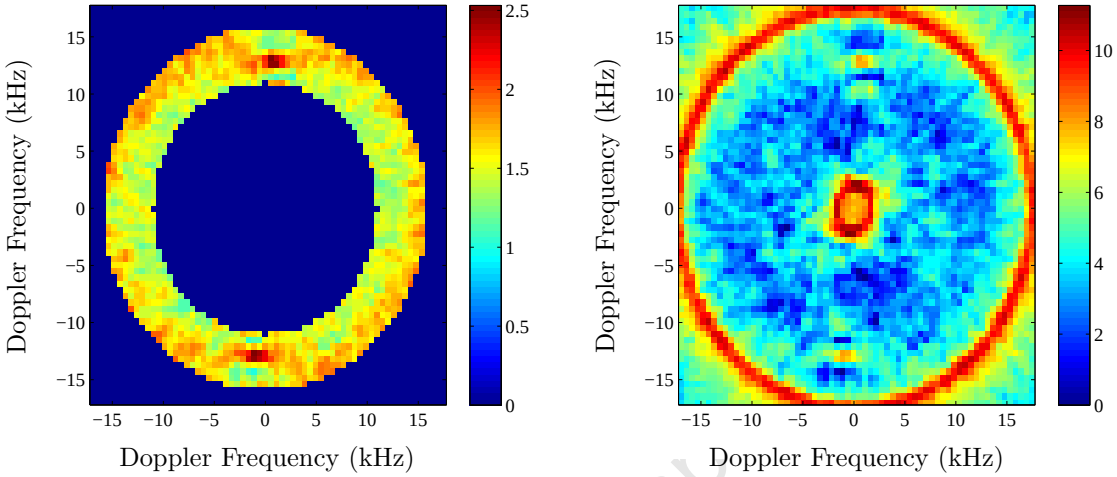

Figure 3.23: Focused 2-D image of the blade tips using the IRT, where in a) the body of the helicopter is masked and in b) it shows the complete focused image.

Figure 3.23 gives a Doppler-Doppler image of the two blade tips of the helicopter. From inspection the number of rotor blades can therefore be determined. From this focused image the main rotor blade parameters such as the number of blades, N, the blade length, L, and the rotation rate, r_ω, can be estimated automatically. This is discussed in Section 3.7.5 that follows.

3.7.5 Parameter extraction

The final step in the algorithm is to extract automatically the various main rotor blade parameters. This section describes the method that is used to estimate the various helicopter blade parameters used to identify a target.

Rotation rate

The first parameter that can be estimated is the rotation rate of the main rotor. This parameter is taken from the focused 2-D image formed by the IRT process, by using the angular velocity, ω_r at which the image focused. The rotation rate, r_ω can be derived

from the angular velocity by using Equation 3.25

$$r_\omega = \frac{60\omega_r}{2\pi} \tag{3.25}$$

Different statistical measures were used to estimated this value. The first approach makes use of the maximum value for each image that is formed. Whenever the blade tips focus, a peak in the maximum value can be observed. The rotation rate at the instance of the peak is then the estimated rotation rate of the main rotor. Another method is to use entropy to determine at what rotation rate the focused image occurs. By definition the entropy of an image would be a minimum if the reconstructed image is focused. The equation for the entropy that was used in the technique can be expressed by

$$H = \sum I_{norm}^2 \log I_{norm}^2 \tag{3.26}$$

where I_{norm} is the normalized vector of each image. Therefore by taking the minimum entropy value in the search space for all the images, the rotation rate can be estimated. Figure 3.24 shows the various values for both the maximum intensity and the entropy plotted against the rotation rate in RPM, as defined by the search space. Both these methods have been normalized to fit on the same axis.

In Figure 3.24 the peak in the maximum intensity occurs at approximately 185 RPM whereas the minimum entropy value is at 182 RPM. The reported rotation rate for the helicopter in the literature is 194 RPM. This shows that the estimator is accurate, and it is believed that the actual rate was closer to between 182 and 185 RPM as estimated, since the rotation rate of a helicopter is not exact as it changes for different loads, manoeuvres and wind conditions.

Number of main rotor blades

From the focused image formed by the IRT the number of main rotor blades can be determined, since it is an image of the blade tips. The manual process therefore involves simply counting the number of blade tips on the focused image through inspection. An automated process can be used to determine the number of blades by extracting samples on a circle that coincide with the maximum value in the image. This then is the intensity representing the circular path of the blade tips, and the number of peaks along this path that cross a certain threshold indicates the number of blade tips in the IRT image. A

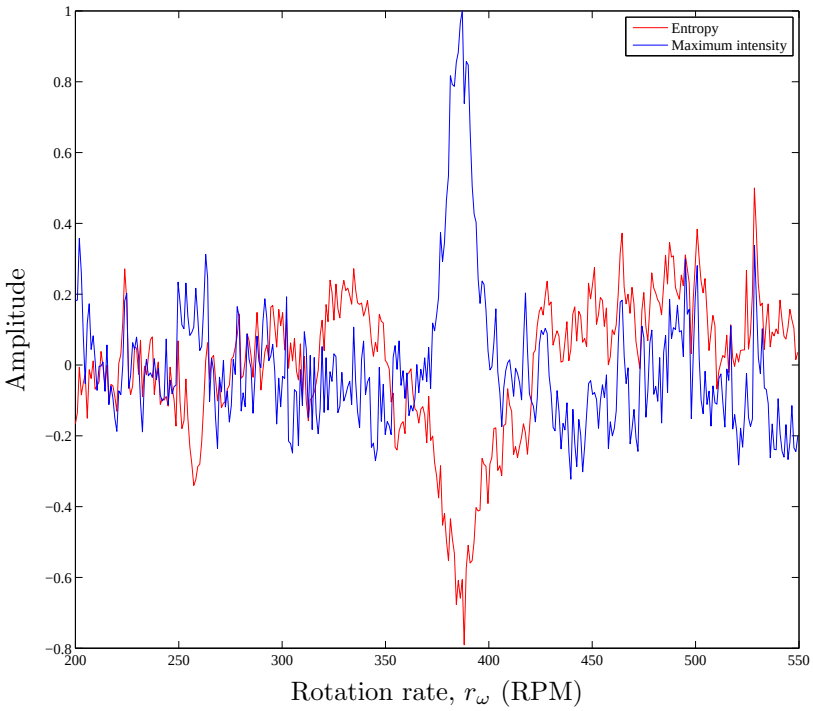

Figure 3.24: Two statistical measures, the normalized maximum intensity and entropy, used to determine the angular velocity at which a focused image occurs. The main rotor rotation rate in RPM can be estimated from this graph, when a peak occurs in the maximum intensity plot or a minimum entropy value occurs.

constant threshold was used to determine the number of blades in the focused image formed in the search space, where the threshold was determined by taking the sum of the standard deviation and the mean value of the data on the circular path where the maximum value occurred in the image. Figure 3.25 shows this method taken from the same data used for Figure 3.24.

Figure 3.25 shows that the threshold has been crossed twice, which indicates that the helicopter in question has two main rotor blades. Since the experiment was controlled and the specific target (Bell 206 LR) with its blade parameters (two main rotor blades) that correspond to the measured data is known, it can be verified that this method seems feasible.

Blade length

Finally, the blade length can also be determined from the focused image of the blade tips at the estimated rotation rate. The first step is to determine the maximum Doppler

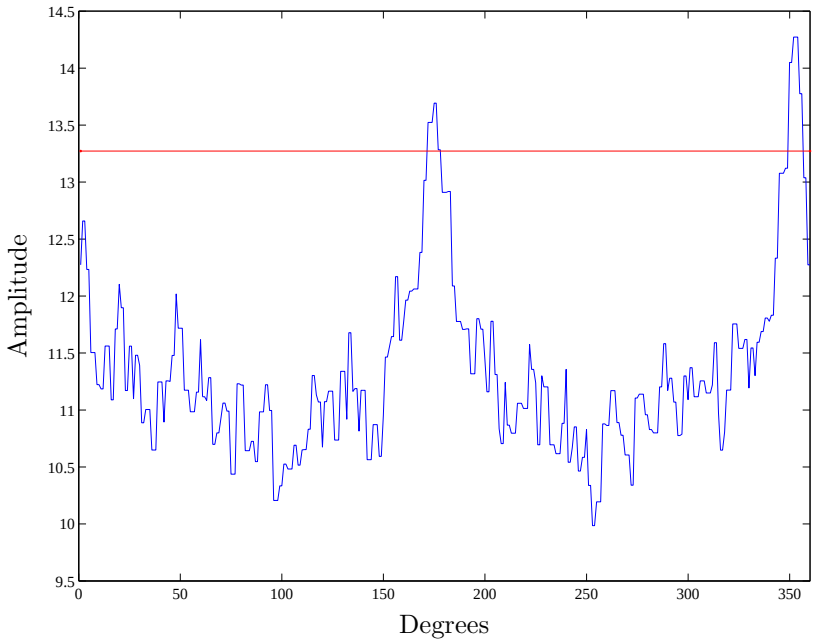

Figure 3.25: Estimation of the number of main rotor blades by taking the number of peaks that cross the threshold. The position of the peaks on the x-axis, corresponds to the phase of the focused blade tips in the focused image of the IRT process.

frequency at the tip of the blade. Since the 2-D image of the blade tips is a Doppler-Doppler image, the pixel with the highest intensity for anyone of the focused blade tips can be used to determine this maximum Doppler frequency at the blade tip. The maximum value is determined first, and then the euclidean distance from the centre of the image is used to determine at which Doppler bin the peak value occurred. To convert the Doppler bin to measured radar Doppler frequency Equation 3.27 is used.

$$f_{d_{est}} = f_{bin}\frac{PRF}{N_{pulses}} \tag{3.27}$$

where the N_{pulses} indicates the number of pulses per burst used in the waveform. The next step for the estimation of the blade length is to calculate the estimated blade tip velocity by using Equation 3.28.

$$v_{tip_{est}} = f_{d_{est}}\frac{\lambda}{2} \tag{3.28}$$

where λ is the wavelength of the transmitted radar signal. An error in the estimated tip velocity is made if the elevation angle of the target to the radar is not compensated for. Figure 3.26 gives the geometrical representation of the elevation angle of the target to the radar.

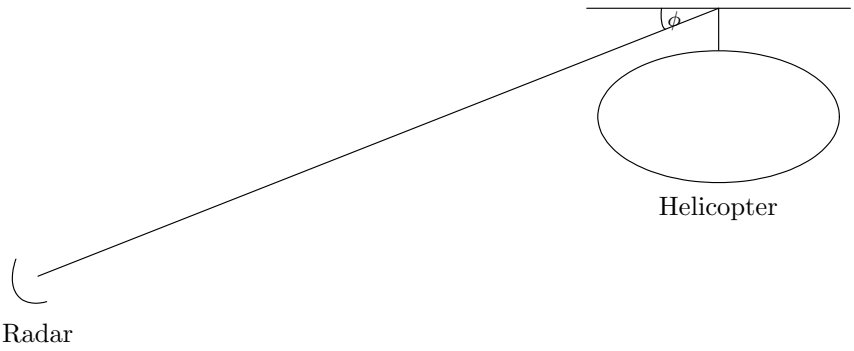

Figure 3.26: Geometric representation of the elevation angle between the radar and the helicopter.

To show how important it is to compensate for the elevation angle, a simulation was performed to investigate the tip velocity estimation error that is caused by the elevation angle (before compensation) of the radar toward the target. The simulation parameters were based on the Bell 206 Jet Ranger with a blade length of 5.08 m, a blade tip velocity of 202.15 m/s and a rotation rate of 380 RPM. The radar transmit frequency was chosen as 8.5 GHz. The simulation was performed for elevation angles ranging from 0 - 45 degrees. Angles of more than 45 degrees were not considered, since in a real world application this would not be realistic.

Figure 3.27 shows the estimated tip velocity as the elevation angle increases. The estimated tip velocity will always be biased to be lower than the actual tip velocity before the elevation angle is compensated for. This implies that for a number of estimated values for the same helicopter, the tip velocity estimate with the highest value would be the most accurate estimate. This of course does not take the SNR into account, since this factor can cause an estimate to be bigger than the actual tip velocity, and therefore be biased to have bigger values than that of the ground truth data. Figure 3.27 shows that, as the elevation angle increases, the estimated tip velocity decreases, which proves why it is necessary to compensate for the elevation angle, ϕ. Figure 3.28 shows the error in the blade tip velocity estimation for increasing elevation angles. It is assumed that the helicopter blades are in the horizontal plane and for 0 degrees elevation angle, the radar is in the same plane as the helicopter blades.

To compensate for this elevation angle, the following equation was used to estimate the tip velocity accurately.

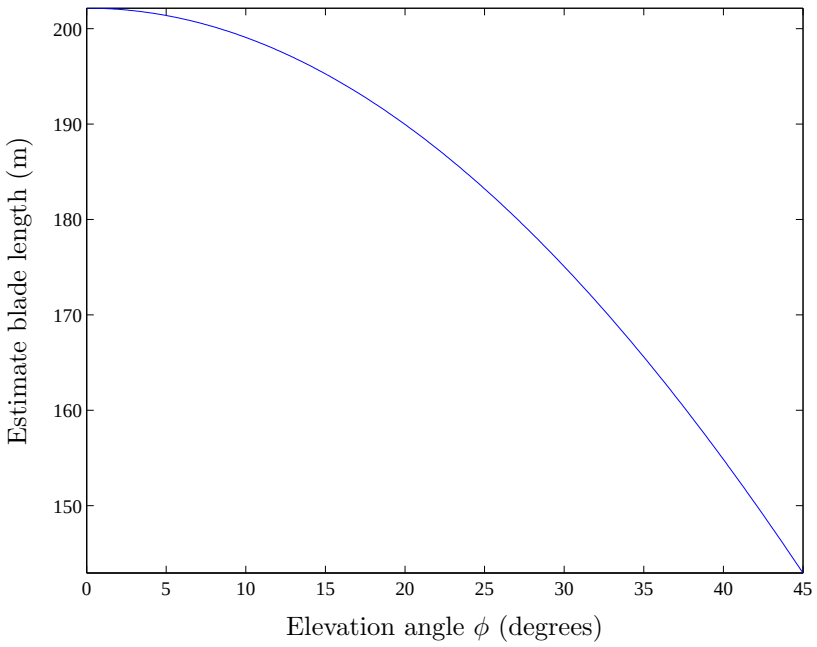

Figure 3.27: Estimated tip velocity (m/s) before elevation angle compensation for a helicopter with a tip velocity of 202.15 m/s with increasing elevation angles ranging from 0 to 45 degrees. As the elevation angle increases, the estimated tip velocity decreases.

$$\begin{aligned} v_{tip_{est}} &= f_{d_{est}} \frac{\lambda}{2} \frac{1}{\cos\phi} \\ &= f_{bin} \frac{PRF}{N_{pulses}} \frac{\lambda}{2} \frac{1}{\cos\phi} \end{aligned} \tag{3.29}$$

The estimated angular velocity that is required to determine the blade length is taken from the rate at which the focused 2-D image occurs. The blade length can thus be determined by Equation 3.30, which shows the effect that all the various parameters have on estimating the blade length of the helicopters.

$$L_{est} = f_{bin} \frac{PRF}{N_{pulses}} \frac{\lambda}{2} \frac{1}{\cos\phi} \frac{1}{\omega_{est}} \tag{3.30}$$

Equation 3.30 shows that all the parameters are linearly related to the blade length. This section illustrated how the various blade parameters (N, L and r_ω) can be estimated. From the focused 2-D image of the helicopter main rotor blade tips, all three parameters can be estimated. A limitation to this method, however, is the fact that two of these parameters are dependent on one another. Hence, if the rotation rate of the main rotor is incorrectly estimated, it will directly influence the estimated blade length, since these two

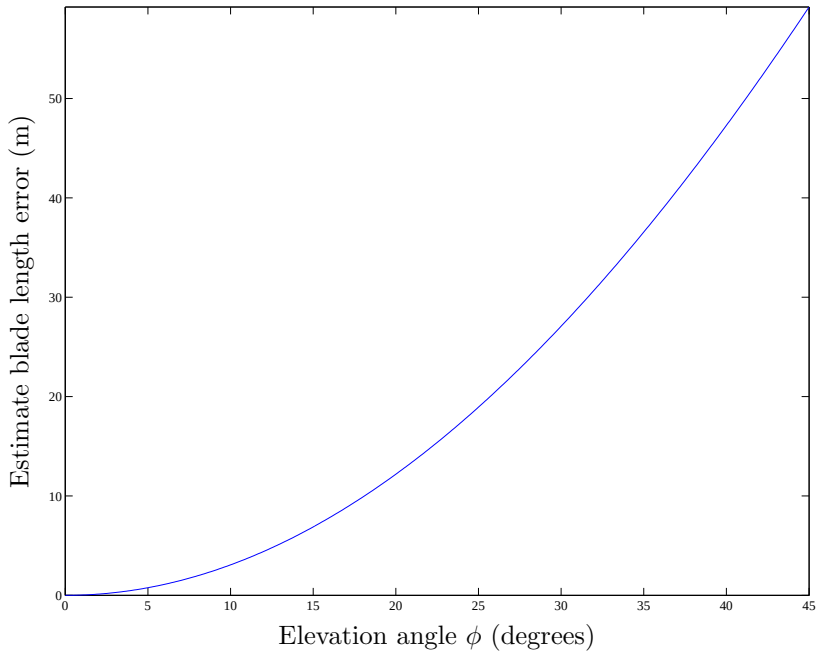

Figure 3.28: Blade tip velocity estimation error (m/s) before elevation angle compensation for a helicopter with a tip velocity of 202.15 m/s with increasing elevation error. As the elevation error increase, so does the error in the tip velocity estimation.

parameters are linearly dependent on each other (see Equation 3.30) . This fact should be taken into account when validating this method with measured helicopter data.

3.8 Summary

Chapter 3 introduced a new technique that uses tomographic imaging to estimate the number of main rotor blades (N), the main rotor blade length (L) and the main rotor rotation ration rate (r_ω) of a helicopter. The method has been developed specifically for tracking radar purposes using high PRF waveforms with long dwell times. The Doppler spectrum data of the helicopter is used as input to the Inverse Radon Transform (IRT), from where these blade parameters are estimated.

A simulation based on a point scatterer model was developed that shows the two key characteristics of the micro-Doppler effect in helicopters, namely the blade flash and the blade tip scattering, which forms a sinusoid in the Doppler-spectrum data. Together with presenting this model, this chapter also looked at the mathematical expressions for a blade flash and the expression for the range from the tip of the rotor blade to the radar. By

comparing these mathematical descriptions of blade modulation with the results from the simulation, it seems that the model is a good representation of the theoretical analysis, albeit with a few limitations.

The simulation together with measured radar data was also used to develop the blade estimation algorithm, which was discussed in detail in the chapter. The range gate Doppler data is used as input to the tomographic imaging process, where the IRT reconstructs a 2-D image of the main rotor blade tips. The image is formed by searching through all possible angular velocities, and a focused image of the blade tips occurs at the actual angular velocity of the main rotors. The three rotor blade parameters are estimated from this image. The rotation rate of the rotor is estimated by determining the angular velocity at which the focused image occurred. The number of blades can be estimated by inspection through counting the number of blade tips, or automatically by using a detection algorithm on the circular path of the IRT values corresponding to the focused image. The blade length is calculated by taking the maximum Doppler frequency of one of the focused blade tips in the 2-D image, and by using Equations 3.28 and 3.30 the estimated blade length is can be determined.

Although the blade parameter estimation technique seems feasible, the algorithm needs to be validated by using measured radar data where various waveforms are used to measure the helicopters. A variety of helicopters performing various flight profiles are needed to make valid statements regarding the performance and accuracy of the algorithm. Chapter 4 gives a detailed description of the measurement trial and of the data that was recorded during the trial in order to perform this validation. The location and duration of the trial as well as the different targets that were used are discussed. The results from the trial are discussed in this chapter, for all the different helicopters performing various flight profiles.

Chapter 4

Experiments and results

In Chapter 3 a new method was introduced to extract certain helicopter blade parameters for the purpose of target identification. The method makes use of joint time frequency radar data and a tomographic imaging process, in the form of the inverse Radon transform, to estimate the number of main rotor blades, the blade length and the rotation rate of the main rotor. A detailed analysis of the algorithm, showing the key processing steps, was presented in the chapter. A simulation based on a point scatterer model was used to generate data that served as input to the algorithm. The results from the simulation were verified with the mathematics of the micro-Doppler effect occurring in the helicopter rotor blades.

Chapter 3 also showed figures of measured helicopter data for the various key processing steps to enhance our understanding of the function of each step since the method was shown to be feasible from a theoretical point of view. The next step would be to validate the method by means of measured radar data, for more than one helicopter, in different scenarios. The performance of the algorithm needs to be assessed, in order to show at which ranges and in which circumstances the algorithm would fail and to understand why this would happen.

Chapter 4 gives a detailed account of a radar trial that was held to start this process of validating the new algorithm. A number of helicopters were measured, for various flight profiles at different ranges from the radar. The chapter first sets out the aims of the experiment, followed by the setup of the trial. The specific helicopters that were used, the schedule of the trial, the designed flight profiles and the radars used for the measurements are discussed in detail. Single results for the various flight profiles for some

of the helicopters are shown as a first validation step, indicating that the method gives promising results at various ranges.

The final section of this chapter gives the results for all the helicopters used during the trial for all the different flight profiles. The results are presented by showing the estimated blade length plotted against range. This gives a very good first approximation of the performance of the algorithm in decreasing SNR levels i.e. as the range increases. WTo Waveform parameters such as the PRF, duty cycle and the radar attenuation factor were also analysed to determine whether some of these parameters would influence the performance of the algorithm. The probability of correctly identifying one of the helicopters used in the trial by distinguishing it from the other targets from the trial is shown.

4.1 Trial description

The first trial took place in May 2007 in Simon's Town. The aim of this first experiment was to determine whether one of the CSIR's radar facilities, MECORT, could successfully measure helicopter data in a high PRF mode and therefore only one helicopter, a Bell 206JR, was used in the two measurement sessions. The measured data was entered into the signal processing algorithm discussed in Chapter 3 and promising results were obtained from this data set.

The second trial took place in August 2007, when a dedicated helicopter trial was held on the campus of the CSIR. The results from the first set of measured data led to the planning of this second trial, since it became clear that more data was needed for the validation of the helicopter blade parameter extraction method. The main goal of this trial was to record radar data for a large variety of helicopters, performing various manoeuvres at various ranges from the radar. By obtaining such a diverse data set the validity of the algorithm could be determined under various conditions. The flight profiles were also designed to be recorded at distances beyond visual range, to investigate the performance of the algorithm at deteriorating SNR levels.

This section gives a detailed account of all the different aspects to the trail, and of the experimental setup.

Table 4.1: Different helicopters used for the helicopter experiment trial in August 2007 on the CSIR campus in Pretoria. Helicopters from three different classes were used, and the rotor and blade parameters are indicated in the table for the nine different helicopters.

Class type: Number of main rotor blades								
2 Blades			**3 Blades**			**4 Blades**		
Helicopter	**L (m)**	r_ω **(RPM)**	**Helicopter**	**L (m)**	r_ω **(RPM)**	**Helicopter**	**L (m)**	r_ω
Bell 206 JR	5.08	380	Colibri EC 120	5	414	Bell 407	5.34	413
Bell 206 LR	5.64	394	AS 350B Squirrel	5.35	390			
Robinson R22	3.85	491	Aloutte II	5.1	-			
Robinson R44	5.05	400	Eurocopter EC 130	5.34	-			

4.1.1 Trial helicopters

Careful thought went into the selection of the different helicopters used for the trial. The aim was to have helicopters of different classes, as well as helicopters of the same class, where a class is defined by the number of main rotor blades. The helicopters within each class were also chosen to have varying blade lengths, ranging from very similar to significantly different. This was done to verify how well the algorithm could separate the different classes and blade lengths within a class.

A large number of private charter companies in the Pretoria and Johannesburg area was contacted and a list was compiled of all the possible helicopters that could be used for the trial. Table 4.1 shows the different helicopters that were used during the trial. These helicopters can be divided into three classes, namely main rotors with two, three and four blades respectively. The table also includes the ground truth parameters from the database of the blade length (L) in metres (m) and rotation rate (r_ω) in RPM for the different helicopters.

Nine different helicopters were used during the trial. Some of the models were used more than once, but were chartered from different companies. This was done to verify whether the same results could be obtained for different helicopters of the same model. One of the key aims of the analysis of this work was to determine the accuracy of the process and how well it would be able to separate helicopters from the same class with very similar blade lengths, such as the EC 130 and the AS 350B.

The photographs in Figures 4.1, 4.2 and 4.3 show some of the helicopters that were used during the trial.

The Bell 206 JR and the Robinson R22 are two of the two-bladed helicopters that were used, whereas the AS 350B Squirrel is a three-bladed helicopter. This specific model (AS

Figure 4.1: Bell 206 Jet Ranger

Figure 4.2: Robinson R22

350B) was used twice during the trial, though from two different charter companies. The three helicopters shown are popular helicopters and are widely used for civilian purposes. It is therefore very valuable to have the capability of positively identifying them.

4.1.2 Trial schedule

The second helicopter trial spanned over two weeks. Table 4.2 shows the schedule of the trial. More specifically, it shows the dates and different sessions, together with the helicopter used during each session. Each day was divided into two morning sessions of

Figure 4.3: AS 350B Squirrel

Table 4.2: Schedule for the helicopter trial that spanned over two weeks. Each day had two sessions with one helicopter per session. Two pre-trial sessions were scheduled to test the radar waveforms and verify whether the designed flight profiles were safe for the pilots to perform.

Date	Session	Helicopter	Charter company
2007-08-22	Pre-trial	Robinson R22	Henley Air
2007-08-24	Pre-trial	Robinson R44	Henley Air
2007-08-27	Session 1	AS 350B	ATS
2007-08-28	Session 1	Bell 206 LR	ATS
	Session 2	AS 350B	Chopperworx
2007-08-29	Session 1	Robinson R22	ATS
	Session 2	EC 120	Chopperworx
2007-08-30	Session 1	Robinson R44	ATS
	Session 2	Bell 206 JR	Chopperworx
2007-08-31	Session 1	Alouette II	ATS
	Session 2	Bell 407	Chopperworx
2007-09-05	Session 3	EC 130	ATS

two hours each. Three different charter companies were used during the trial, namely Henley Air, Aviation Toward Success (ATS) and Chopperworx. The trial started with two pre-trial sessions that were used to test the various waveforms properly and conduct a test run of the helicopters performing the different flight profiles, and to ensure that these were safe for the pilots to perform. The R22 and R44 helicopters were used due to their low hourly rates. These two helicopters were used again the following week during the trial, though from another charter company, to capture another set of data and thus make it possible to compare the different data sets. The AS 350B Squirrel was also chartered from two different companies, to investigate whether the same results were obtained for different helicopters of the same model.

4.1.3 Trial location

As mentioned in the introduction, the trial was held on the campus of the CSIR in Pretoria, using the MECORT experimental radar facility and Fynmeet, a RCS measurement facility. The photographs in Figures 4.4 and 4.5 were taken from one of the helicopters during the trial. It shows MECORT as well as some of the team members from the Radar and EW group at the Defence, Peace, Safety and Security (DPSS) division of the CSIR, who assisted during the trial.

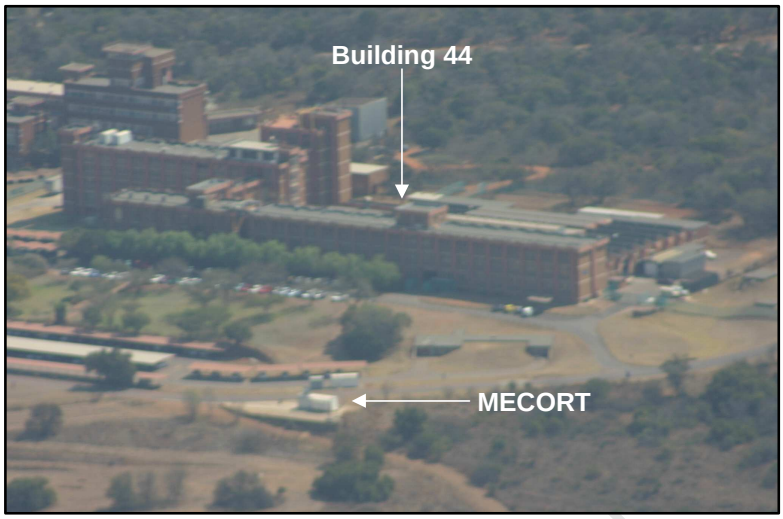

Figure 4.4: One of the radar facilities, MECORT, that was used during the trial to record the helicopter data. This photograph of the radar was taken from one of the helicopters during a measurement session.

Figure 4.5: MECORT together with the radar operators from the Radar and EW group at DPSS, after a helicopter measurement session.

4.1.4 Flight profiles and GPS data

To validate the algorithm for different flight scenarios, three different flight profiles were used, namely:

- Racecourse profile
- Circling hover profile
- Hill descent profile

These specific profiles were used so that new insight could be gained from each flight scenario, and so that the HBM algorithm could be verified for different conditions. The racecourse profile was approximately 12 km in length, and stretched to the North-Eastern side of Pretoria. This profile was chosen primarily to record data of the helicopter during in- and outbound runs. By using this profile beyond the visual range data could be captured, and the algorithm could therefore be tested in low SNR environments. The circling hover profile was chosen to record data of the helicopter from all aspect angles. The use of tail rotor modulation to aid in the identification of helicopters is still a question that needs to be answered and it was hoped that the data from a circling hover profile would be very useful, since the tail rotor will be visible for some aspect angles and obscured by the fuselage of the helicopter at other times. This hover profile was performed between 2 and 4 km from the radar.

The last profile was the hill descent. The pilots were asked to approach a hill in Faerie Glen (approximately 3 from the position of the radar) and to descend behind the hill. The body of the helicopter would be obscured first, isolating the returns from the main rotor blades and hub, providing more insight into the Doppler modulation close to the main body of the helicopter, which was the aim of this flight profile.

A Global Positioning System (GPS) was taken on the helicopters for some of the flights. The GPS data of the flight was able to contribute significantly to the analysis of the data, since the profile and manoeuvre of the helicopter could be easily determined by looking at the GPS track. The GPS data could further be used to show the altitude and azimuth and elevation angles from the helicopter to the radar, since the exact GPS location of the radar was known. Figure 4.6 shows the GPS data from the second session on the 30th of August. The helicopter used during this session was the Bell 206 JR.

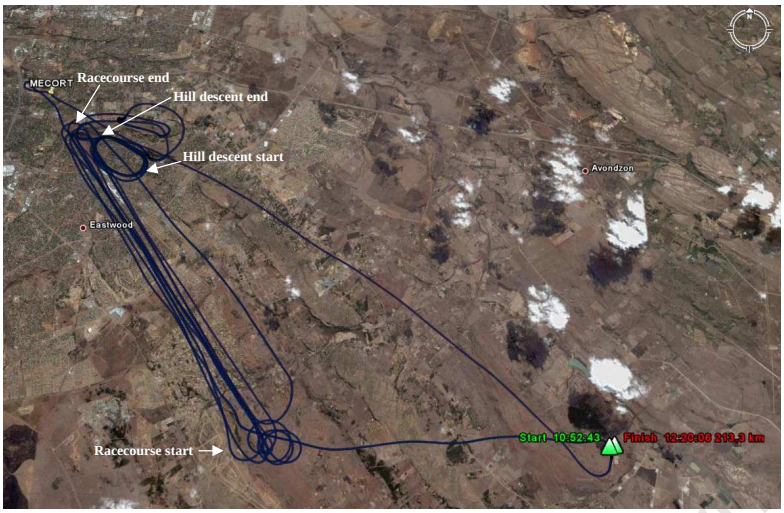

Figure 4.6: GPS data points for an entire recording session (30th of August, session 2). The data points are plotted in Google Earth, indicating both the different flight profiles and the position of the radar (MECORT).

Figure 4.6 shows the GPS data mapped in Google Earth. The racecourse and hill descent profiles are indicated. The range profile of the helicopter to the radar is showed in Figure 4.7. The different flight profiles that were performed can be identified by looking at this graph.

By looking at the range profile of the GPS data the three different flight profiles can be easily identified. Figure 4.8 shows the altitude above sea level for the same session.

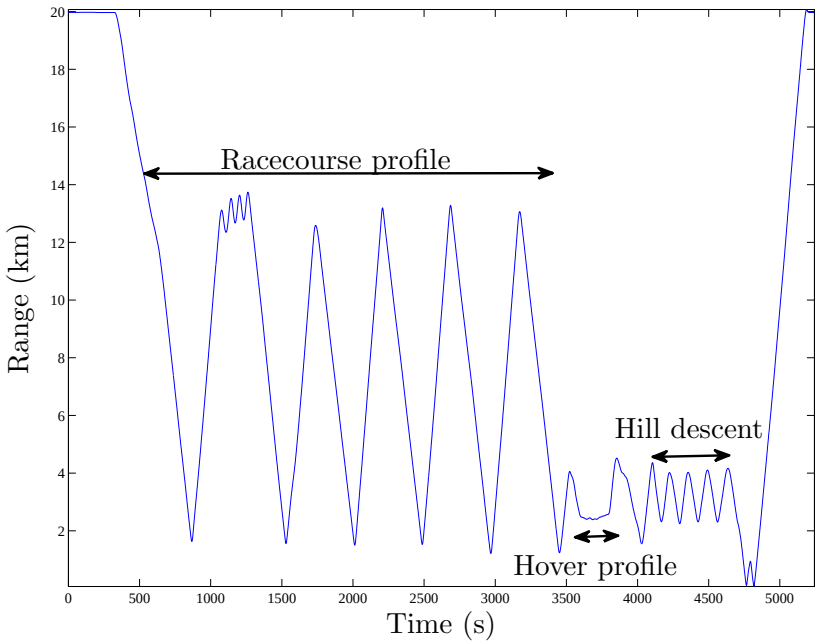

Figure 4.7: GPS data showing the range in kilometres from the target to the radar for an entire recording session (30th of August, session 2). The three flight profiles can be identified from the range tracks indicated on the figure.

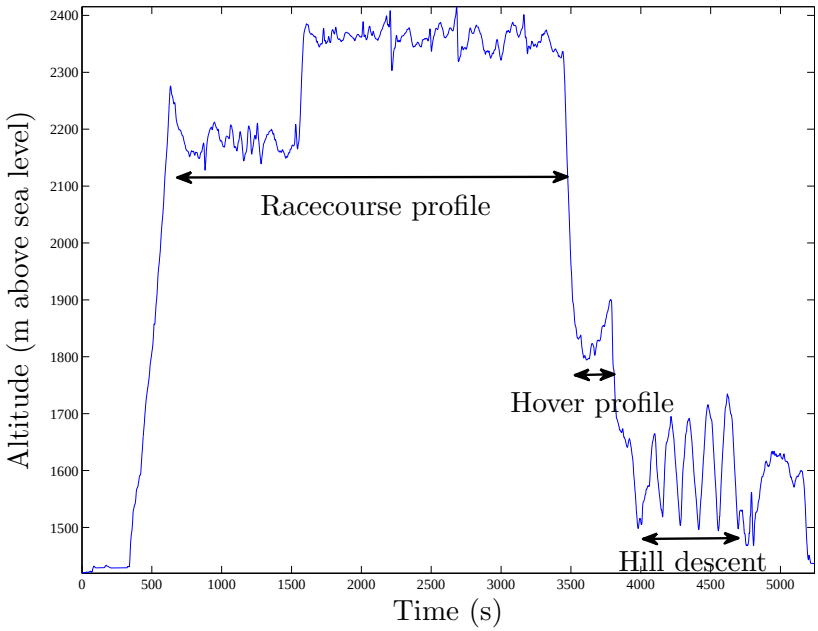

Figure 4.8: GPS data showing the altitude in metres above sea level for an entire recording session (30th of August, session 2).

Figure 4.8 shows the different altitude levels for the different profiles. The hill descent profile can be easily identified as the triangular signal seen in the latter part of the figure.

4.1.5 Radar waveforms used

To obtain valid data sets from the trial the radar waveforms were chosen very carefully. It is firstly important to understand the waveform capability of MECORT (the primary measurement facility of the trial). The radar is capable of transmitting up to 12 bursts in a pattern before the pattern is repeated. Each burst in the pattern can have its own PRF and number of pulses, and it can either be changing frequency from pulse to pulse or a constant frequency for the burst can be used. The waveforms used for the trial only made use of a single frequency, however in a pattern there were both high and low PRF bursts. The low PRF burst, or tracking burst were required to ensure unambiguous range tracking. The other bursts in the pattern, called measurement bursts, or in this case, helicopter blade modulation (HBM) bursts had high PRF values ranging from 22 to 35 kHz, with 64 pulses in the burst. The PRF of the tracking burst varied between 7.5 and 10 kHz, with 14 pulses in the burst. Figure 4.9 shows a diagram of the four different types of waveforms that were used during the trial. All the bursts were transmitted at 8.55 GHz. The only difference between the 4 types of waveforms is the number of HBM bursts in the pattern. The waveforms varied between values of one, two, six and ten HBM bursts in a pattern. The waveforms with six and ten HBM bursts within the pattern effectively have a higher duty cycle.

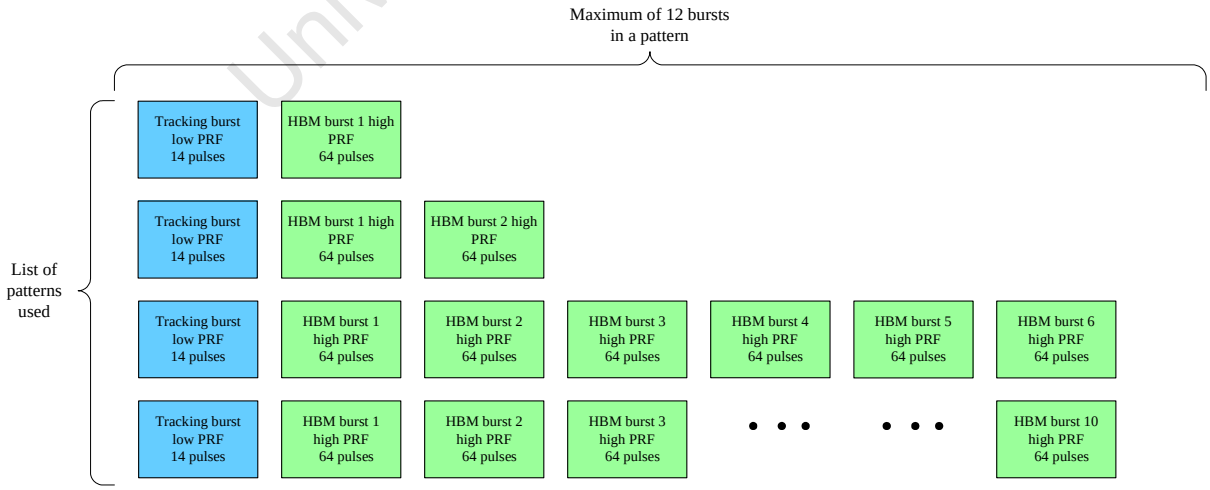

Figure 4.9: Diagram of the various radar waveforms used for the meausrement trial.

4.2 Examples of helicopter trial results

In this section, the results from the measured data of the trial are presented. The aim of this section is not to give a detailed analysis and discussion of the results (this is given in Section 4.3; rather, it is to show some of the examples of the data that was recorded during the trial and the estimated blade parameters for this data, determined by the HBM algorithm. This section shows data and results from all the flight profiles with a different helicopter for each profile. Four helicopters, representing all three classes, were chosen for this section, viz. the Bell 206 LR, Bell 407, AS 350 and R22.

This section is divided into subsections according to the flight profiles. The racecourse profile section gives results for two different helicopters, at different ranges. For each flight profile the data and results for the estimated blade parameters are shown. This gives a good indication of how well the technique works. The Doppler spectrum after velocity compensation and the data representing the processing interval for the IRT are shown, together with the focused image of the IRT. A plot showing the maximum intensity and entropy values for each IRT image is given, showing where each method is able to predict a focused image. The estimated blade parameters for each helicopter and the estimation errors are summarized in a table.

4.2.1 Racecourse profile

The data shown in this section represents both inbound and outbound runs of the racecourse profile. For the outbound leg of the racecourse profile, data from the Bell 206 LR is presented. Data from the AS 350B was used as an example of the inbound run.

Bell 206 LR

The data shown for this helicopter was recorded during one of the outbound runs. Figure 4.10 shows the experiment parameters for the specific recording, which includes the range of the target from the radar, the elevation and azimuth angles and the altitude of the target above the radar antenna.

Figure 4.10 shows the outbound path of the helicopter from 7 - 7.3 km from the radar. The duration of the measurement for this flight is approximately 4 seconds. The altitude

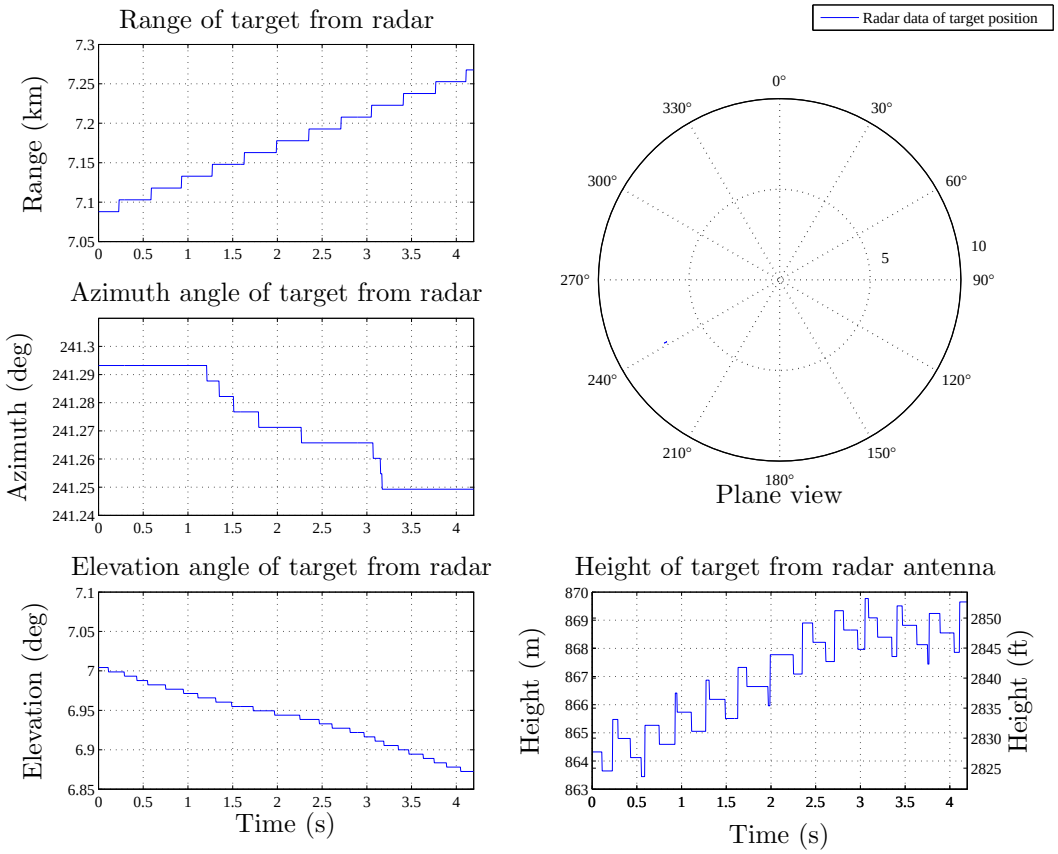

Figure 4.10: Measured radar data showing the position of the target (Bell 206LR) with respect to the radar. The range, elevation and azimuth angles as well as the height of the target are shown. The total duration of the measurement (in seconds) for the specific data file is indicated on the x-axis of each sub-figure.

of the helicopter is relatively constant for this period and the change in azimuth angle with respect to the radar is very small. The Doppler spectrum data after velocity compensation for the complete data file is shown in Figure 4.11.

The micro-Doppler effect from the helicopter rotor blades and the return from the fuselage in the Doppler-spectrum data are visible for the entire data file, shown in Figure 4.11. The time-frequency data used as the input to the IRT process is shown in Figure 4.12. This shows a zoomed-in view of the spectrogram, with a time window of approximately 400 ms.

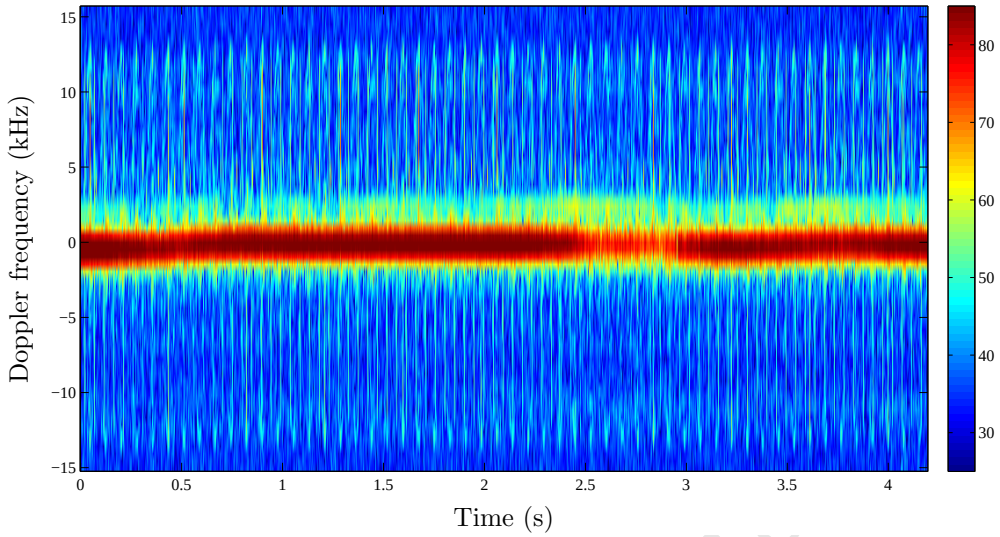

Figure 4.11: Doppler spectrum of measured data for the Bell 206LR, on an outbound course. The PRF of the waveform used for the measurement is 31 kHz.

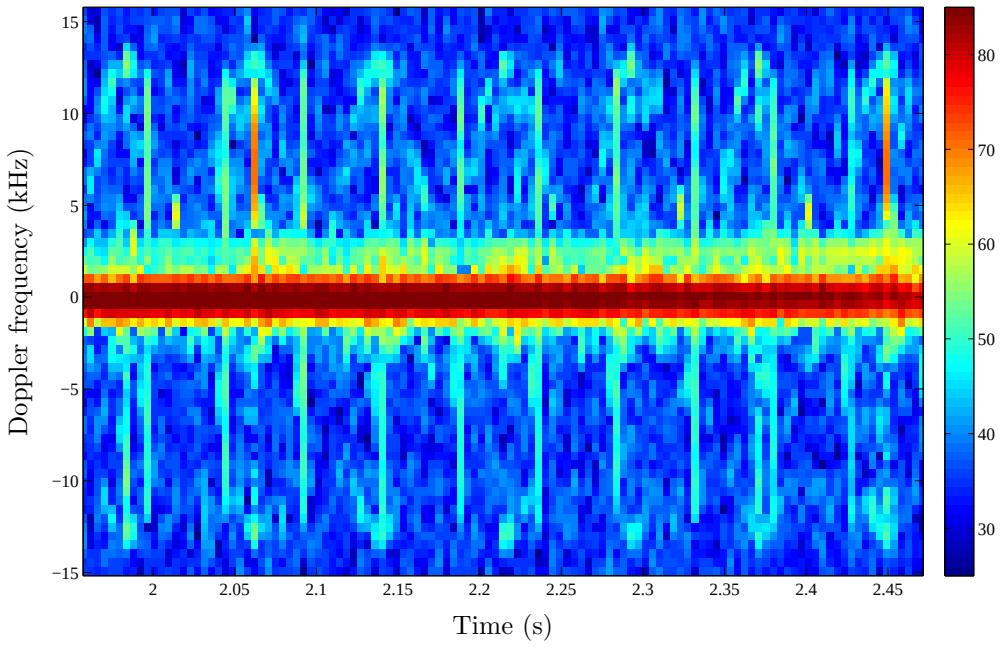

Figure 4.12: Doppler spectrum of measured data for the Bell 206LR that was used as input to the IRT process with a time interval of approximately 400 ms. The tail rotor is visible in the data, with the flashes occurring more frequently than those of the main rotor blade.

Blade flashes from both the main and tail rotor are present in the helicopter data in Figure 4.12. The tail rotor blade flashes are more frequent due to the gear ratio between the two rotors and can be seen due to the aspect angle of the helicopter. Although the main rotor blade flash is not sampled for every flash, the tips of the sinusoids for both the approaching and receding blades are seen. It is therefore still possible to form a 2-D image of the blade tips, since the IRT uses the sinusoids as 1-D projections of the blade tips. Figure 4.12 again confirms that the return from the approaching blade is more pronounced than that of the receding blade, since stronger blade flashes and sinusoids are observed for the positive Doppler frequencies. The even parity of the main rotor is also apparent from the data represented in Figure 4.12.

As discussed in Chapter 2, the rotation rate of the main rotor blade is determined by using the statistics of each image that is formed during the IRT process, thus at each search angle (angular velocity, ω_r). Figure 4.13 shows the estimation of the main rotor rotation rate by using both the maximum intensity value and entropy at each image. The two methods can be compared to determine which statistical method gives the most accurate estimate.

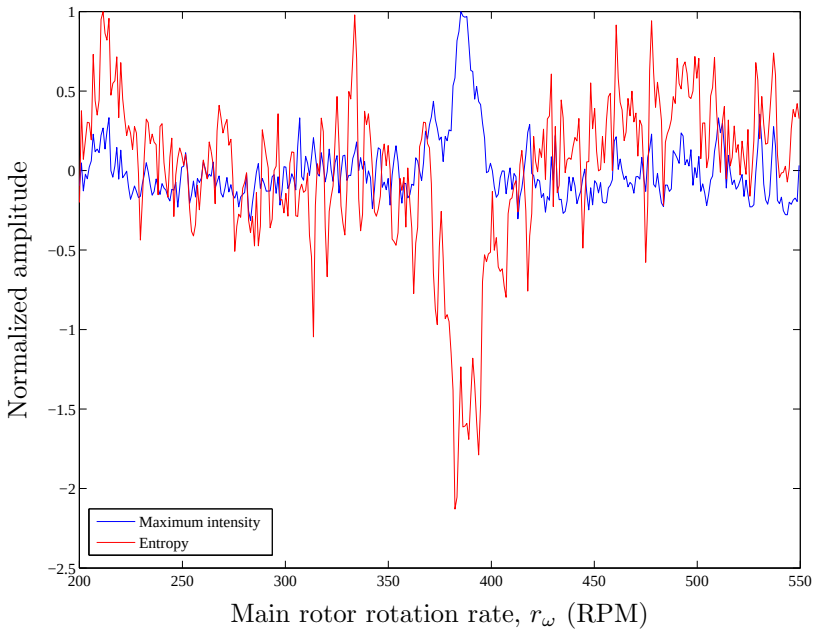

Figure 4.13: Normalized maximum intensity and minimum entropy values for each 2-D image produced by the IRT over the rotation rate search space. The process was performed for rotation rates between 200 and 550 RPM. The estimated rotation rates are chosen when a maximum value for the maximum intensity method and a minimum value for the entropy method occur.

Figure 4.13 shows the results from the two statistical methods to estimate the rotation rate of the main rotor. The maximum intensity value gives a slightly lower rotation rate. The differences in the estimated rotation rates will result in differences in the estimated blade lengths as well. It is therefore important to analyse more data to determine which method gives the smallest estimation errors. Figure 4.14 shows the focused IRT image of the helicopter blade tips that was formed by using the data from Figure 4.12 as input. From this focused image the maximum Doppler frequency at the blade tips is determined, which can then be related to the blade tip velocity. The figure on the left shows the IRT with the body of the helicopter as well as the outer circle masked, to increase the dynamic range of the image. The figure on the right shows the complete image at the estimated rotation rate.

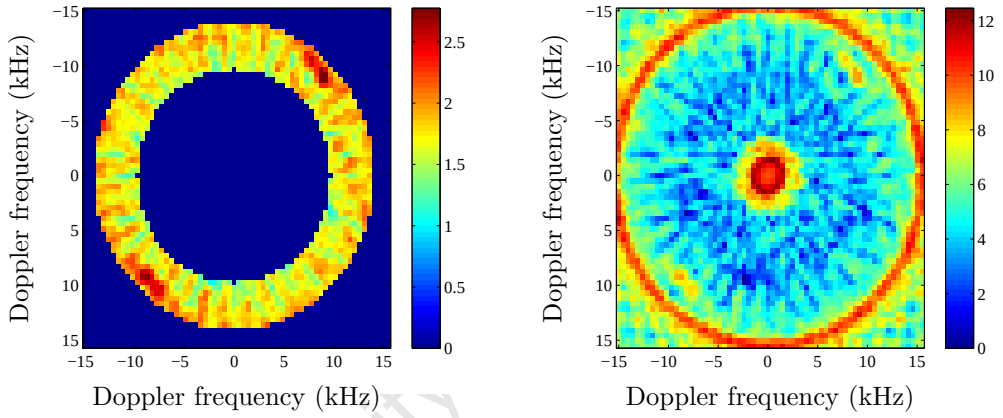

Figure 4.14: Focused 2-D image of the two helicopter blade tips by using the IRT. The estimated rotation rate from the maximum intensity method was used for this image. The image on the left had the body of the helicopter masked to increase the dynamic range of the image.

The rotation rate for the specific image corresponds to the estimated rate by using the maximum intensity method. The remaining blade parameter estimations calculated for the specific data shown in Figure 4.12 are summarized in Table 4.3. The actual blade parameters are also given in the table, as are the errors that are made with the estimation. Table 4.3 indicates that both the blade length and rotation rate were estimated fairly accurately. The blade length has an estimation error of 10 cm, whereas the rotation rate was correctly estimated within 1 RPM. Referring back to the separability analysis in Chapter 2 and specifically to Figure 2.11, which only considered the blade length with an estimation error of 0.1 m (as indicated in Table 4.3), the probability of correct identification is only 45% over the complete data set, and 60% for the class of two main rotor blade helicopters.

Table 4.3: Measured data results for the Bell 206LR performing an outbound run in the racecourse profile. The helicopter was at a distance of approximately 7 km from the radar. The three estimated blade parameters are indicated together with the ground truth data taken from the database for this helicopter.

Helicopter Parameters			**Estimated Parameters**			**Estimation Error**	
N	**L (m)**	r_ω **(RPM)**	**N**	**L (m)**	r_ω **(RPM)**	**L (m)**	r_ω **(RPM)**
2	5.64	394	2	5.54	393	0.1 m	0.25 %

AS 350B

The measured data shown for this helicopter performing an inbound run of the racecourse profile was recorded during the second session on the 28th of August. Figure 4.15 shows the experiment parameters for one of the data files captured during this measurement.

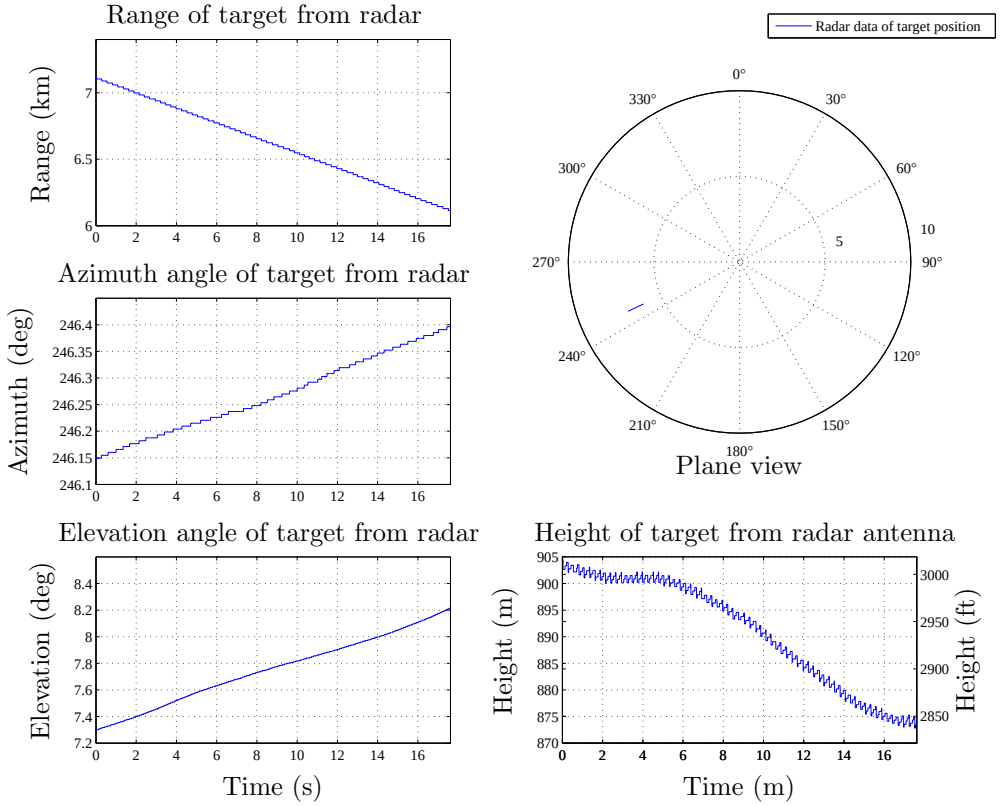

Figure 4.15: Measured radar data showing the position of the target with respect to the radar. The range, elevation and azimuth angles as well as the height of the target are shown. The duration of the data file is indicated on the x-axis of each sub-figure.

Figure 4.15 shows that the helicopter was inbound from approximately 6 to 7 km, for the data file of 16 seconds. The azimuth angle varies by only 0.3 degrees. The figure shows that the altitude of the helicopter decreased by almost 25 m over the period of the

data file. Figure 4.16 shows the Doppler-spectrum data for the data file before velocity compensation.

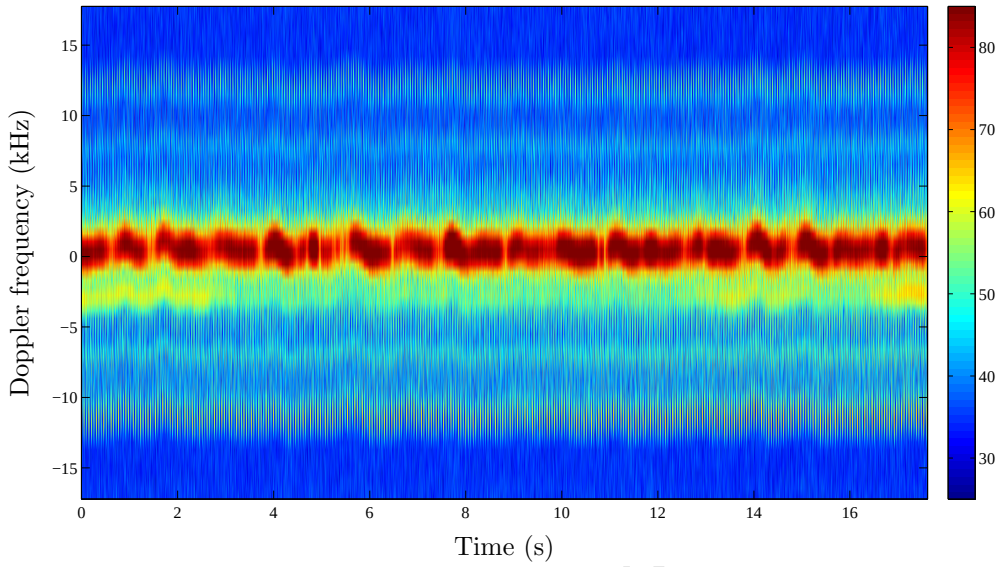

Figure 4.16: Doppler spectrum of the measured data for the AS 350B during an inbound run in the racecourse profile after velocity compensation.

The IRT input data (Doppler spectrum data after velocity compensation) is shown in Figure 4.17. A processing interval of approximately 400 ms was chosen, as explained in Chapter 3.

Figure 4.17 shows the time-frequency data used as input to the IRT. Unlike the previous example of the Bell 206 LR, it seems that the return signal from the receding blades is larger than that of the approaching blades. This seems to be especially true for the blade tip scattering, since the sinusoids for the receding blades are much more prominent than those for the approaching blades. The parity of the rotor can be easily determined from this figure. To estimate the rotation rate of the main rotor, Figure 4.18 shows the entropy as well as the maximum intensity values calculated for each 2-D blade tip image from the IRT at a certain search angle (rotation rate).

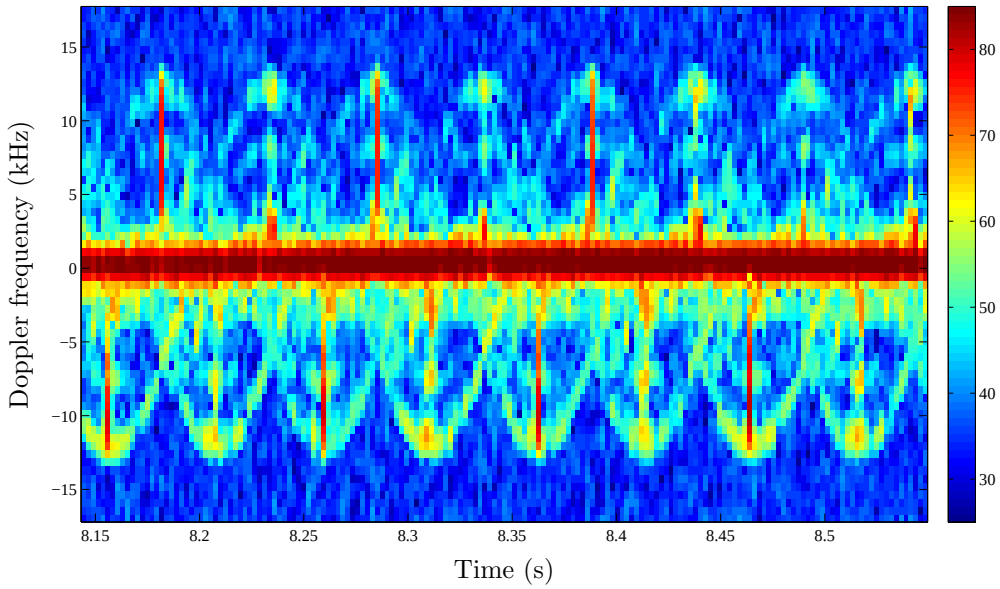

Figure 4.17: Doppler spectrum of the AS 350B used as input to the IRT process. The processing interval was chosen to be approximately 400 ms. The blade flashes and sinusoidal tip scattering is prominent in both the approaching and receding blades.

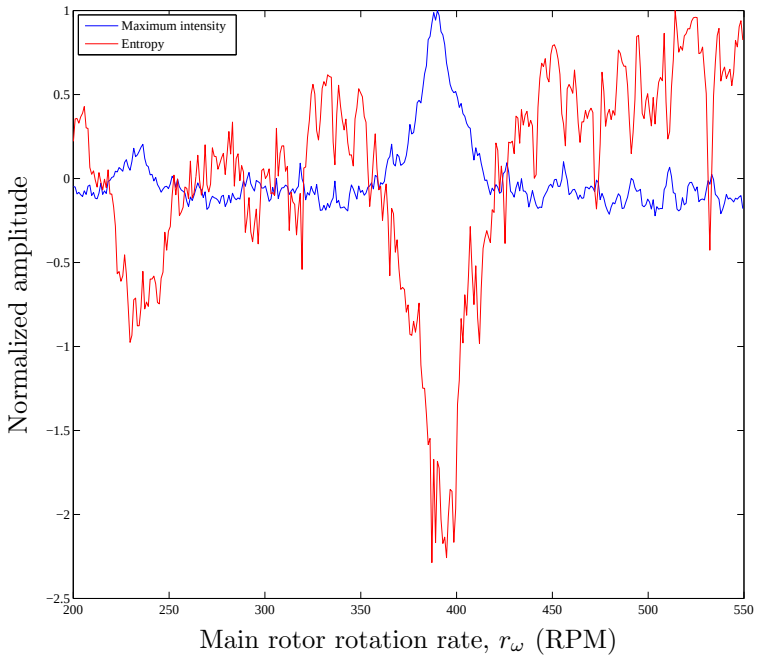

Figure 4.18: Normalized maximum intensity and minimum entropy values for each 2-D image produced by the IRT over the rotation rate search space for AS 350B. The process was performed for rotation rates between 200 and 550 RPM. The estimated rotation rates are chosen when a maximum value for the maximum intensity method and a minimum value for the entropy method occur.

The focused 2-D image from the IRT process is shown in Figure 4.19. The rotation rate at which the focused image occurs corresponds to the estimated rotation rate by means of the entropy method. The figure shows two images, one where the body of the helicopter has been masked, and the other IRT image with the return from the fuselage included. The masked image was used to estimate the parameters.

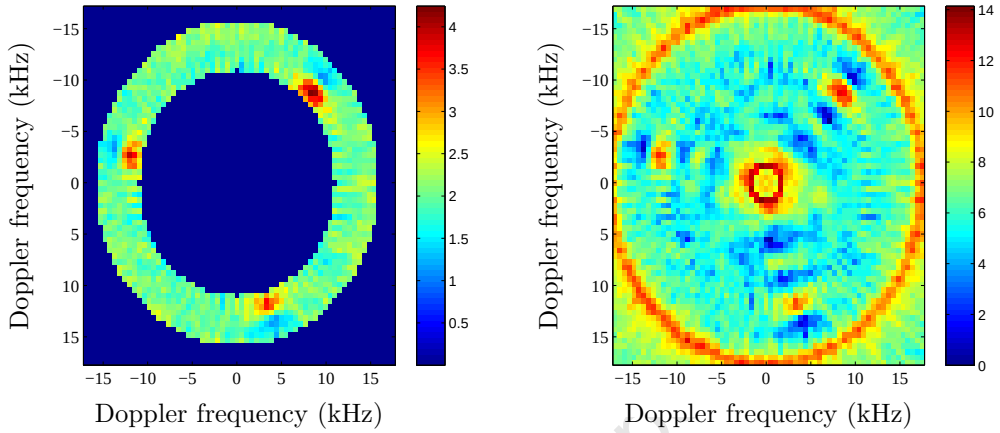

Figure 4.19: Focused 2-D image of the three helicopter blade tips of the AS 350B helicopter by using the IRT. The estimated rotation rate from the entropy method was used for this image. The image on the left had the body of the helicopter masked to increase the dynamic range of the image.

The blade parameters that were estimated from Figure 4.19 for the data file presented are shown in Table 4.4. The estimated parameters as well as the ground truth parameters for the helicopter are shown together with the estimation error for both the blade length and the rotation rate parameters.

Table 4.4: Measured data results for the AS 350B performing an inbound run in the racecourse profile at a distance of 7 km from the radar. The estimated blade parameters are indicated together with the ground truth data taken from the database.

Helicopter Parameters			**Estimated Parameters**			**Estimation Error**	
N	**L (m)**	r_ω **(RPM)**	**N**	**L (m)**	r_ω **(RPM)**	**L (m)**	r_ω **(RPM)**
3	5.35	390	3	5.23	387	0.12 m	0.77%

Table 4.4 shows that an estimate error of 12 cm was made for the blade length and that the rotation rate was estimated within 3 RPM of the value in the database. According to Figure 2.11 the probability of correct identification given the blade length estimation error is 44% over the complete data set, and only 40% for the class of three main rotor

blades. This indicates that, although the results from Table 4.4 would separate the helicopter from several targets in the database, it is not accurate enough to contribute to the positive identification of a helicopter make and model.

4.2.2 Hover profile

This section gives an example of measured data for the circling hover profile. For this profile the helicopters were at a range between 2.5 and 3.5 km from the radar. The data shown in this subsection was measured on the 31st of August, during the second session, with the Bell 407 helicopter.

Bell 407

Figure 4.20 shows the experiment parameters for one of the data files recorded during the hover profile. Figure 4.20 shows that the range from the radar to the helicopter does not

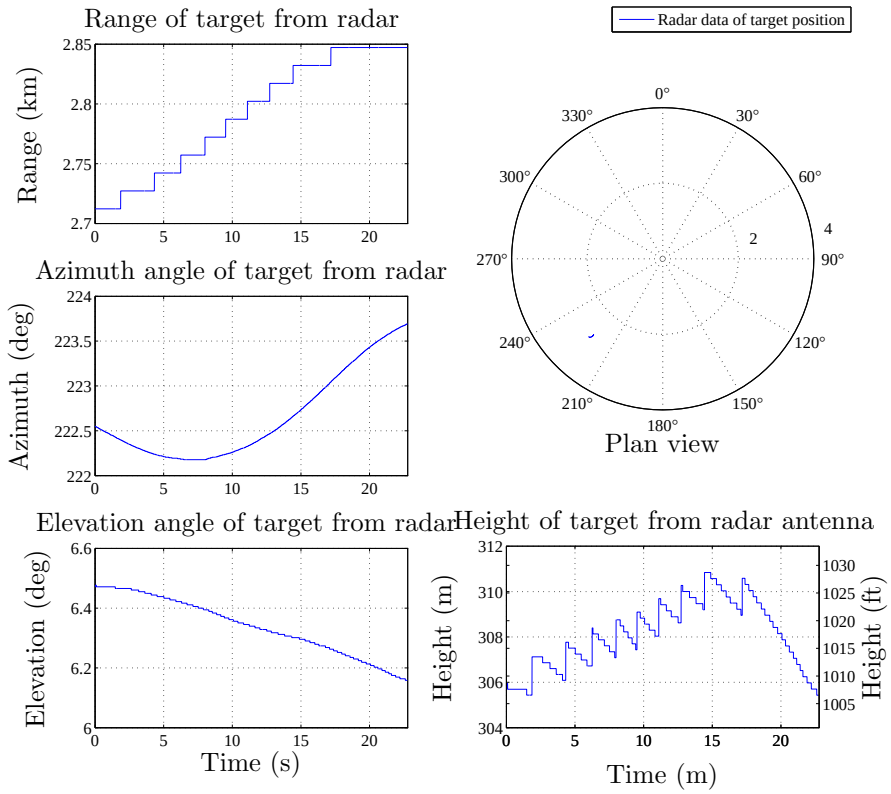

Figure 4.20: Measured radar data showing the position of the target with respect to the radar. The range, elevation and azimuth angles as well as the height of the target are shown. The duration of the data file is indicated on the x-axis of each sub-figure.

vary by more than 25 m for this data file of 20 s. The Doppler spectrum data is shown in Figure 4.21.

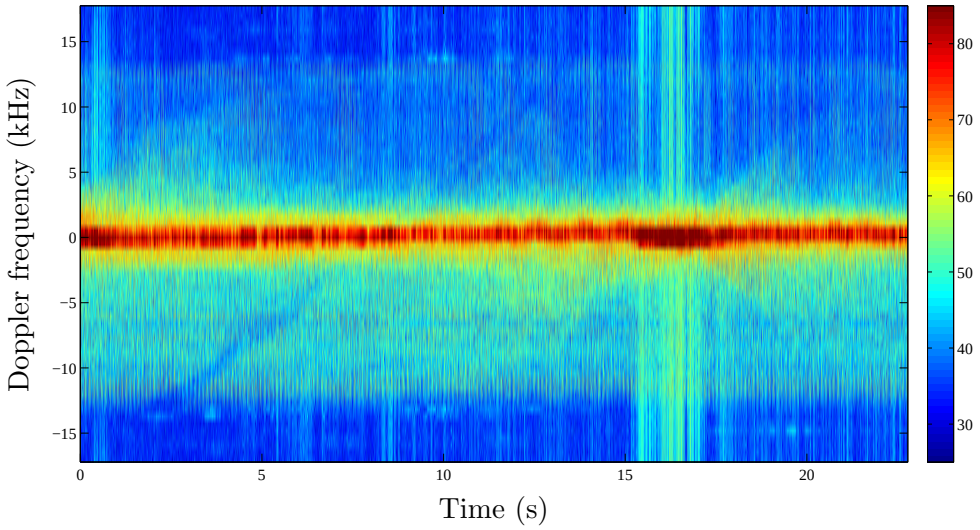

Figure 4.21: Doppler spectrum after velocity compensation for one of the hover profile data files. The target is a Bell 407.

The time-frequency data that was used as the input for the IRT process is shown in Figure 4.22 where the processing interval is in the order of 440 ms.

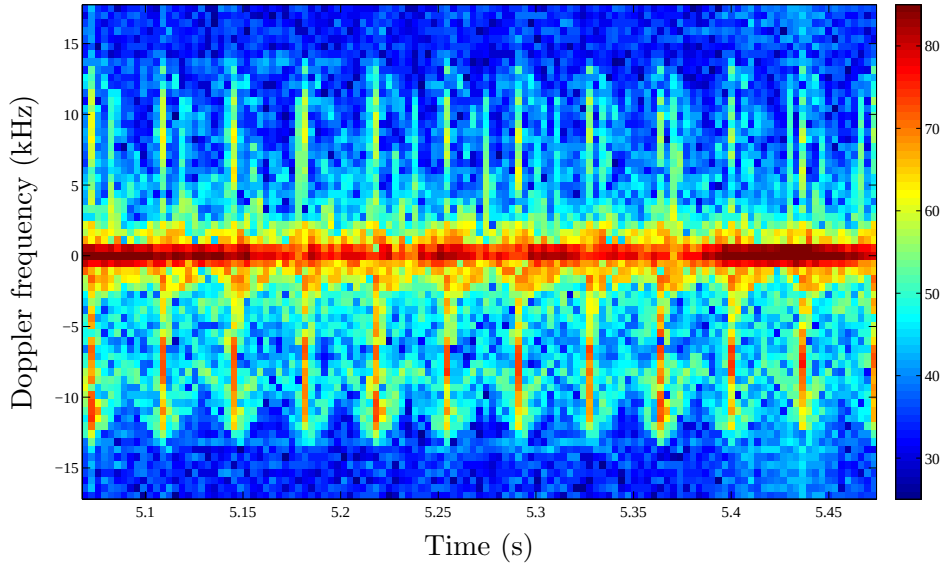

Figure 4.22: Doppler spectrum of the IRT input data with processing interval of approximately 440 ms. The receding blades give a bigger return than the approaching blades.

Figure 4.22 shows that once again the return signal from the receding blades is bigger than the return from the approaching blade. The blade flashes with positive Doppler frequency are significantly smaller and the sinusoids are only visibly at the turning points at maximum Doppler frequency. Figure 4.22 is a very good example of a case where it is not possible to count the number of sinusoids in order to determine the number of main rotor blades. The parity of the main rotor can however still be determined. The entropy and maximum intensity values for each 2-D image from the IRT are shown in Figure 4.23, from which the estimated main rotor rotation rate is determined.

Figure 4.23 shows that, unlike the previous two examples, the maximum intensity and entropy methods fluctuate significantly over the search space, and the peak and minimum values are not separated significantly from the other values. The IRT image that corresponds to the minimum entropy value, which occurs at 412 RPM, is shown in Figure 4.24.

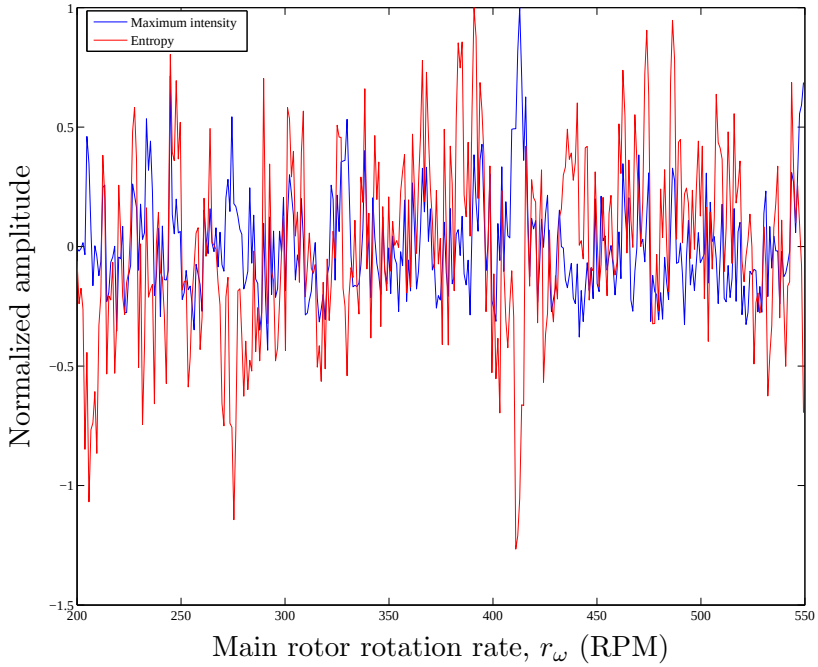

Figure 4.23: Normalized maximum intensity and minimum entropy values for each 2-D image produced by the IRT over the rotation rate search space for the Bell 407. The process was performed for rotation rates between 200 and 550 RPM. The rates at which a maximum value occurs for the maximum intensity method and at which a minimum value occurs for the entropy method are the estimated rotation rates for the two methods.

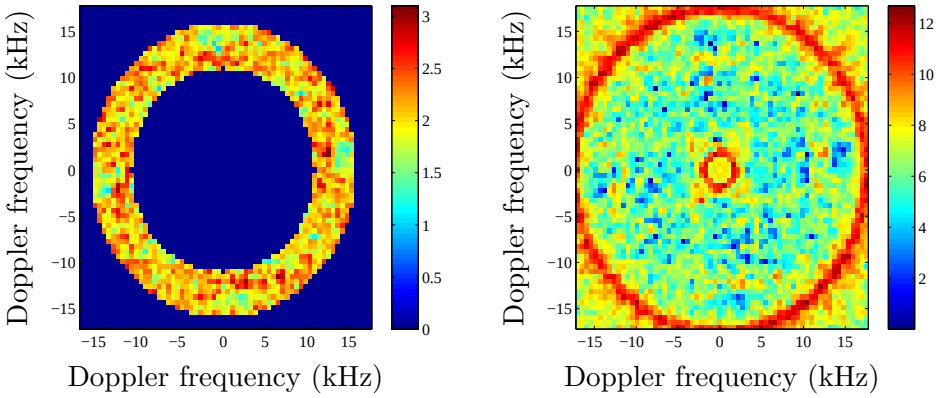

Figure 4.24: Focused 2-D image of the four helicopter blade tips by using the IRT. The estimated rotation rate from the entropy method was used for this image. The image on the left had the body of the helicopter masked to increase the dynamic range.

Table 4.5: Measured data results for the Bell 407 performing a circling hover profile. The helicopter was at a distance of approximately 2.8 km from the radar. The three estimated blade parameters are shown together with the ground truth data taken from the database for this helicopter and the estimated error.

Helicopter Parameters			**Estimated Parameters**			**Estimation Error**	
N	**L (m)**	r_ω **(RPM)**	**N**	**L (m)**	r_ω **(RPM)**	**L (m)**	r_ω **(RPM)**
4	5.34	413	4	5.38	412.9	0.04 m	0.02%

The four main rotor blade tips are more prominent in the masked IRT image than in the other image. From the image on the right it is very difficult to determine the number of main rotor blades, since the focused blade tips and the noise are in the same order of magnitude. Table 4.5 shows all the estimated blade parameters.

Even though the result from the IRT did not seem promising, the estimated parameters are quite accurate. The estimation error of 4 cm for the blade length relates to a probability of correct identification of 66% over the complete dataset and 65% for the four-bladed helicopter class (see Figure 2.11). This probability of correct identification is calculated by only making use of the blade length as an identification feature.

4.2.3 Hill descent profile

One of the measurements that was made during the hill descent profile is shown in this section, together with the estimated blade parameter results. The helicopter that was measured during this session was the Eurocopter EC 130.

Eurocopter EC 130

The data shown in this section was recorded on the 5th of September during the only session on that day. The helicopter measured during this session was the three-bladed EC 130. The data presented in this section is of the helicopter descending behind a hill. This profile was performed to isolate the main rotor returns from the returns from the body of the helicopter, and thus to investigate whether returns from the main rotor hub were visible, in the absence of the fuselage return. Figure 4.25 shows the experiment parameters for the data file. Figure 4.25 shows the descending helicopter as the range toward the radar decreases. Figure 4.26 shows the Doppler spectrum data for the data capture. Figure 4.26 furthermore shows how the track on the helicopter was lost as it disappeared

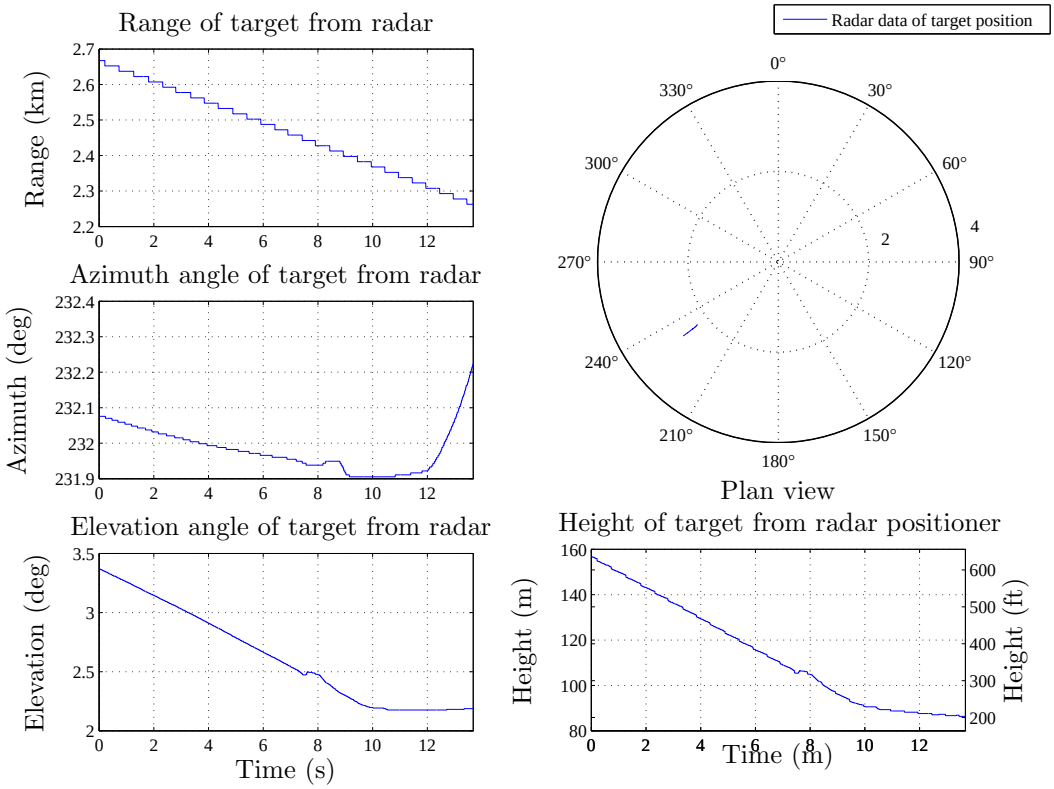

Figure 4.25: Measured radar data showing the position of the target (EC 130) with respect to the radar. The range, elevation and azimuth angles as well as the height of the target are shown. The total duration of the measurement (in seconds) for the specific data file is indicated on the x-axis of each sub-figure.

behind the hill. This data serves as a good example of the descend profile. From this measured data the isolated return signal from the rotor hub can be investigated, once the body of the helicopter has descended behind the hill. Figure 4.27 shows the Doppler spectrum data used as input to the IRT.

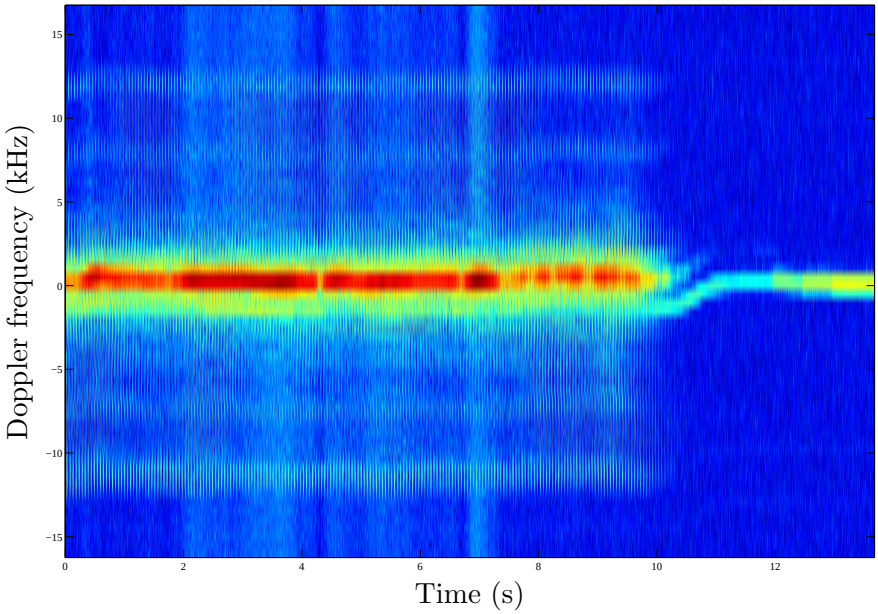

Figure 4.26: Doppler spectrum data of the EC 130 as it is descending behind the hill. The helicopter completely disappeared behind the hill after approximately 9.5 s into the measurement and thus the track was lost. This is a good example to investigate the return signal from the main rotor hub.

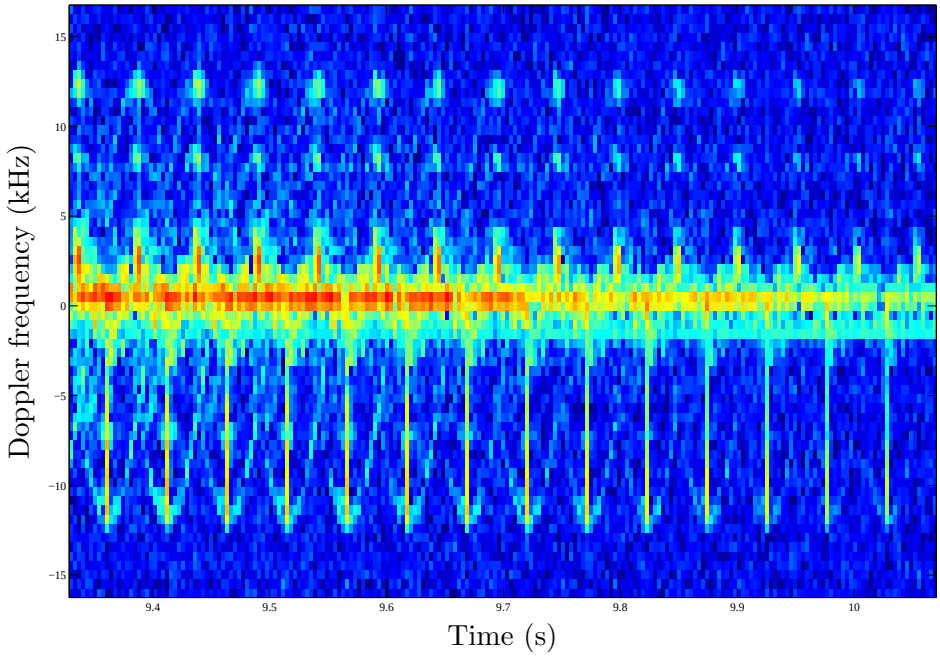

Figure 4.27: Doppler spectrum of measured data for the EC 130. The return signal from the hub can be seen, as the main rotor is isolated from the fuselage.

Figure 4.27 shows that more detail of the return signal from the rotor hub can be seen, due to the isolation of the main rotor. Flashes with a very low Doppler frequency are present for the positive Doppler frequencies of the return signal. This can be due to the push rods that form part of the main rotor hub. When concentrating only on the return close to the zero Doppler line, small sinusoidal returns on the negative Doppler frequencies of the Doppler spectrum can be seen. These sinusoids are at a slight offset to the right of the blade flash. One possible explanation for these sinusoids is that the rotating hub causes these sinusoidal returns, and since the velocity of the hub is much smaller than of the blade tip, these returns have a lower Doppler frequency. The returns from the receding rotor blades are once again stronger than those from the approaching blades, as can be seen from the negative Doppler frequencies in Figure 4.27; however, the short blade flashes from the push rods are not seen in the receding blade flashes. This asymmetry in the spectrum of the measured data may be helpful for the identification of a helicopter, especially if it occurs consistently for a certain helicopter. To estimate the rotation rate of the main rotor, the normalized statistics from the maximum intensity and entropy values of each 2-D IRT image were used for this example. The various values for the rotation rate search space are shown in Figure 4.28. The peak of the maximum intensity method and the minimum entropy level are both at approximately 390.03 RPM. The focused image that corresponds to the search angle that produced a minimum value by using the entropy method is shown in Figure 4.29.

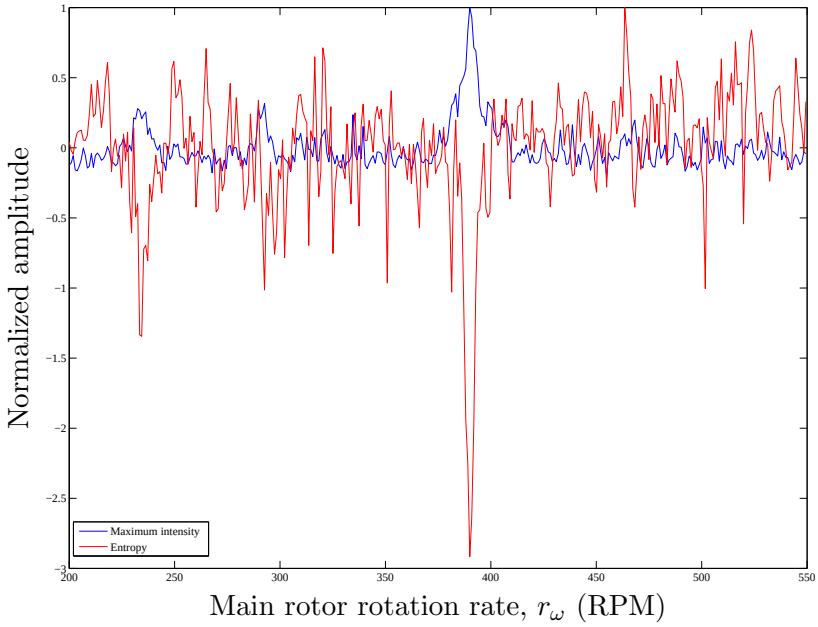

Figure 4.28: Normalized maximum intensity and minimum entropy values for each 2-D image produced by the IRT over the rotation rate search space for EC 130. The process was performed for rotation rates between 200 and 550 RPM. The rates at which a maximum value occurs for the maximum intensity method and the rates at which a minimum value occurs for the entropy method are the estimated rotation rates for the two methods.

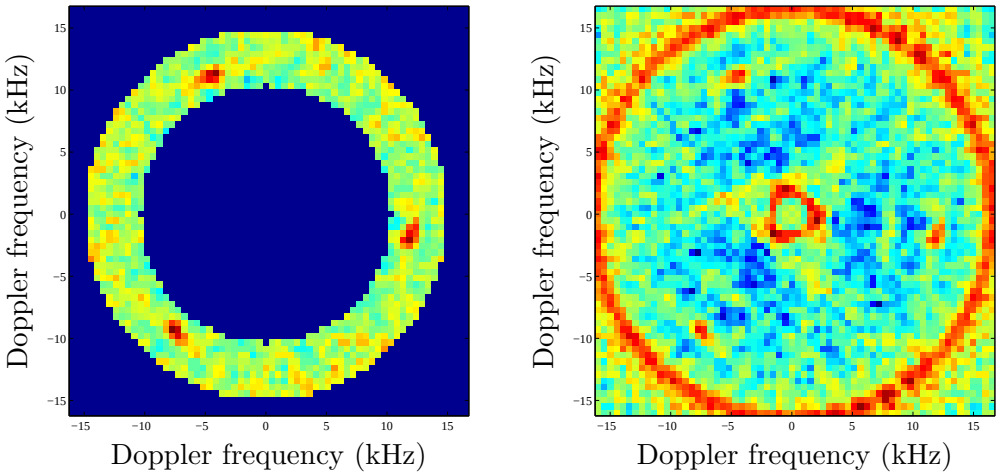

Figure 4.29: Focused 2-D image of the three helicopter blade tips by using the IRT. The estimated rotation rate from the entropy method was used for this image. The image on the left had the body of the helicopter masked to increase the dynamic range of the image.

The estimated values for the various parameters are shown in Table 4.6 together with the ground truth data and the estimation errors for each parameter. The derived blade

Table 4.6: Measured data results for the EC 130 while descending behind a hill. The helicopter was at a distance of approximately 2.3 km from the radar for the processed data. The three estimated blade parameters are shown together with the ground truth data taken from the database for this helicopter.

Helicopter Parameters			**Estimated Parameters**			**Estimation Error**	
N	**L (m)**	r_ω **(RPM)**	**N**	**L (m)**	r_ω **(RPM)**	**L (m)**	r_ω **(RPM)**
3	5.34	-	3	5.19	390	0.15 m	-

parameters obtained from the HBM algorithm for this data capture show that the blade length is under-estimated by 15 cm. The number of blades was correctly estimated. The rotation rate for this helicopter is not known, and therefore together with the estimated rotation rate error it is not included in Table 4.6. Due to the relationship between the blade length and the rotation rate of the helicopter, and because the helicopter rotor is designed such that it has a tip velocity between 0.7 and 0.9 of the speed of sound, the normal rotation rate value for this helicopter can be roughly estimated. By comparing the blade length to other helicopters in the database with the same blade length, an estimate of between 390 and 394 RPM can be used for the RPM of the helicopter (using the data for the AS 350B and the AS 550 Fennec). Since an error of 15 cm was made and the blade length and rotation rate parameters are linearly dependent, it is true to say that some error was made either in the calculation of the main rotor rotation rate or in the estimation of the maximum Doppler frequency at the blade tip.

4.3 Analysis of helicopter trial results

The results presented in this section represent data of all the measured helicopters for all the different flight profiles. A batch processor was developed in which data for an entire run of a certain flight profile was processed. The time-frequency data was divided into chunks of 400 ms, with an overlap of 200 ms, i.e. 50% overlap. The estimated blade parameters, N, L and r_ω were obtained for each chunk.

The analysis of the results from the batch processor includes the blade length estimation error over range for all the different helicopters for both the in- and outbound runs of the racecourse profile. Together with this, the analysis shows the change in waveform,

PRF, duty cycle and the attenuation factor (in dBs) over range in order to investigate the possible causes for change in the blade length estimation error.

This section also presents the probability of correct identification, given the estimated blade length parameter, L as feature, and uses the database discussed in Chapter 2 to determine the probabilities. For this analysis the helicopters were firstly separated into classes according to the number of main rotor blades. The probability of correct identification of a helicopter is therefore calculated for every helicopter within the class. This probability is also shown over range for each profile and each helicopter. All the results of the various analysis are shown for both the entropy and maximum intensity methods that were used to estimate the rotation rate of the main rotor. These two methods can therefore be compared to determine which method produces the best results.

For the hover profile, however, the range to the target is almost constant and the probabilities for correctly identifying each helicopter are shown over time. The racecourse profile has been divided into two sections: an outbound and inbound run section. By analysing the results from the racecourse profile, the performance of the algorithm in decreasing SNR conditions can be seen, since the racecourse profile has a maximum range of more than 14.5 km.

The probability of correct classification for each of the helicopters was determined by assuming a Gaussian distribution for the blade length error. The results from the trial show, however, that for most of the cases this error has a Rayleigh-like distribution rather than a Gaussian distribution, as will be shown in the following section. The results from the analysis of the probability of correct classification therefore gives a more theoretical analysis of the performance of the algorithm. It also takes all the helicopters from the database into account to determine the probability of correct classification, which gives a worst case scenario answer, since all the helicopters in the database are not found in South Africa.

The probability of correct identification given the rotation rate or the change in the estimated rotation rate over range is not shown in this section, since the rotation rate and blade length of a helicopter main rotor are linearly dependent. This implies that if the rotation rate is inaccurate the blade length will be incorrectly estimated as well. Furthermore, since there are helicopters in the database with unknown rotation rates, showing the probability of correct identification given the rotation rate as feature would not be a true account of the algorithm's performance.

By showing these results, new insights are gained. For instance, it became clear that for some helicopters the scattering from the blade tip is very small, resulting in poor blade parameter estimation, whereas for other helicopters the return from the blade flash is very small. Some of these effects are discussed in more detail in the following subsections. This study therefore also highlighted some of the limitations of the algorithm, and these will be discussed in more detail in Chapter 5.

4.3.1 Racecourse profile - Outbound run

The probability of correct identification and the analysis of the blade length estimation error from the measured helicopter data for a complete outbound run is presented in this section. The range for this outbound run is from approximately 1.75 to 14.5 km. Due to corrupt data files, or errors caused by the radar, all the helicopters are not shown over the entire range.

Results from the entropy method

Figure 4.30 shows the probability of correct identification where the entropy method was used to estimate the main rotor rotation rate.

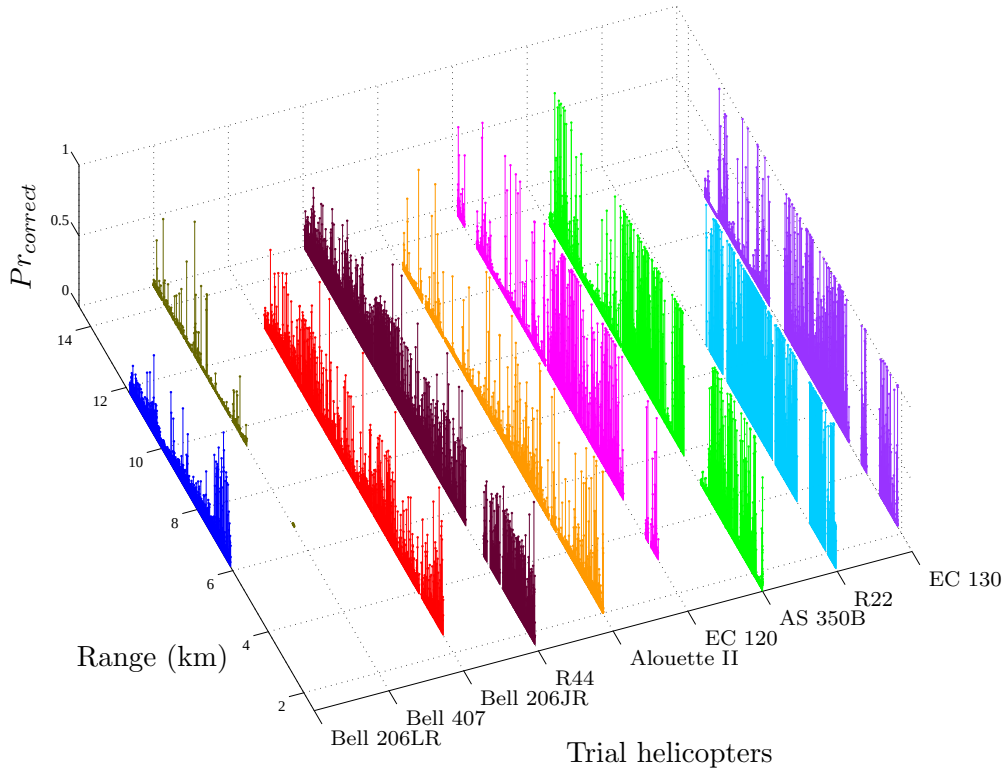

Figure 4.30: Probability of correct identification for an outbound run between 1.75 and 14.5 km. The estimates were determined by using the entropy method. The results for all the helicopters used in the trial are shown, with each helicopter indicated on the x-axis.

Figure 4.30 shows that the probability of correctly identifying helicopters such as the AS 350B, EC 130 and the R22 is very good. The reason for the high probability in the case of the R22 is that it has the shortest blade length. Therefore, for all the estimated blade lengths smaller than 3.85 m, the helicopter will be correctly identified. The reason for the high probability on the two three-bladed helicopters is a result of the blade tip scattering. Doppler-spectrum data for both these helicopters showed that even at long ranges such as 12 km a strong return from the blade tips is present and since the return from the blade tips is used by the IRT process as input data, accurate estimation results are achieved.

To investigate the actual blade length error distribution over range for the outbound run given the entropy method, the blade length estimation errors of each helicopter together with the distribution of the errors are shown in Figures 4.31, 4.34 and 4.37. These figures also indicate the change in the waveform during the measurement, as well as the change in the radar attenuation factor (in dB) with increasing range. The radar attenuation factor was changed manually during the radar measurements as the target range increased.

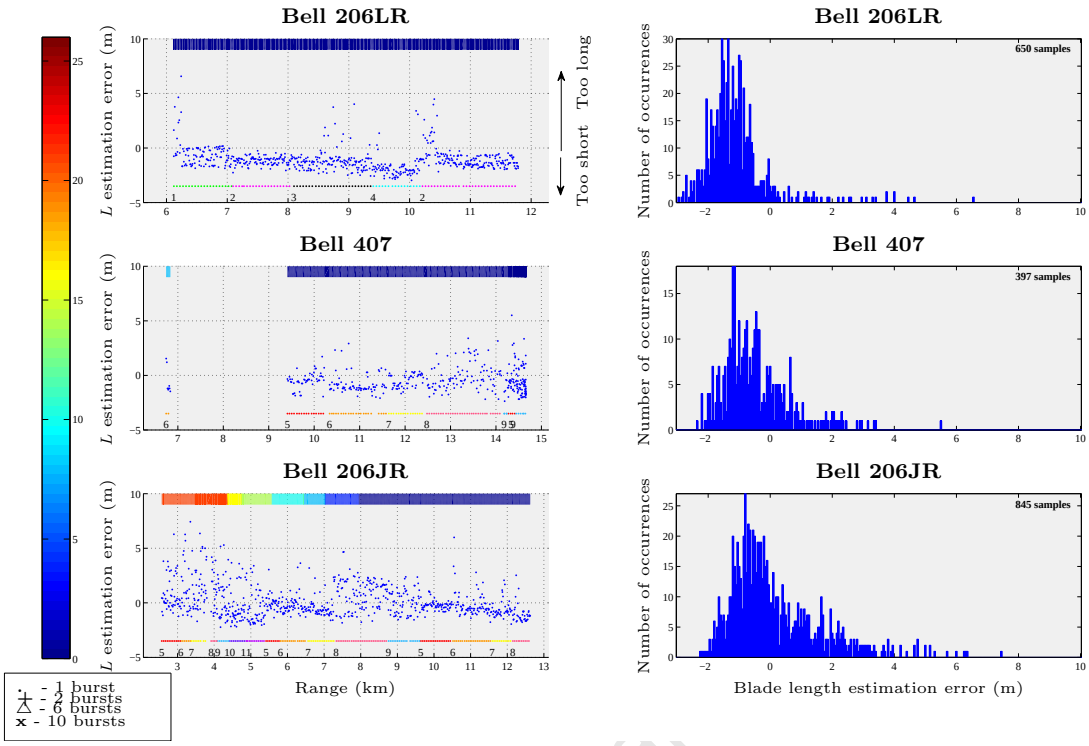

Figure 4.31: The blade length estimation errors and error distribution using the entropy method for the Bell 206LR, Bell 407 and the Bell 206JR over range for the outbound run of the racecourse profile.

Figure 4.31 shows the results for the Bell 206LR, Bell 407 and the Bell 206JR. The difference between the measured blade length and the actual blade length of the helicopter indicated in the database is given in the first column of the figure. The arrows next to the first graph indicate that for errors greater than zero the blade length is over-estimated, and for errors smaller than zero the blade length is under-estimated. The radar attenuation factor during the measurements is indicated by the colour bar at the far left of the figure. For the Bell 206LR a constant attenuation factor of $0dB$ was used. For the Bell 206JR, the attenuation factor was decreased as the range increased, causing less attenuation of the received signal. The various waveforms that were used during the measurements are indicated at the bottom of each graph. Each waveform is represented by a different colour, and the number of the waveform is also indicated. All the waveforms used during the measurement of these three helicopters had one tracking burst, followed by a single HBM burst (as explained earlier in this chapter). The main difference between the tracking burst and the HBM burst is the shorter PRI for the HBM burst, as well as the shorter pulse width in the latter. Appendix A gives a detailed description of the various

waveforms that were used also indicating the number of each waveform as indicated in the figure.

The distribution of the blade length estimation errors is shown in the second column of the figure. This clearly indicates that the error does not have a Gaussian distribution as previously assumed, and that a long tailed distribution, for instance the Rayleigh distribution could be fitted on the data, since this could provide a better fit. The number of samples used for each histogram is showed in the top right corner of each graph. It is also clear that the distribution of the estimated blade length errors do not have a mean value around zero, but it is offset with a negative mean which relates to an under estimation of the main rotor blade length.

As mentioned earlier the duty cycle of the waveforms used in the measurements were also analysed together with the change in PRF. The results from this analysis is given below. The percentage duty cycles used during the measurement for these three helicopters (Bell 206JR, Bell 206LR and Bell 407) are shown in Figure 4.32 against increasing range. The duty cycle was determined by dividing the pulse width in a burst with the PRI of that burst. The waveforms are once again indicated both by their various colours and numbers.

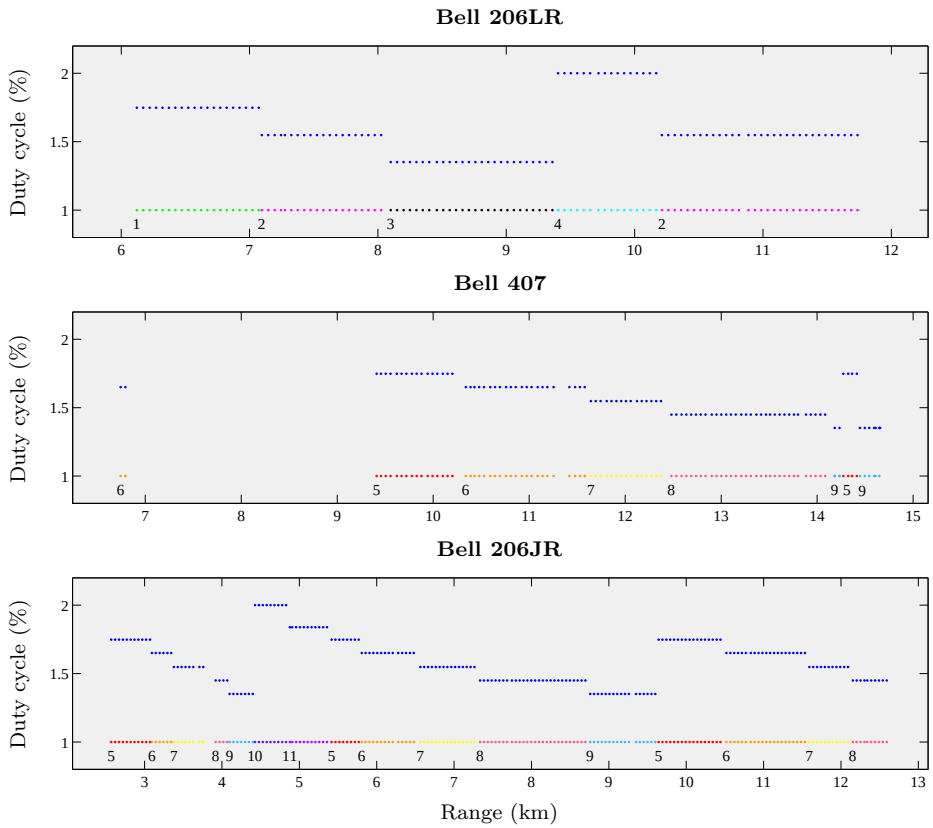

Figure 4.32: The duty cycle of the various waveforms used for the Bell 206LR, Bell 407 and the Bell 206JR over range for the outbound run of the racecourse profile.

Figure 4.32 shows the change in duty cycle as the waveforms are switched. A maximum duty cycle of 2% was used. The change in duty cyle is clearly shown as the waveforms are changed. To explain the changes and errors in the blade length estimation another waveform parameter, aside from the duty cycle was investigated, namely the PRF. There is an hypothesis that as the PRF decreases during the waveform changes the absolute estimation errors will increase. Figure 4.33 shows the PRF for every waveform over range for the three helicopters.

The blade length estimation error and error distribution for the next three helicopters, the Robinson R44, the Alouette II and the EC120, are shown in Figure 4.34.

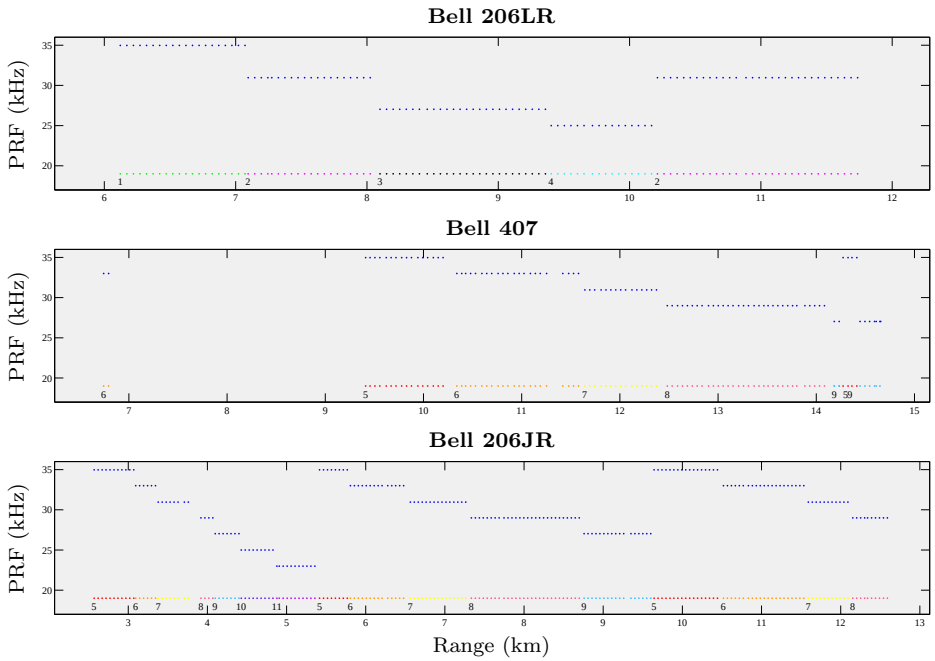

Figure 4.33: The PRF of the various waveforms used for the Bell 206LR, Bell 407 and the Bell 206JR over range for the outbound run of the racecourse profile.

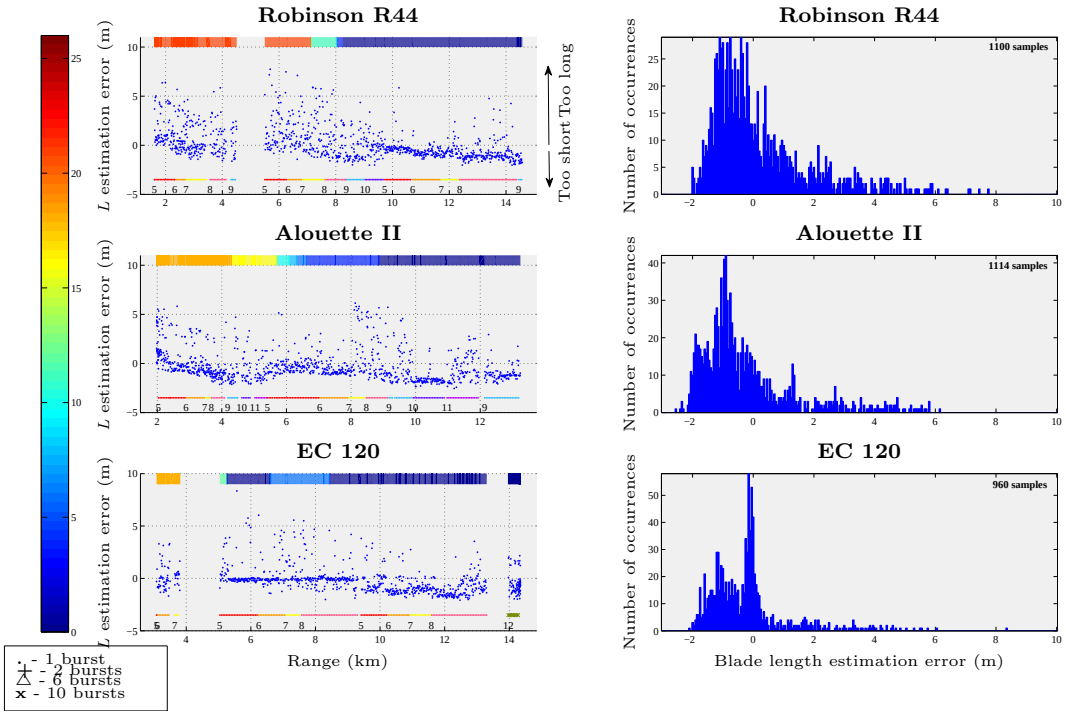

Figure 4.34: The blade length estimation errors and error distribution using the entropy method for the Robinson R44, the Alouette II and the EC 120 over range for the outbound run of the racecourse profile.

Figure 4.34 gives the same information as Figure 4.31. The blade length error for the EC 120 has a mean value of approximately zero between 5 and 9.5 km, but at the waveform change from waveform 8 to 5, the error jumps to approximately −1 m. This is also indicated in the histogram of the blade length estimation error. For most of the waveforms used for these helicopters, only one HBM burst was used. However, for the EC 120, waveform 12 was used at 14 km with 10 consecutive HBM bursts. This effectively implies longer continuous time on the target. However, since the target is at 14 km the SNR will be lower which would still explain the high blade length errors. The duty cycles of the various waveforms that were used for these three helicopters are shown in Figure 4.35. The PRF for the waveforms used in this data set is showed in Figure 4.36.

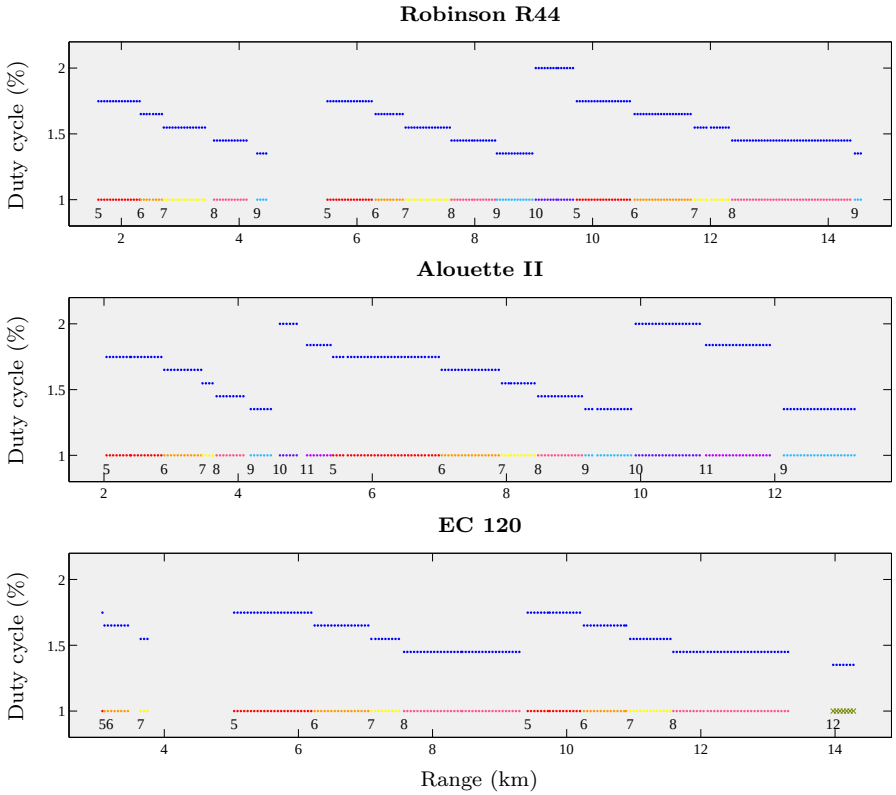

Figure 4.35: The duty cycle of the various waveforms used for the Robinson R44, the Alouette II and the EC 120 over range for the outbound run of the racecourse profile.

One of the recommendations for future work would be to investigate the role that the PRF of the waveform plays in the performance of the algorithm in more detail. It seems to be true to say that for some cases the change in PRF plays a role in the performance of the algorithm. It is therefore important to do a study on choosing the optimal waveform, with PRF as one of the parameters to achieve the good and reliable results. Figure 4.37

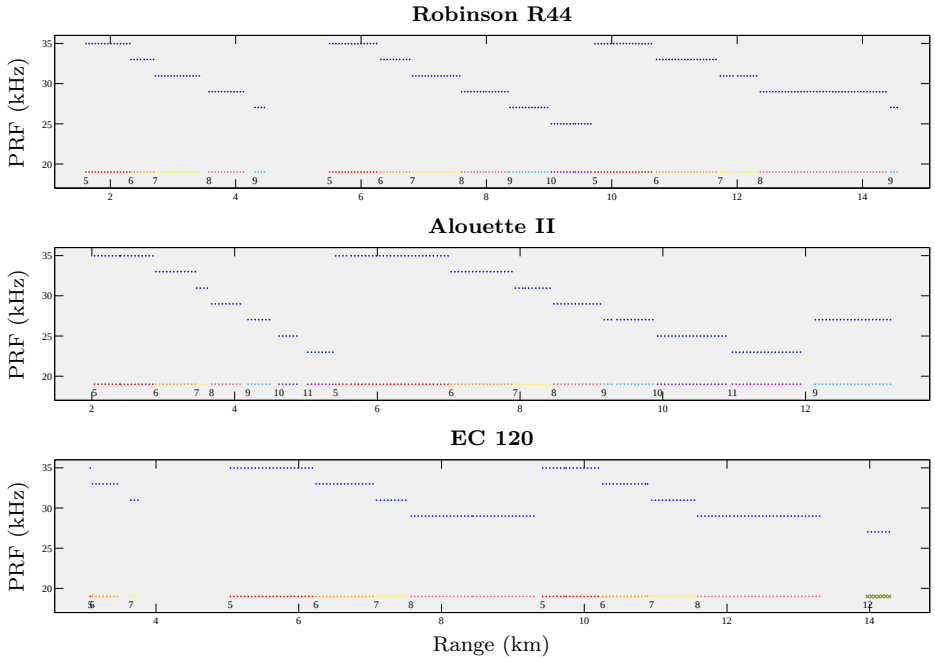

Figure 4.36: The PRF of the various waveforms used for the Robinson R44, the Alouette II and the EC 120 over range for the outbound run of the racecourse profile.

gives the results for the AS 350B, the Robinson R22 and the EC 130 while performing an outbound run. The results were also calculated by using the entropy method.

For all 9 helicopters it is interesting to note that the errors are relatively large at close ranges to the radar. There are two possible explanations for this. Firstly, it may be a result of the actual manoeuvre of the helicopter. The helicopters performed a teardrop turn at approximately 2 km from the radar to start the outbound run. Due to the large blade tilt during the turn the Doppler frequency of the helicopter blade may be estimated incorrectly. Another possibility is that due to the large return from the helicopter blade flash at such a small range, the small return signals from the sinusoids may be suppressed.

The duty cycles for the various waveforms used for the AS 350B, the Robinson R22 and the EC 130 are shown in Figure 4.38. Once again the changes in PRF for the different waveforms used for this dataset is showed in Figure 4.39.

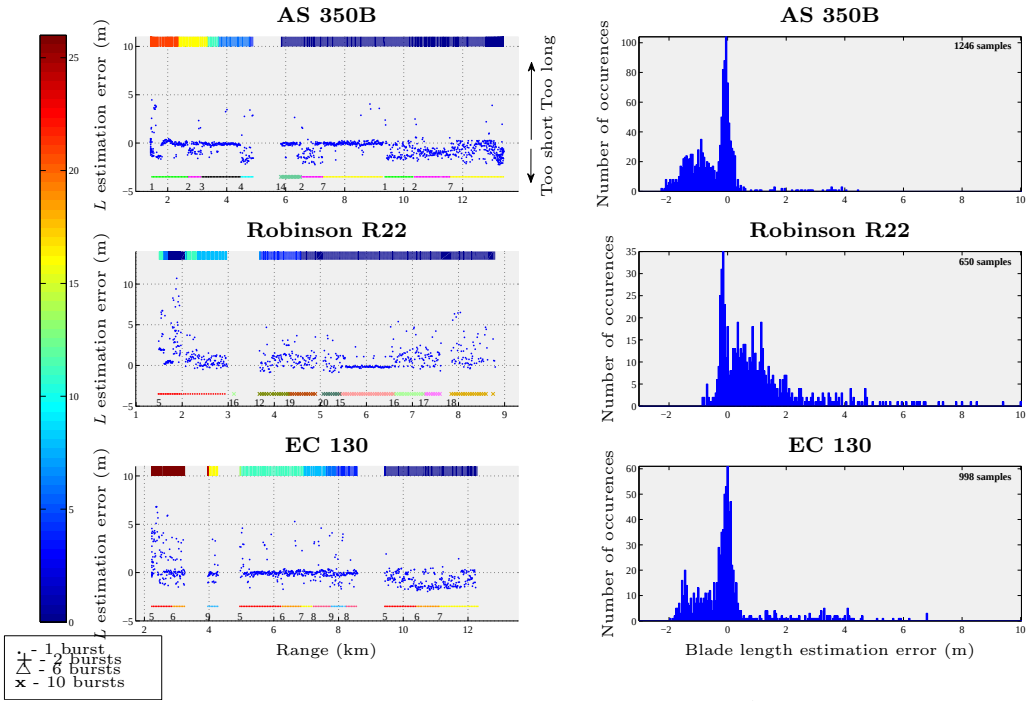

Figure 4.37: The blade length estimation errors and error distribution using the entropy method for the AS 350B, the Robinson R22 and the EC 130 over range for the outbound run

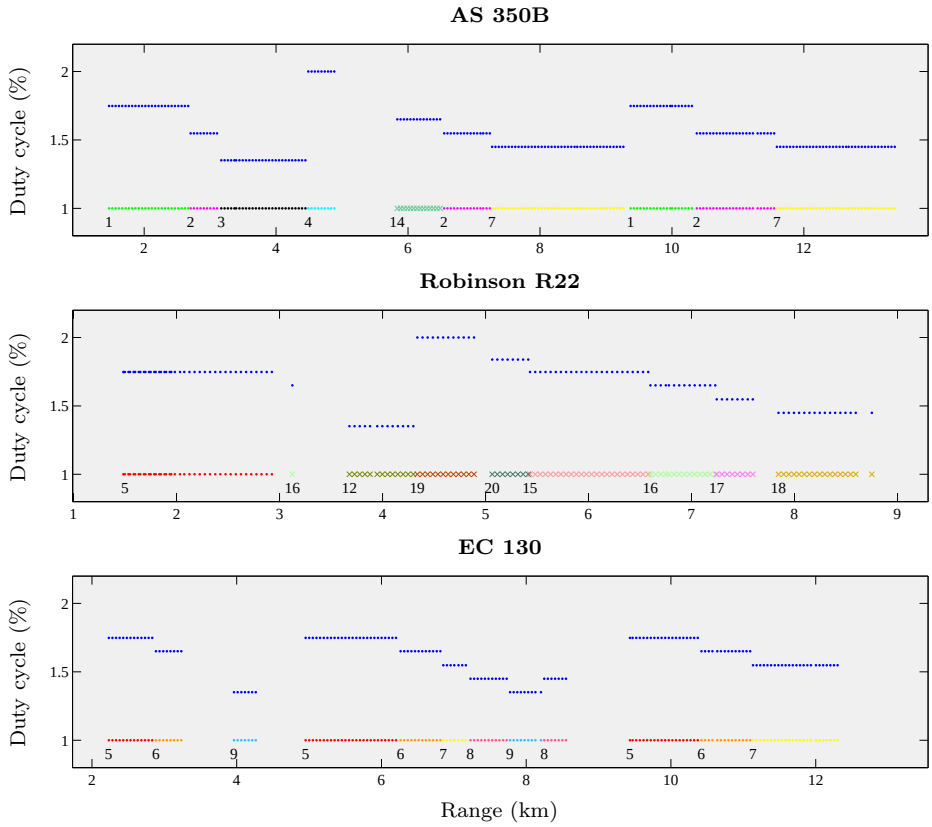

Figure 4.38: The duty cycle of the various waveforms used for the AS 350B, the Robinson R22 and the EC 130 over range for the inbound run of the racecourse profile.

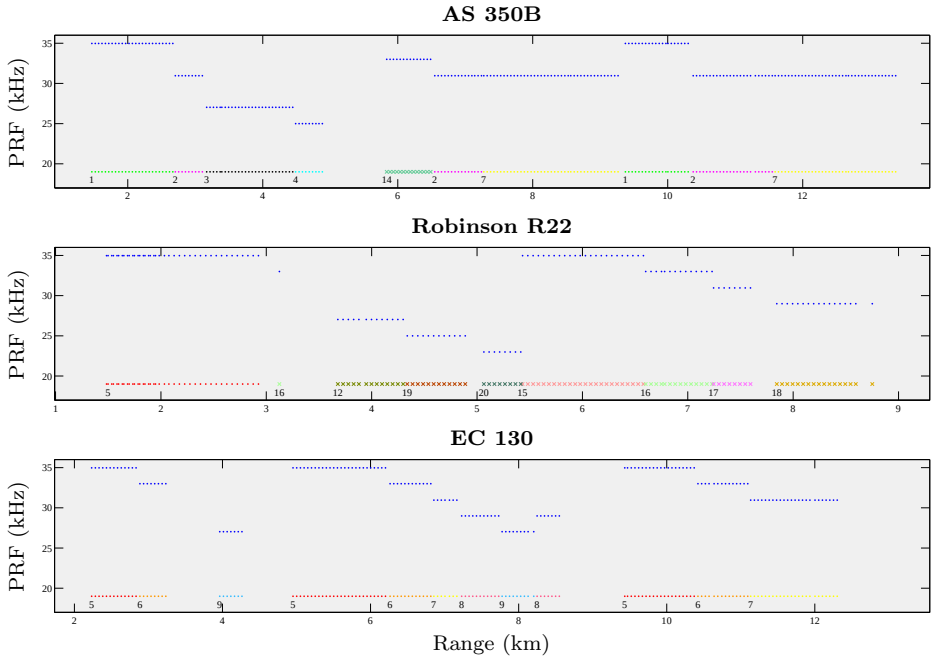

Figure 4.39: The PRF of the various waveforms used for the AS 350B, the Robinson R22 and the EC 130 over range for the inbound run of the racecourse profile.

Results from the maximum intensity method

Figure 4.40 shows the probability of correct identification for the same outbound run, hence the same measured data, but using the maximum intensity method to estimate the rota

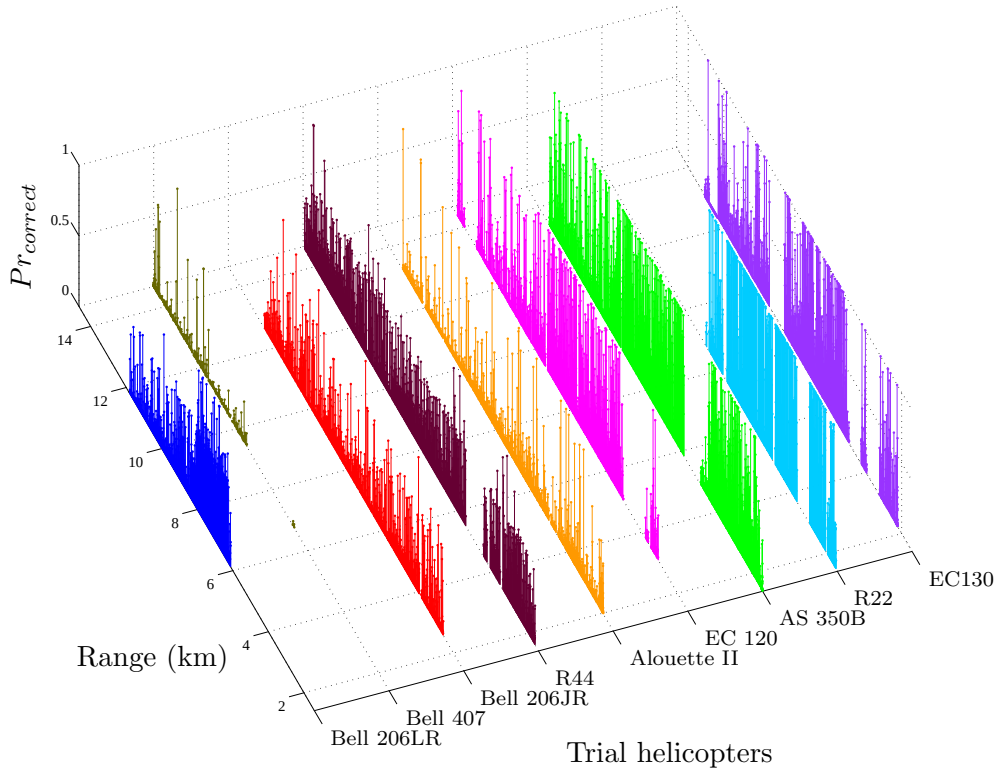

Figure 4.40: Probability of correct identification for an outbound run between 1.75 and 14.5 km. The blade parameters were determined by using the maximum intensity method. The results for all the helicopters used in the trial are shown, where each helicopter is indicated on the x-axis.

By comparing the results from Figures 4.30 and 4.40, it is clear that the results for the Bell 206LR and the EC 120 are significantly better when using the maximum intensity method. The blade length estimation errors and the distribution of these errors by using the maximum intensity method are shown in Figure 4.41 for the Bell 206LR, the Bell 407 and the Bell 206JR.

By comparing Figures 4.41 and 4.31, it is evident that the maximum intensity method gives very stable answers for the Bell 206LR from 6 to 8 km. The estimations for ranges further than 8 km are however very scattered, and do not give reliable answers. The same is true for the other two helicopters, and this is also portrayed in the histogram

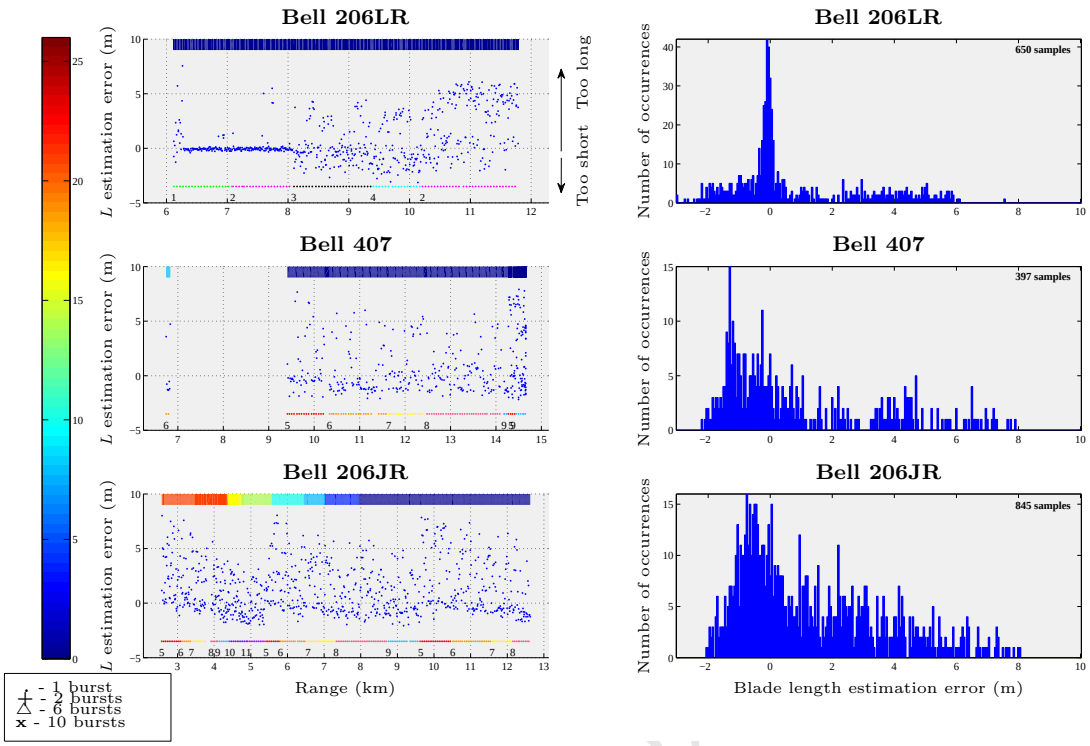

Figure 4.41: The blade length estimation errors and error distribution using the maximum intensity method for the Bell 206LR, the Bell 407 and Bell 206JR over range for the outbound run of the racecourse profile.

of the blade length estimation error. From the data used for these three helicopters it seems that the entropy method gives more accurate results than the maximum intensity method. The duty cycles of the waveforms are not shown again, since the different processing methods were performed on the same data sets.

Figure 4.42 shows the results for the Robinson R44, the Alouette II and EC 120. By

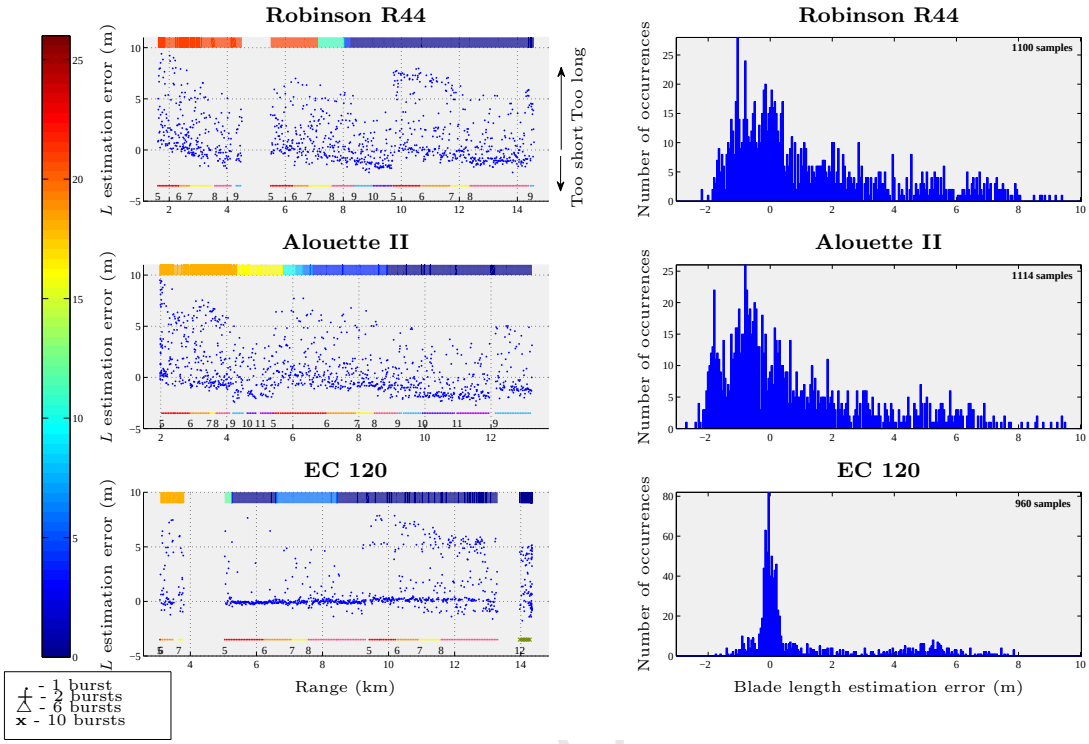

Figure 4.42: The blade length estimation errors and error distribution using the maximum intensity method for the R44, the Alouette II and EC 120 over range for the outbound run of the racecourse profile.

analysing the results shown in Figure 4.42 it seems once again that the estimated blade length errors are considerably more scattered when using with the maximum intensity method. It does however appear that, when very accurate results are obtained, the variance of the error is much smaller than for the case of the entropy method. This can be seen from the data given of the EC 120. Very accurate results are shown with a small variance compared to that of the other helicopter, which can also be seen in the histogram of the error. By comparing this to the results for the same helicopter shown in Figure 4.34, this hypothesis seems to hold true.

It would therefore be more effective to use both methods for estimating the blade length. The entropy method can be used first in a rough search space, and then the maximum intensity method can be used in a finer search space in the IRT process to obtain a more accurate estimation of the blade length.

The results for the AS 350B, the Robinson R22 and lastly the EC 130 are shown in Figure 4.43.

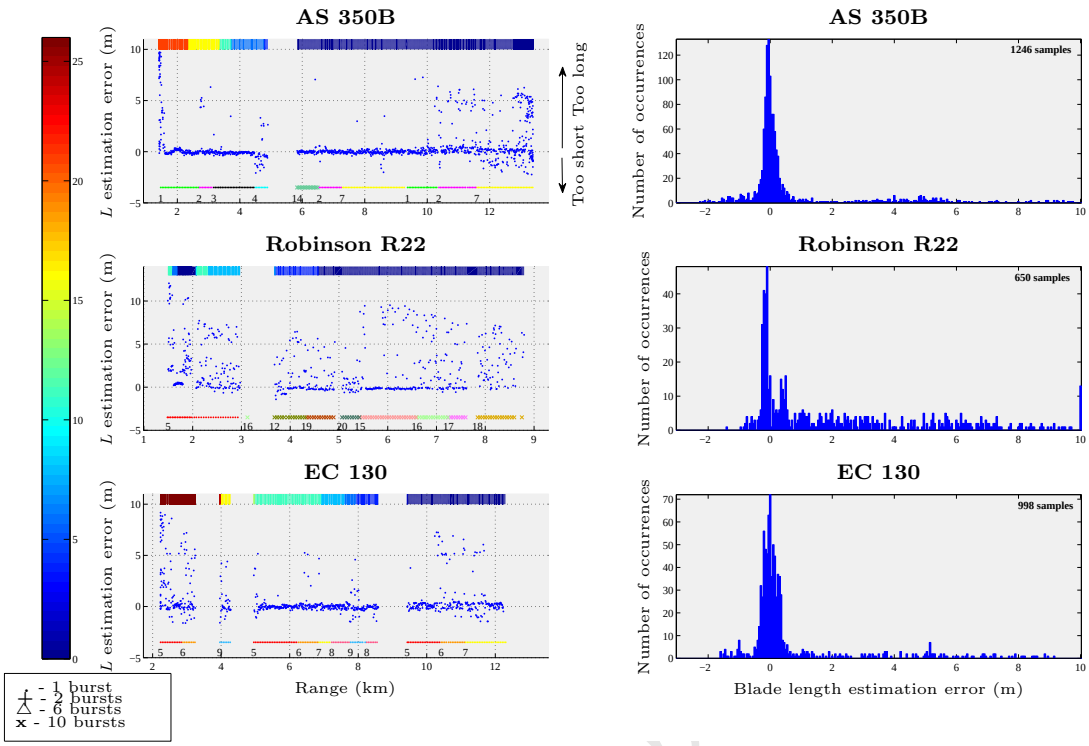

Figure 4.43: The blade length estimation errors and error distribution using the maximum intensity method for the AS 350B, Robinson R22 and EC 130 over range for the outbound run of the racecourse profile.

The hypothesis discussed above is once again confirmed by analysing the results from Figure 4.43. Very accurate results are obtained for parts of the data, with a small variance in the statistics of the errors.

4.3.2 Racecourse profile - Inbound run

The results from an inbound run are shown in this section for a range between 2 and 14 km. Some of the helicopters' data over the complete range is not shown because some data files were corrupt. In some other cases, waveforms with a too low PRF were used, which caused the Doppler spectrum data to alias. Since the proposed algorithm requires a minimum PRF equal to the Doppler frequency at the blade tip, these data files could not be used.

Results from the entropy method

Figure 4.44 shows the probability of correct identification off all nine helicopters in the database by using the entropy method to calculate the rotation rate of the main rotor.

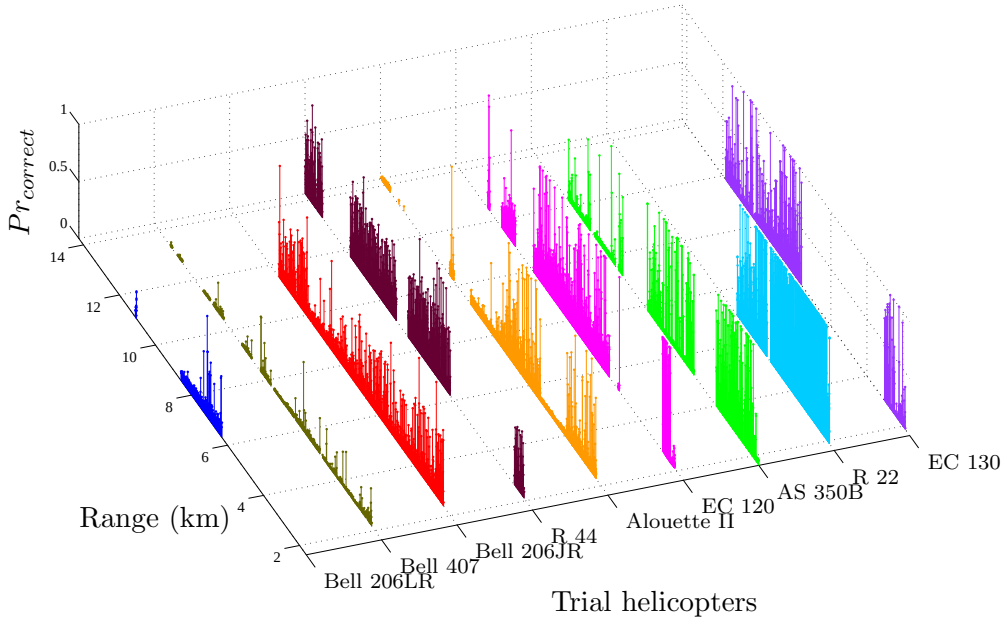

Figure 4.44: Probability of correct identification for an inbound run between 2 and 14 km. The blade parameters were determined by using the entropy method. The results for all the helicopters used in the trial are shown, with each helicopter indicated on the x-axis.

One of the limitations of the HBM algorithm is highlighted by Figure 4.44. The probability of correct identification for the AS 350B and EC 130 is high, except for very small ranges. At these small ranges the helicopters were performing a teardrop turn to start the next outbound run. The position of the angled rotor blades, i.e. not in the horizontal plane, caused the return Doppler signal to have a much lower tip Doppler frequency. The HBM algorithm would therefore give lower estimates of the blade length, resulting in misidentification.

The algorithm does not perform very well for the 4-bladed helicopter, the Bell 407. There are two possible explanations for this. There are a large number of helicopters in the class of four rotor blades, which have similar blade lengths (see Figure 2.7 in Chapter 2). The estimated parameters therefore need to be extremely accurate in order to identify this helicopter correctly. Contributing to this problem is the fact that the IRT process does not form a very focused image of the four blade tips, resulting in poor estimation of the

blade length. As a result of this the question of whether the HBM method can be used for helicopters with four main rotor blades or more forms part of the future work discussed in Chapter 5.

Figure 4.45 shows the blade length estimation error for the Bell 206LR, Bell 407 and Bell 206JR.

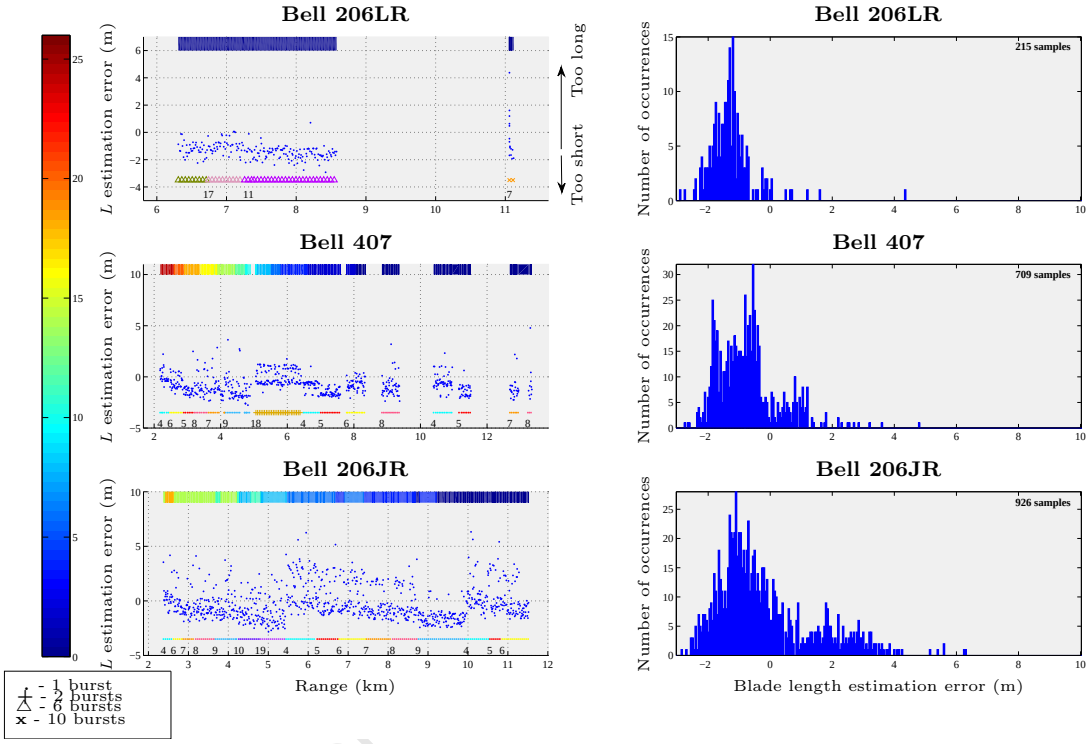

Figure 4.45: The blade length estimation errors and error distribution using the entropy method for the Bell 206LR, Bell 407 and Bell 206JR over range for the inbound run of the racecourse profile.

The waveforms indicated by a triangle used 6 HBM bursts followed by one tracking burst, whereas the waveforms indicated by a cross had 10 consecutive HBM bursts. The waveforms indicated by a plus sign had 2 HBM bursts for every tracking burst. The variance of the error for the three helicopters is quite large, as can be seen in the histogram of the blade length estimation error and once again the mean value is offset to have a negative blade length estimation error.

Figures 4.46 and 4.47 give the percentage duty cycle and the PRF of the various waveforms (indicated by the different colours in the figure) for the data used in Figure 4.45.

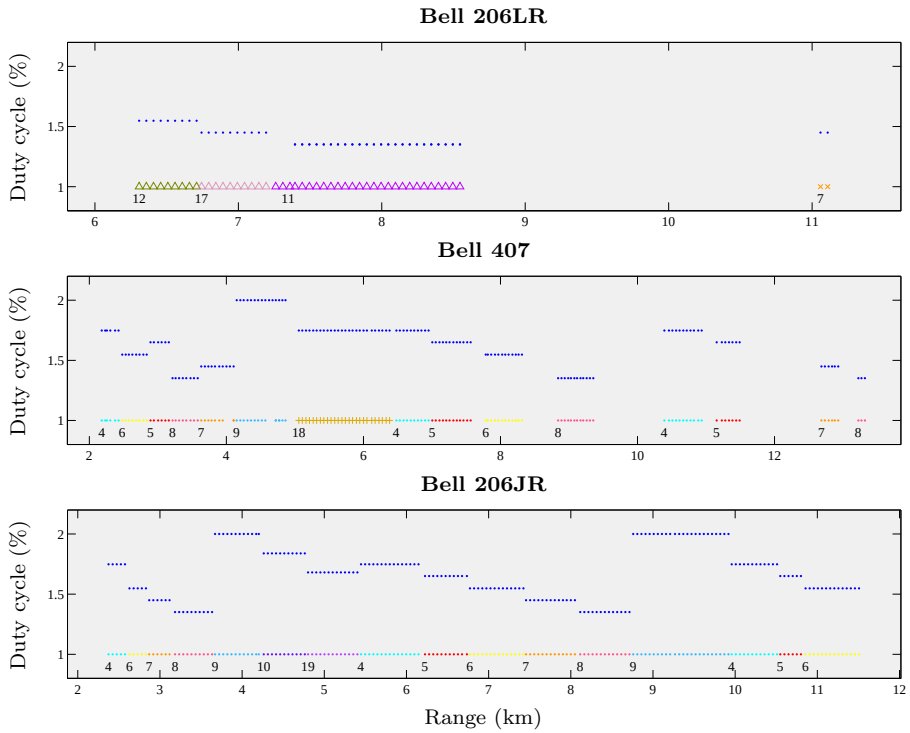

Figure 4.46: The duty cycle of the various waveforms used for the Bell 206LR, Bell 407 and Bell 206JR over range for the inbound run of the racecourse profile.

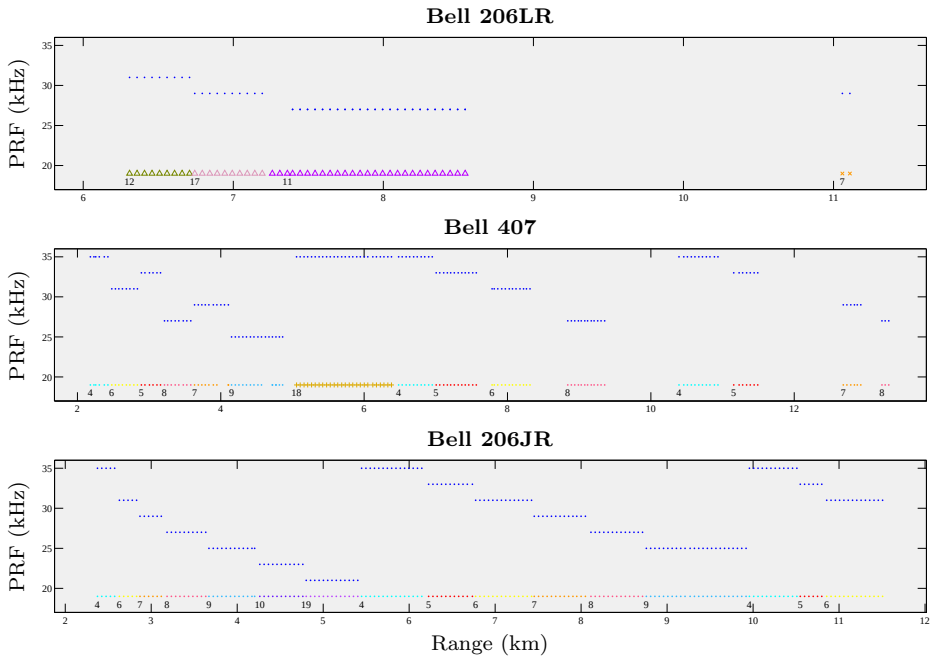

Figure 4.47: The PRF of the various waveforms used for the Bell 206LR, Bell 407 and Bell 206JR over range for the inbound run of the racecourse profile.

The results for the Robinson R44, the Alouette II and the EC 120 are given in Figure 4.48.

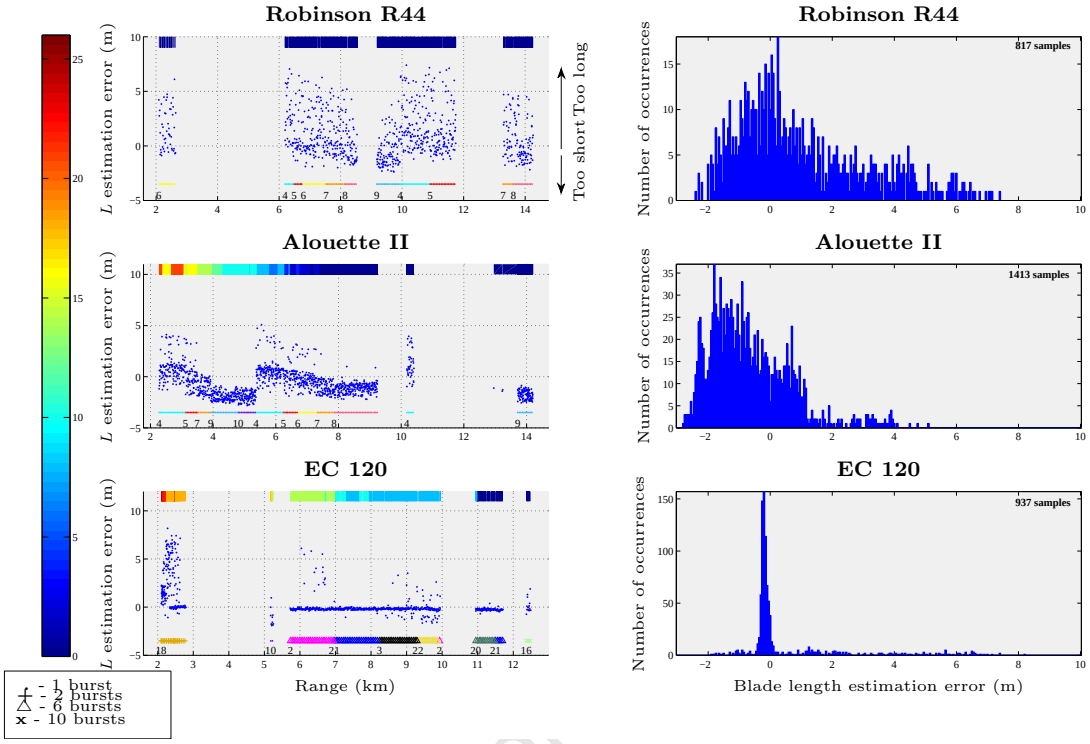

Figure 4.48: The blade length estimation errors and error distribution using the entropy method for the R44, Alouette II and EC 120 over range for the inbound run of the racecourse profile.

The results from Figure 4.48 show that for both the Robinson R44 and the Alouette II the estimated errors are very scattered, causing a very large variance in the estimated errors. When examining the data for the Alouette II at approximately 5 km, a large jump occurs when the waveforms are switched from 10 to 4. The duty cycle decreases for these two waveforms but the radar attenuation factor was lowered at exactly that moment. This could therefore be a possible reason for the change in estimation error.

As mentioned before a very important aspect in the performance of the algorithm is that of the optimal waveform to use for these measurements. The results for the EC 120 show very accurate blade length estimations with a very small variance in the estimated error. The waveform used for the majority of this measurement had 6 HBM bursts for every tracking burst. It would seem therefore that more accurate results can be obtained by only using waveforms with more than one HBM burst.

The duty cycles of the waveforms used for the measurements of the three helicopters are shown in Figure 4.49.

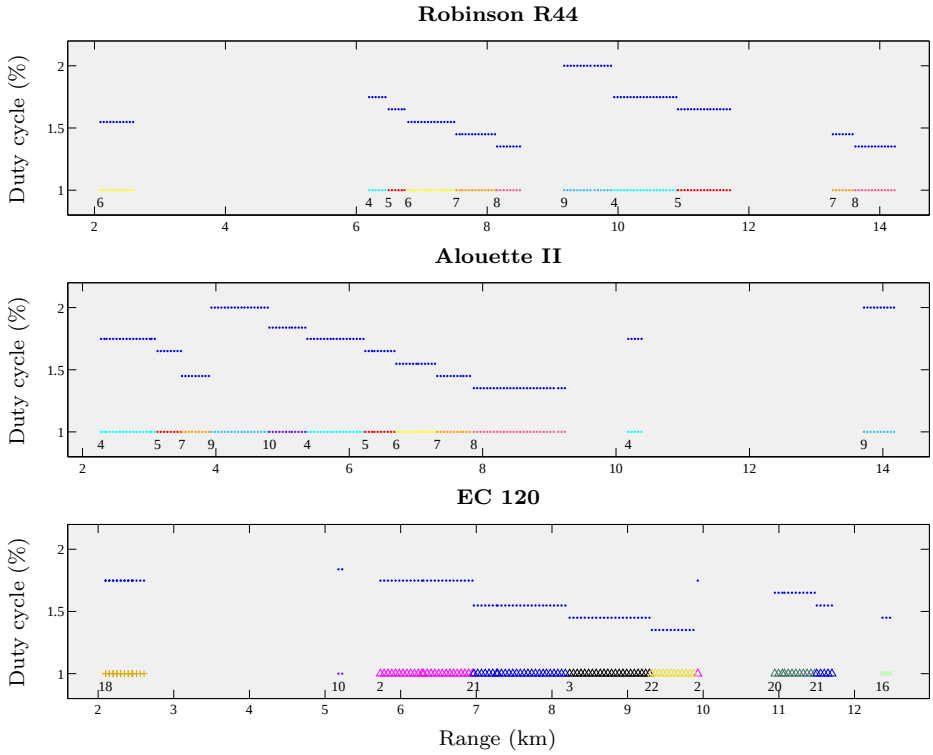

Figure 4.49: The duty cycle of the various waveforms used for the Robinson R44, Alouette II and EC 120 over range for the inbound run of the racecourse profile.

Figure 4.50 shows the PRFs for the waveforms used during the measurements for the R44, Alouette II and the EC 120.

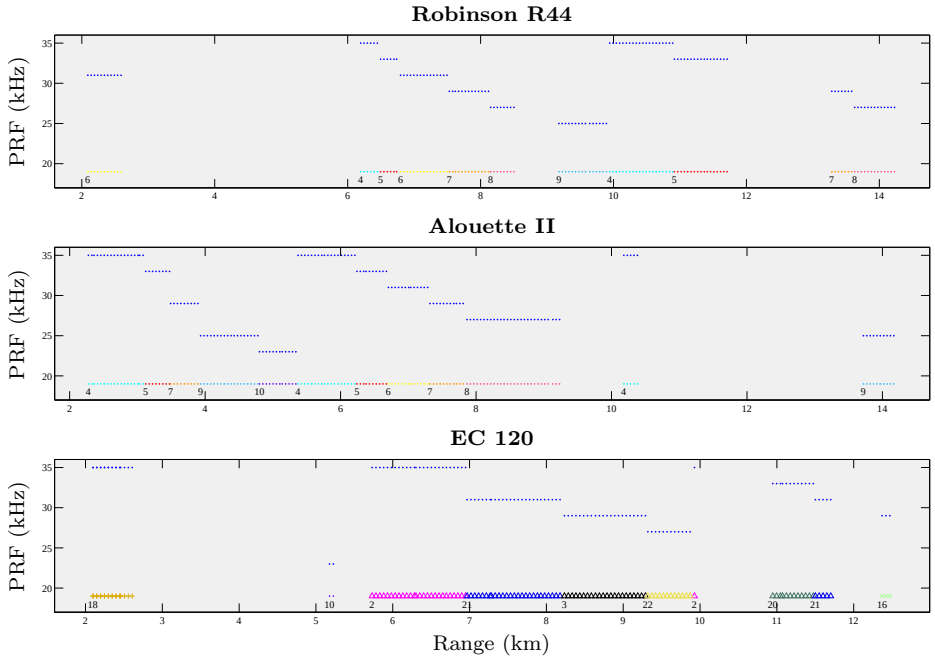

Figure 4.50: The PRF of the various waveforms used for the Robinson R44, Alouette II and EC 120 over range for the inbound run of the racecourse profile.

Figure 4.51 shows the estimated blade length errors for the AS 350B, Robinson R22 and EC 130.

The results from Figure 4.51 show that even for waveforms with only one HBM burst accurate results with a very small variance can be obtained (see the Robinson R22). The results for the AS 350B show a very interesting distribution of the error, where two clusters are formed. All the waveforms used for the measurements of the EC 130 have 10 HBM bursts.

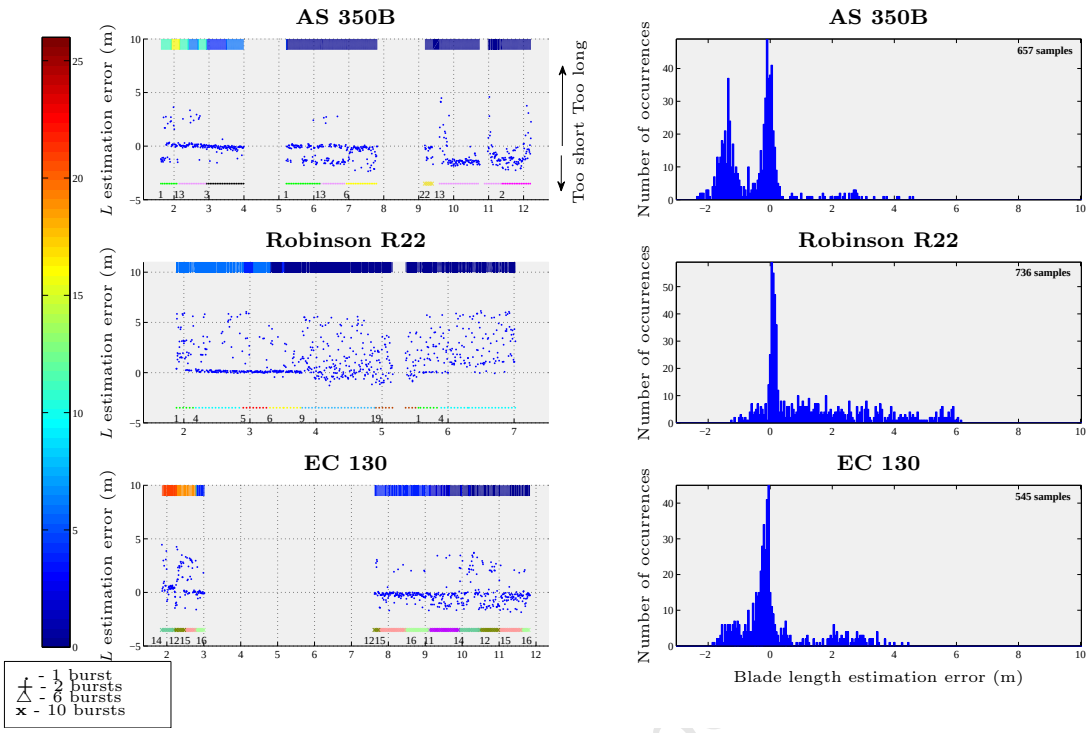

Figure 4.51: The blade length estimation errors and error distribution using the entropy method for the AS 350B, Robinson R22 and EC 130 over range for the inbound run of the racecourse profile.

The duty cycles and PRFs for the various waveforms are shown in Figures 4.52 and 4.53.

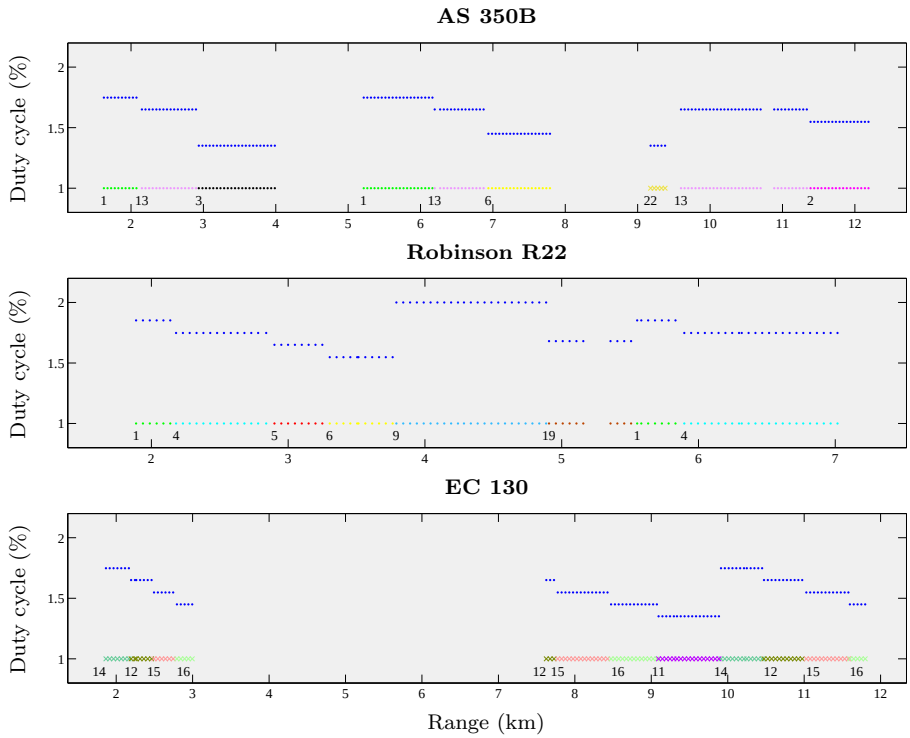

Figure 4.52: The duty cycle of the various waveforms used for the AS 350B, Robinson R22 and EC 130 over range for the inbound run of the racecourse profile.

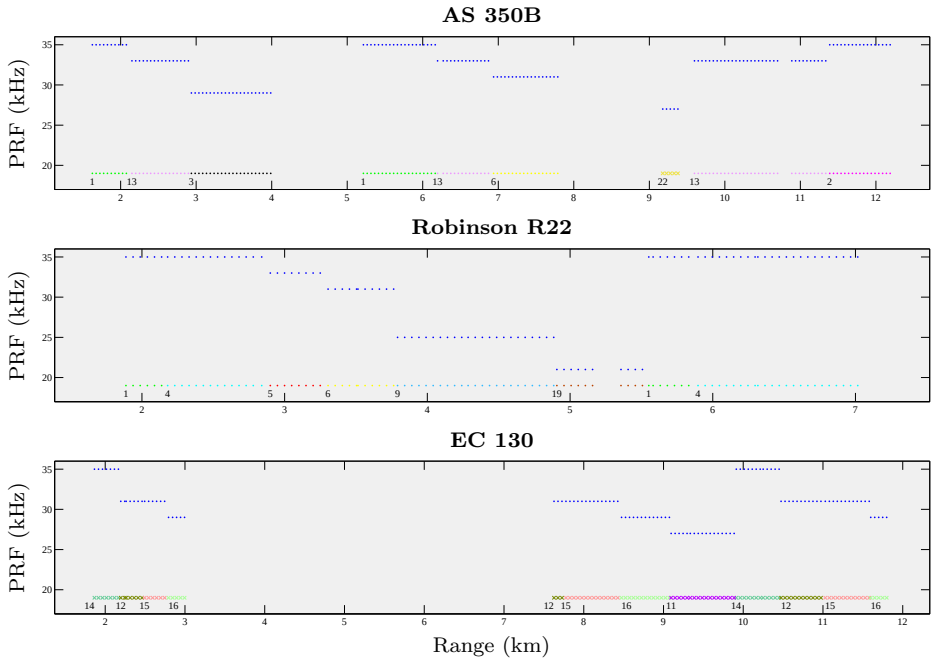

Figure 4.53: The PRF of the various waveforms used for the AS 350B, Robinson R22 and EC 130 over range for the inbound run of the racecourse profile.

Results from the maximum intensity method

To compare the results of the above entropy method with those of the maximum intensity method, Figure 4.54 shows the probability of correct classification for the measured helicopter data in an inbound run using the maximum intensity method.

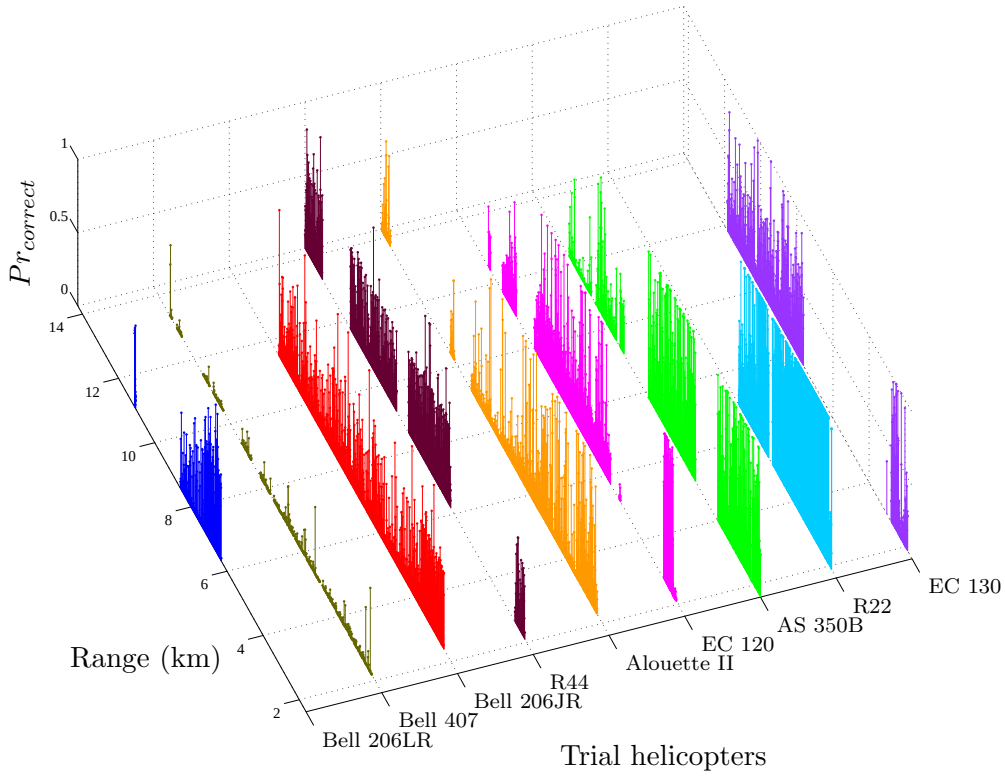

Figure 4.54: Probability of correct identification for an inbound run between 2 and 14 km. The blade parameters were determined by using the maximum intensity method. The results for all the helicopters used in the trial are shown, with each helicopter indicated on the x-axis.

Figure 4.54 shows that higher probabilities were obtained for the Bell 407 and EC 120 by using the entropy method, which is in contrast with what was seen in the outbound run. The poor results for the EC 120 may be due to interference signals from the radar, since the algorithm performed relatively well for this helicopter in the outbound run. The Robinson R44 has promising results even at a range of 14 km.

The same analysis of the estimated blade length errors in the inbound run are once again shown for the maximum intensity method. Figure 4.55 shows the results from the measurements of the Bell 206LR, Bell 407 and Bell 206JR.

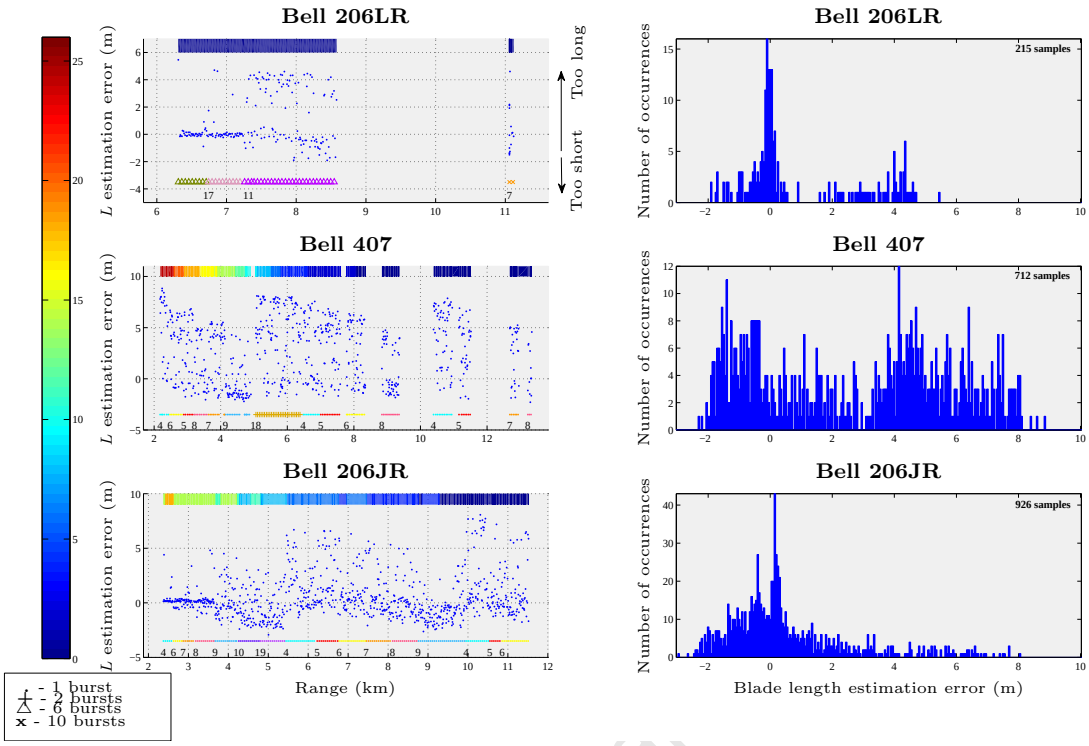

Figure 4.55: The blade length estimation errors and error distribution using the maximum intensity method for the Bell 206LR, Bell 407 and Bell 206JR over range for the inbound run of the racecourse profile.

Figure 4.55 shows that, as in the case of the maximum intensity method for the inbound run data, the blade length estimation errors are very scattered especially for the four-bladed Bell 407, irrespective of the number of HBM bursts in the waveform (see waveform 18). By comparing these results with Figure 4.45 it would seem that the entropy method gives more accurate results, although the errors are still very scattered.

Figure 4.56 shows the results from the inbound measurements of the Robinson R44, Alouette II and EC 120.

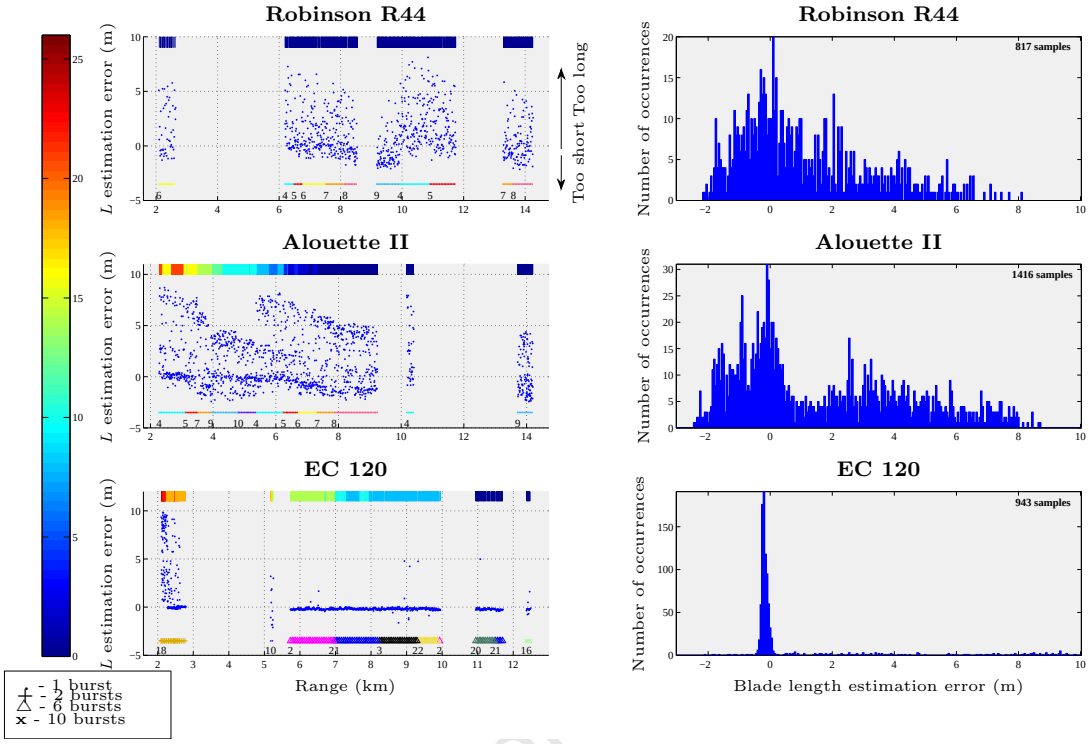

Figure 4.56: The blade length estimation errors and error distribution using the maximum intensity method for the R44, Alouette II and EC 120 over range for the inbound run of the racecourse profile.

For the first two helicopters, the R44 and the Alouette II, the blade length errors are very scattered, once again more so than in the results from the entropy method. In contrast, the results for the EC 120 are once again very accurate, with a very small variance in the distribution of the errors. This was again for a waveform with 6 HBM bursts for every tracking burst (see Appendix A for a detailed description of the waveforms).

Finally, Figure 4.57 shows the results from the maximum intensity method of the AS 350B, the Robsinson R22 and the EC 130 while performing an inbound run.

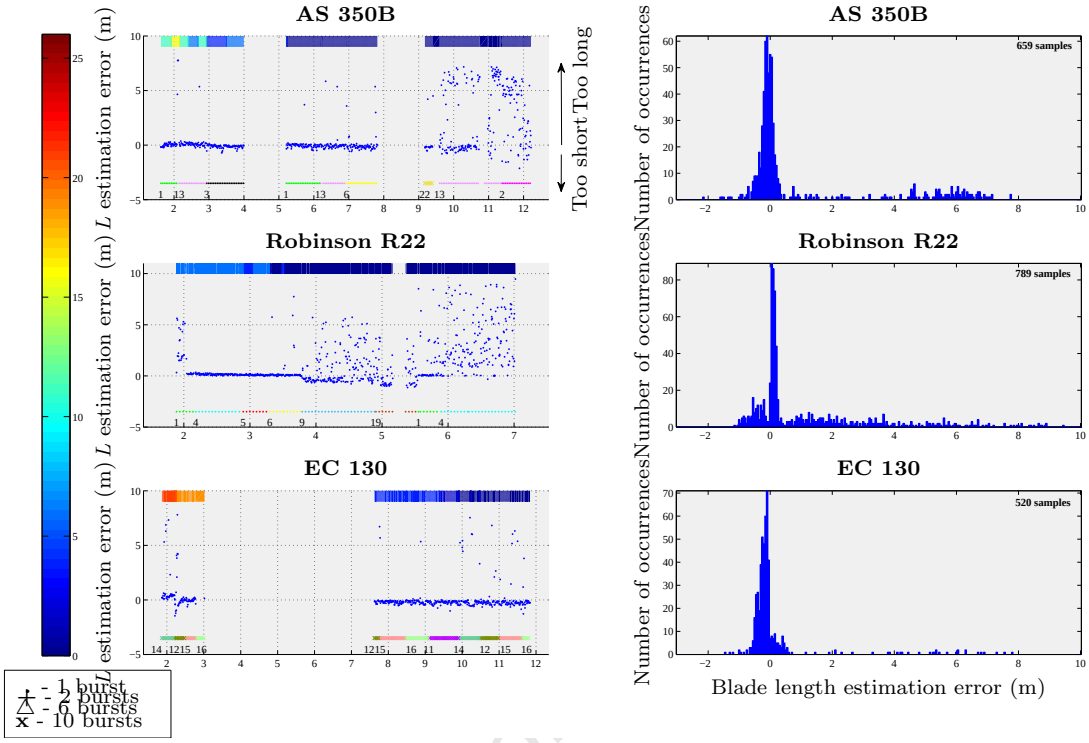

Figure 4.57: The blade length estimation errors and error distribution using the maximum intensity method for the AS 350B, Robinson R22 and EC 130 over range for the inbound run of the racecourse profile.

Very accurate blade length estimations were obtained from the maximum intensity method for all three helicopters. This is shown by all three figures in the right hand column of Figure 4.57. Even at a range of 12 km accurate results were achieved for the EC 130. Other than in the previous cases it should be noted that, irrespective of the waveform, these results were obtained together with a fairly constant attenuation factor.

From the analysis of the racecourse profile done in this section it shows that, by carefully choosing the correct waveform and processing method, accurate blade length estimations can be made. There are several possible reasons why some large blade length estimation errors do occur (errors up to 10 m), and although none of these possible reasons can be formally proven, the results obtained are still very valuable since a number of new insights have been gained by analysing them.

4.3.3 Circling hover profile

The probability of correct identification for all the trial helicopters performing the circling hover profile is discussed in this section. Since the range of the helicopters was relatively constant, varying from 2.5 to 3.3 km for the different helicopters, the probability of correct identification is shown over time. The number of data chunks was not the same for every helicopter, as a result of which the time for each helicopter differs. Data files with a non aliasing waveform were chosen for each of the hover profiles, as well as files with no interference from the radar system. Therefore the results for some of the helicopters are only for small time intervals. Figure 4.58 shows the probability of correct identification for all the helicopters used in the trial, performing the circling hover profile.

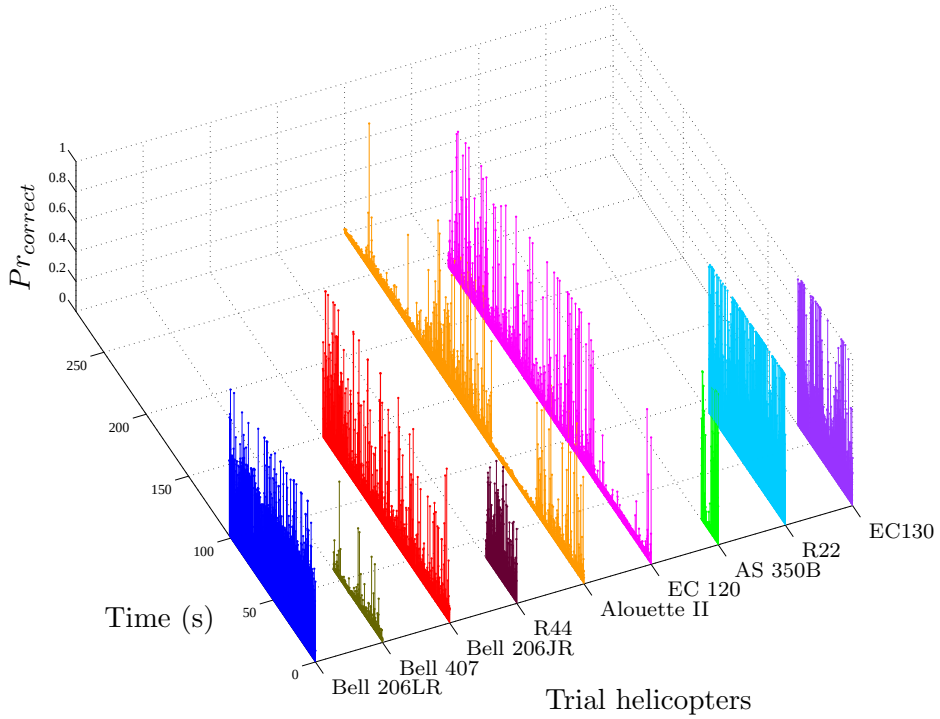

Figure 4.58: Probability of correct identification vs time for the circling hover profile. The blade parameters were determined by using the entropy method. The average range for the helicopters is 3 km.

Both the EC 130 and the R22 have very high probabilities of correct identification. Despite the fact that the Bell 206LR and Bell 206JR are in a class of helicopters in the database with very similar blade lengths, the probability of correct identification for both helicopters are on average above 60% for this hover profile. The results for the Bell 407, however, is not good, even at this close range of 2.8 km. Figure 4.59 gives the probabilities

for the different helicopters by using the maximum intensity method to estimate the main rotor rotation rate.

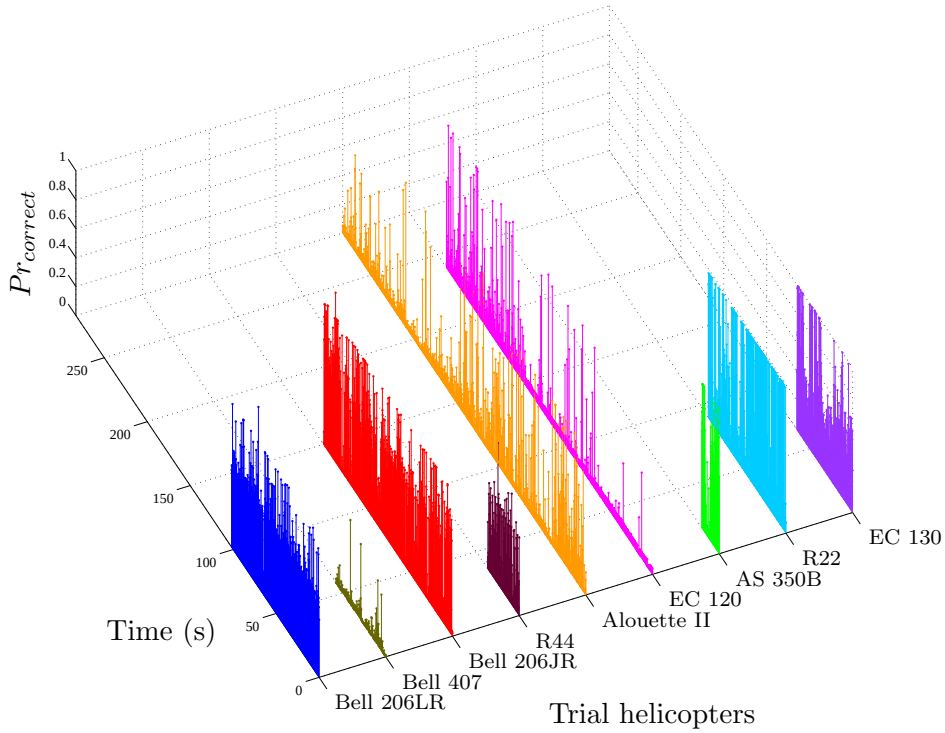

Figure 4.59: Probability of correct identification vs time for the circling hover profile. The blade parameters were determined by using the maximum intensity method. The average range for the helicopters is 3 km.

Comparing Figures 4.58 and 4.59 suggests that the results for the two estimation methods are very similar, unlike the previous two cases (inbound and outbound data). For most of the helicopters the algorithm gives good estimated values.

4.3.4 Descending profile

The probability of correctly identifying the helicopter performing the descending profile is presented in this section. At close ranges to the radar the probability of correct identification decreases, since the helicopter is behind the hill. The range at which the track of the helicopter is lost is not identical for each helicopter, since some helicopters descended earlier than others. This range from 2.5 to 3.5 km is shown in the figures presented in this section. Figure 4.60 shows the probability of correct identification given the entropy method of estimating the blade parameters.

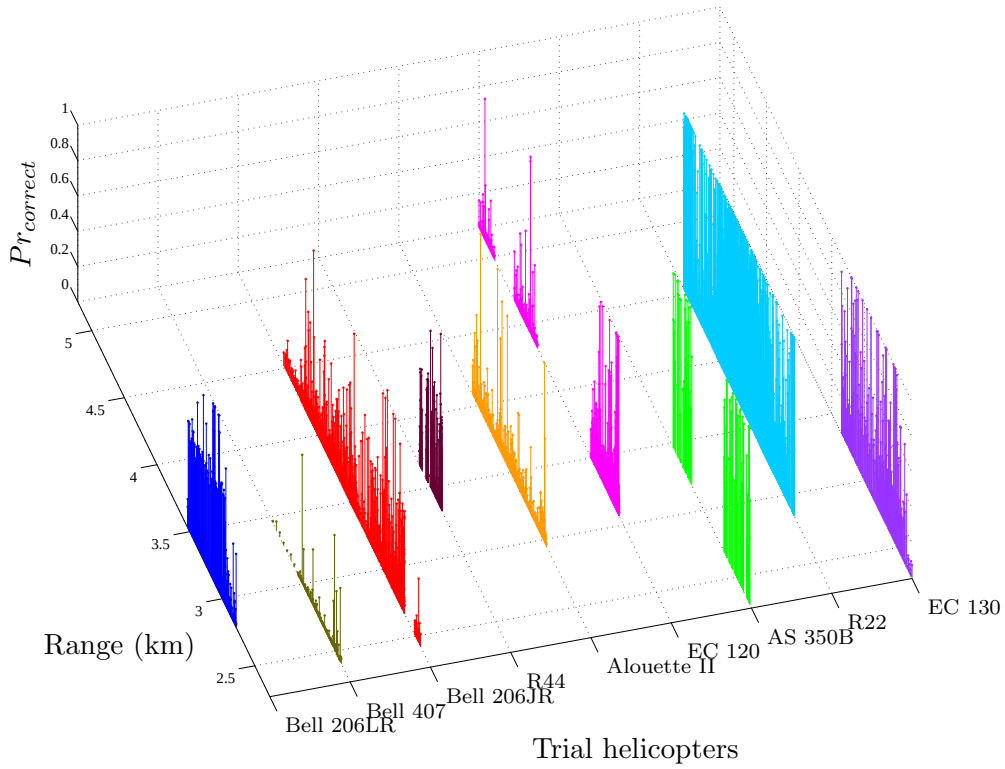

Figure 4.60: Probability of correct identification for the descending profile. The blade parameters were determined by using the entropy method. The results for all the helicopters used in the trial are shown, with each helicopter indicated on the x-axis.

Once again the algorithm gives very good results for the R22 but performs badly for the Bell 407. The decrease in the probability at close ranges can be seen in the Bell 206LR, Bell 206JR and EC 130. Figure 4.61 shows the results obtained by using the maximum intensity method for the same descending profile data.

Figure 4.61 shows very similar results as Figure 4.60. The probability of correctly identifying the Bell 407 is again very low, but a higher probability is obtained for the EC 120. The results from this section showed that, trying to separate the helicopter blade from the body of the helicopter does not give a significant gain in the accuracy of the blade parameter estimations.

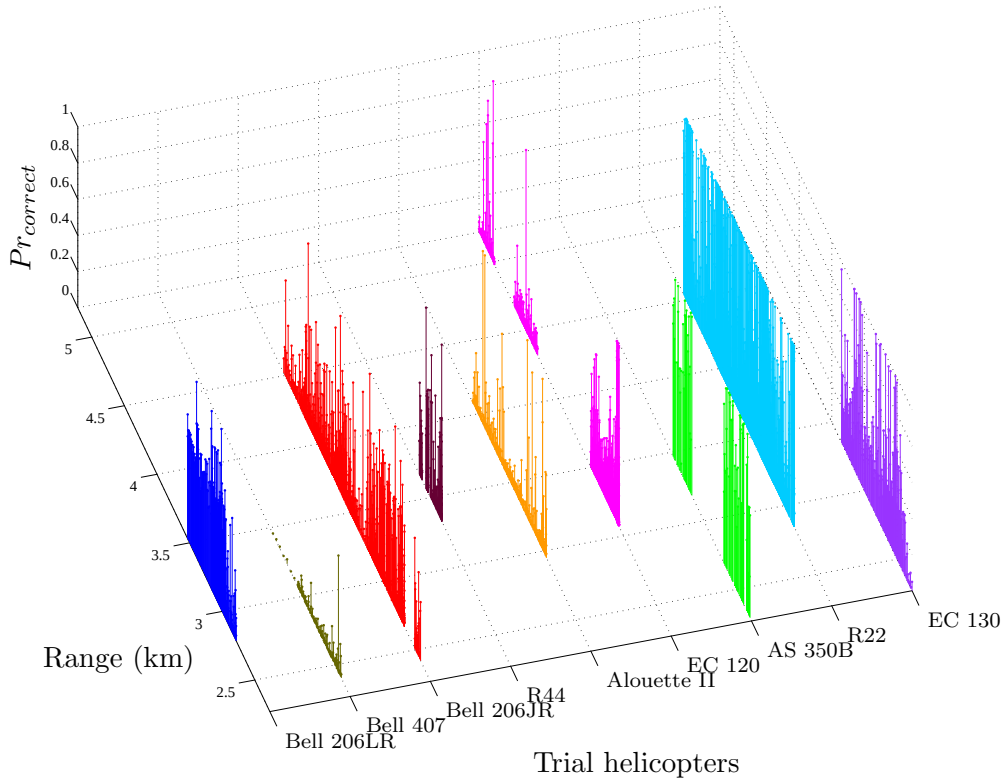

Figure 4.61: Probability of correct identification for the descending profile. The blade parameters were determined by using the maximum intensity method. The results for all the helicopters used in the trial are shown, with each helicopter indicated on the x-axis.

4.4 Summary

This chapter gave a detailed account of the helicopter trial that was conducted and discussed all the various aspects of the trial. By showing some of the results from the trial, this chapter proved that the HBM technique gives promising results that will aid in the process of identifying a helicopter according to make and model.

The final section in this chapter gave a more detailed analysis of all the helicopters performing the different flight profiles. The probabilities of correct identification for the nine helicopter were shown for each profile as well as a detailed analysis of the blade length estimation error over range. The results obtained with both methods that were used to estimate the main rotor rotation rate are shown and compared for each flight profile. The analysis of the estimation error included the change in waveform, PRF, radar attenuation factor and duty cycle for the results obtained. This was performed to gain a better understanding of the performance of the algorithm, and to determine

under which circumstances the algorithm did not perform well. As future work the design of an optimal set of waveforms could flow from this analysis. The probability of correct identification of each helicopter was performed by firstly separating the helicopters according to the number of blades. The performance of the algorithm was then shown for increasing ranges in the outbound and inbound runs of the racecourse profile. Although this is not a formal SNR analysis of the HBM algorithm, it shows the performance of the algorithm for decreasing SNR values. This section also indicated some of the limitations of the algorithm, which will be addressed in the final chapter.

The conclusions and research question for future work are discussed in the following chapter, which also presents some of the current known limitations of the algorithm.

Chapter 5

Conclusions and future work

This chapter gives the conclusions of the research presented in this dissertation. It gives a detailed summary of the work, as well as some of the limitations of the proposed technique. The research questions that arose from this work are discussed in the section on future work.

5.1 Conclusions

Chapter 2 introduced the problem of using the radar return signal from a helicopter to aid in the identification of a target. A summary was given of the research presented in open literature, highlighting some of the methods used to address the problem of target identification. Some papers showed that by exclusively knowing the number of main rotor blades,N, the blade length, L, and the rotation rate of the main rotor, r_ω, the positive identification of a helicopter becomes possible.

Chapter 2 concluded with a helicopter separability analysis based on a database developed at the CSIR to determine to what extent the helicopters can be separated from one another by using the three blade parameters. This study determined the required accuracy of the estimated parameters in order to separate the helicopters from one another. The study showed that, if the number of main rotor blades is known and the helicopters are sorted accordingly, the probability of correct identification increases by up to 13% for the helicopters with two main rotor blades, given a blade length estimation error of 0.1 m. For other classes, such as helicopter with six main rotor blades, however, this

probability is lower by almost 20% given an estimation error of 0.1 m. The reason is that three of the helicopters from that class have the same blade length.

The study also showed that the rotation rate of the main rotor can be used to aid in the identification of a helicopter, although this value is not published for all the helicopters in the database. Unlike the blade length, the rotation rate of the main rotor is not a fixed value due to the design of the rotor. Depending on wind conditions or the manoeuvre of the helicopter, this value can change with relation to the ground truth value (as given in the database). This implies that, even though the rotation rate can aid in the identification of a helicopter, it should not be used in isolation.

Chapter 3 discussed the mathematical analysis of the micro-Doppler effect caused by the main and tail rotors of a helicopter. The mathematical expression of a blade flash was introduced, showing that a blade flash occurs when the turning blade is perpendicular to the radar. The return signal contains Doppler frequencies over the entire blade when the flash occurs. The chapter also showed the RCS of a single blade flash, modelled on the RCS of a flat plate. This model was adjusted to take the leading edge of the blade into account, and a half-cylindrical form was used to estimate the RCS of the blade flash.

The time varying distance from the radar to the blade tip of the main rotor was derived in Chapter 3. The equation expressed as

$$R(t) = R_0 + L\cos\theta(t) \tag{5.1}$$

shows that, apart from the range to the target R_0, a time varying sinusoidal term $\cos\theta(t)$ represents the range from the blade tip to the radar. By taking the time derivative of Equation 5.1, the velocity of the blade tip as a function of time was determined. The expression in Equation 5.1 implies that a sinusoid resulting from the rotating blade tips can be seen in the time-frequency data of the return signal. A point scatterer model was introduced in the chapter to show the key characteristics of the micro-Doppler effect in helicopters: the blade flash and the sinusoidal tip scattering. The Doppler spectrum of the simulation showing these two effects was verified by the mathematics shown in the chapter.

A helicopter blade parameter estimation algorithm was developed and presented in Chapter 3. This algorithm uses the time-frequency domain data of the return signal, for either simulated or measured data, and by using a tomographic imaging technique estimates the number of blades (N), the blade length (L), and rotation rate of the main rotor (r_ω).

The chapter discussed the different processing steps of the algorithm in detail, showing examples of measured data to illustrate each processing block. The chapter concluded that, although the HBM algorithm has been verified with simulated data, it needs to be validated with measured helicopter data to determine the performance and stability of the algorithm.

Chapter 4 presented a detailed description of the helicopter trial conducted in Pretoria. The aim of the trial, different targets and flight profiles were discussed in the chapter. Nine civilian helicopters were used during the trial from the two-, three- and four-bladed helicopter classes in the database. Three different flight profiles were designed - each profile testing the performance of the algorithm in different scenarios. Examples of some of the results from the trial were shown for a few helicopters, which performed the various flight profiles. The results showed the estimated blade parameters as well as the estimation error made by the algorithm. The data for each example was shown, as was the focused IRT image of the blade tips.

The final section in Chapter 4 presented the results for all the helicopters performing all the flight profiles. The results are shown in the form of a probability of correct identification given the estimation of the blade parameters for the helicopters over range. The results for the racecourse profile give an indication of the performance of the algorithm over decreasing SNR values, as the range increases. The results for both statistical methods used to estimate the rotation rate of the main rotor are shown. By comparing these two methods, it seems that for some scenarios, such as the racecourse profile, the maximum intensity method gives more accurate estimations, whereas the opposite is true for the hover profile.

These results showed that, for certain helicopters such as the AS 350B, the algorithm performs well for ranges up to 14 km. For other helicopters, such as the Bell 407, the algorithm does not perform well even at close ranges.

For the inbound and outbound runs of the racecourse profile the blade length estimation error was also shown against range, together with the distribution of this error. The aim of this analysis was to investigate possible causes for some of the very large errors that occurred even at close ranges. The various waveforms together with the radar attenuation factor, duty cycle and PRF of the measurements were indicated on the graphs to determine whether a relationship exists between the increasing absolute error and the change in waveform, PRF, duty cycle or attenuation factor. From this analysis it

was further found that careful planning regarding the waveform design is required. In general blade length estimation errors for all nine helicopters during both the inbound and outbound runs had the smallest value for waveforms with two or more HBM bursts in a pattern.

The two methods used to estimate the blade parameters namely the entropy method and maximum intensity method were both evaluated and it seems that the entropy method gives more accurate estimations over a large data set, however, with a higher variance in the error than achieved with the maximum intensity method. The latter method showed that from some cases, especially with waveforms containing only one HBM burst, the errors of the estimated blade length were very large and scattered. For other cases, however, very accurate results were achieved even at ranges beyond 9 km, with very small variances in the error. This analysis therefore showed that it might be a good practise to use both methods, where the entropy method are used to obtain a first estimate of the blade parameters, and then in a fine search space the maximum intensity method can be used, to obtain more accurate results.

5.2 Limitations

Chapter 3 and 4 showed that the HBM algorithm performs well under certain conditions and for certain helicopters. There are, however, several limitations to this algorithm. This section gives a brief discussion of some of the limitations that have been identified during this research.

Aliasing

In order to estimate the blade parameters accurately it was mentioned that a high PRF waveform is required. A requirement of this waveform is that the minimum PRF used during a measurement should be equal to the maximum Doppler frequency at the blade tip. For waveforms with a lower PRF than f_d, aliasing in the Doppler spectrum data will occur, and both the blade flash and sinusoids will be folded over. Figure 5.1 shows an example of measured helicopter data from the trial where the PRF of the waveform was less than the required value.

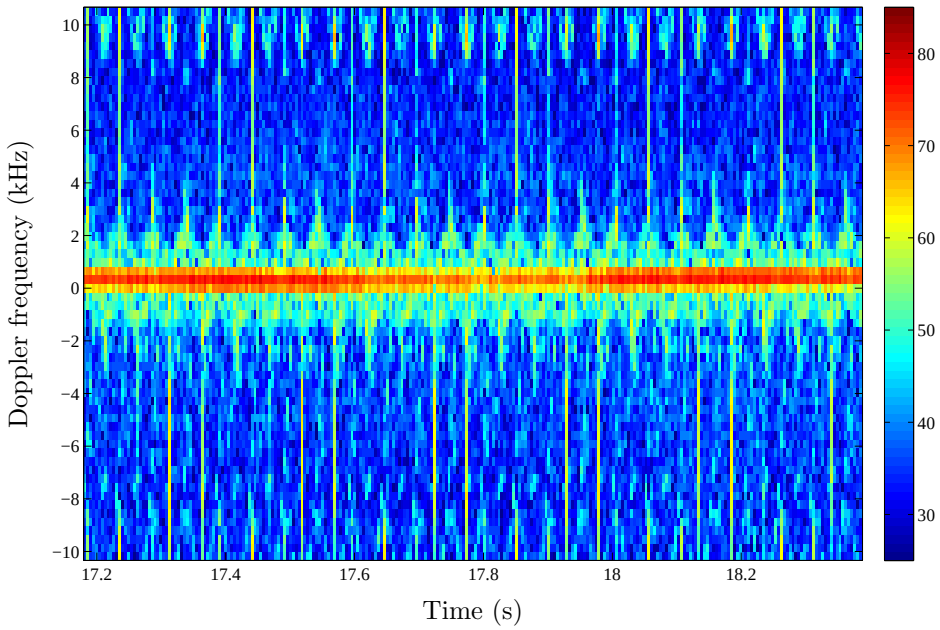

Figure 5.1: Aliased Doppler spectrum data for an EC 130. The PRF of the measurement was 21 kHz, resulting in the aliasing of both the blade flash and the sinusoids.

Figure 5.1 shows the measured data of the EC 130, where a waveform with a PRF of 21 kHz was used for the measurement. Both the blade flash and the sinusoids at the blade tip are aliased. Since the IRT process uses the sinusoids in the Doppler spectrum data as the 1-D projections for reconstructing the 2-D image of the blade tips, the process will not return a focused image of the blade tips, resulting in inaccurate blade parameter estimations. Figure 5.2 shows the IRT image for the data presented in Figure 5.1.

The 2-D images in Figure 5.2 show that, due to the low PRF, the IRT does not produce focused blade tips. The estimated parameters for this case are 3.19 m for the blade length with an estimation error of 1.81 m, and a rotation rate of 474 RPM with an estimation error of 60 RPM.

One method to alleviate this problem is to make two copies of the Doppler spectrum data used as input to the IRT. These copies should then be added above and below the original Doppler spectrum data. By using the top and bottom data, the sinusoids of the original data will be completed and the IRT will receive the completed sinusoids as input.

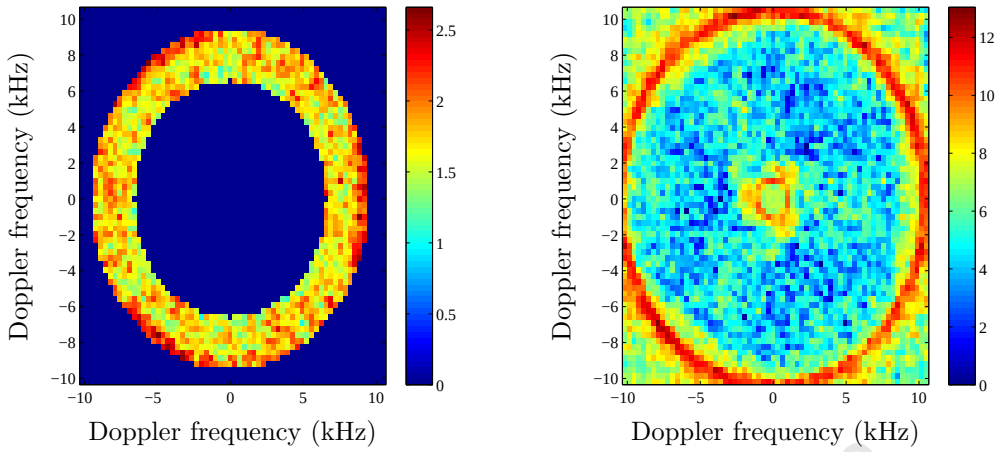

Figure 5.2: 2-D IRT image of the EC 130 measured with a waveform that is ambiguous in velocity. Due to the aliasing of the Doppler data, the IRT does not produce a focused image.

Dwell time

One of the limiting factors of the algorithm is the time interval required for the input to the IRT process. As mentioned in Chapter 3, a processing time of approximately 400 ms is required for the tomographic technique. This inherently implies that the algorithm is best suited for tracking radar purposes, since the dwell time of a search radar is significantly shorter than the required interval. At present the algorithm is therefore limited to tracking radars.

Turning helicopter

Another limitation in the accuracy of the algorithm is encountered in scenarios where the helicopter blades are not in the horizontal plane, for instance, when the helicopter is performing a teardrop turn. Due to the elevation angle of the blade with the horizontal plane, the Doppler return will be lower than when the blades are in the horizontal plane. The reduced Doppler frequency at the blade tip will furthermore result in an estimation error of the blade length. To illustrate this, Figure 5.3 shows measured data of the AS 350B while performing a teardrop turn.

The figure shows that the Doppler frequency of the tail rotor tip is greater than that of the main rotor tip, while the helicopter is making the teardrop turn. Figure 5.4 shows the Doppler-spectrum of the same recording after 16 seconds. The helicopter has finished

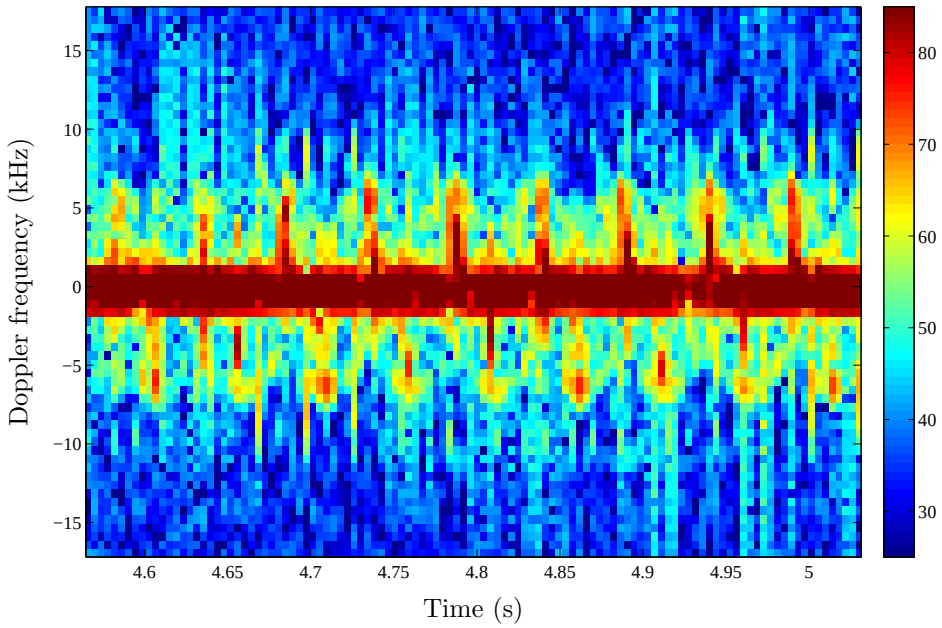

Figure 5.3: Doppler spectrum of the AS 350B while making a teardrop turn. Note the low Doppler frequency of the blade tip, and the higher frequency return of the tail rotor flashes.

the turn and is flying a straight profile once again, with the rotor blade in the horizontal plane.

Note the difference in the Doppler frequency at the blade tip between Figures 5.3 and 5.4. By using the HBM algorithm the blade parameter estimations will be completely inaccurate for the first scenario. The algorithm is therefore designed to give the best results for scenarios where the helicopter blades are in the horizontal plane.

Scattering of helicopter blade tips

By analysing the measured data from the trial it was found that the blade flash and blade tip scattering for some of the helicopters were very small, compared to those of other helicopters such as the AS 350B and Bell 206LR. The R44 is one of the helicopters where the receding blade flashes are sometimes not visible, and where for both the approaching and receding blades the sinusoids from the blade tip scatterers are very small. Figure 5.5 shows the Doppler spectrum data for one of the measurements of the R44, at a range of 3 km.

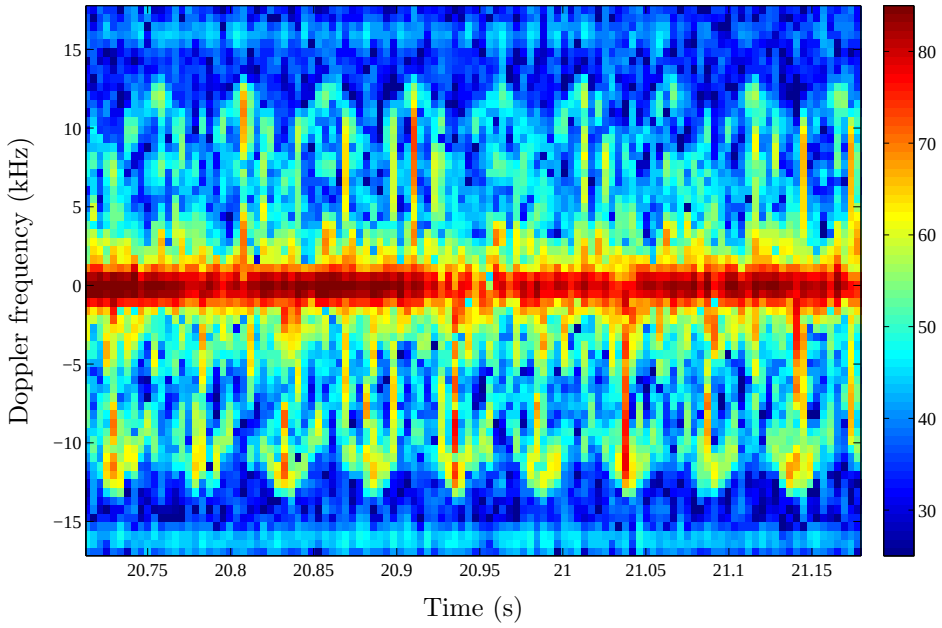

Figure 5.4: Doppler spectrum of the AS 350B after making a teardrop turn.

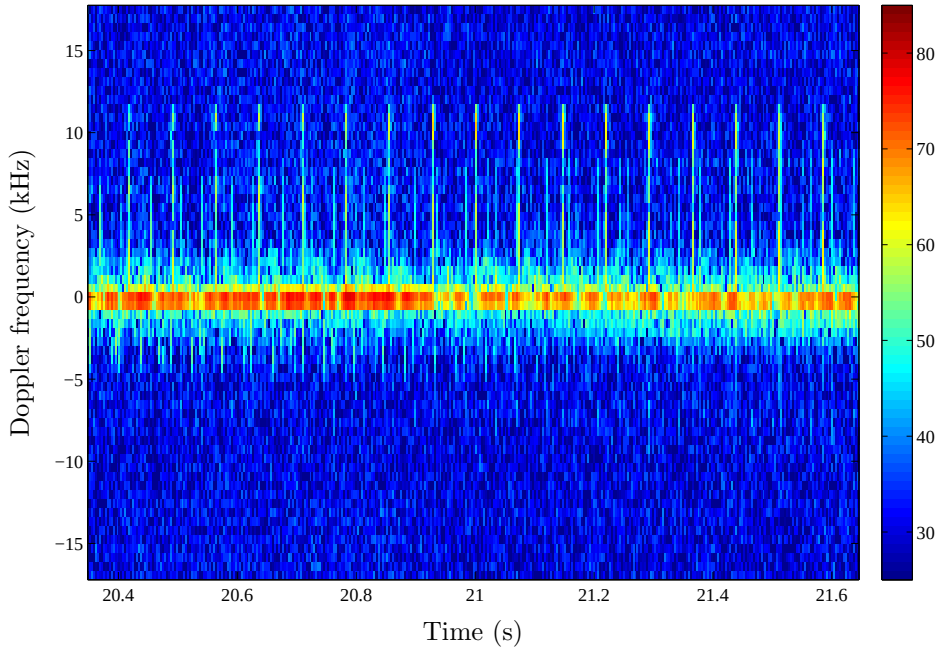

Figure 5.5: Doppler spectrum of the R44 at 3 km. The sinusoids are barely visible at the blade tips, and the receding blade flashes are not seen at all.

The estimated blade parameters from this data would not be accurate at all due to the lack of scattering from the blade tips of the helicopter. This specific helicopter therefore indicates a limitation of the algorithm, in that it is not possible to identify certain helicopters correctly due to the composition of the main rotor blades, which give very small reflections. Although the Doppler spectrum of the R22 showed very similar findings, however since it has the smallest blade length in the database, the probability of correctly identifying a R22 is still very high.

5.3 Future work

During the course of this study several research questions arose, which should be addressed in future research work on the problem of helicopter identification. This section gives some of the topics that should be investigated further.

5.3.1 Tail rotor analysis

The presence of the tail rotor blade was seen in the Doppler spectrum for all the measured data where the aspect angle of the helicopter provided a high Doppler frequency return from the tail rotor. Since the rotation rate of the tail rotor is on average 5 times higher than that of the main rotor, the sinusoids resulting from the tail rotors are not seen in the time-frequency data. This implies that, by using the current method, the number of tail rotor blades and the blade length cannot be determined. However, the number of tail rotor flashes that occur between two consecutive main rotor blade flashes can be determined more easily, given that the helicopter is not flying parallel to the radar. By estimating the number of tail rotor flashes the gear ratio of the helicopter can be determined. This might prove to be another parameter that can be used to aid in the identification of the helicopter. It is also a useful parameter since it is not dependent on the blade length of the main rotor.

5.3.2 Extension of current database

Following on from the previous section the database should be extended to include the gear ratio of the helicopters and the separability study should be extended to determine

whether this parameter would contribute to the positive identification of a helicopter. Only half of the entries in the database have a known main rotor rotation rate. It would be ideal if the rotation rates for all the helicopters were known, so that this parameter can be used for identification purposes.

5.3.3 Helicopter classifier

Although the number of blades, blade length and rotation rate can be estimated for a helicopter to a certain degree of accuracy, it is for many cases not sufficient information to have a positive identification of the target, since a number of helicopters have the same blade parameters. This problem can be addressed by the development of a helicopter classifier that not only takes the three estimated blade parameters into consideration, but also includes valuable information such as the velocity of the target, the altitude of the target and the geographical information of the position of the target. The classifier should also be weighted by the frequency of helicopters occurring in a certain area. Therefore helicopters that occur frequently in a certain area inland should be weighted more in the classifier than a helicopter that is only used for search and rescue missions at the coast.

5.3.4 Analysis of data measured at C-band

In Chapter 4 it has been mentioned that data was recorded by using the Fynmeet measurement radar. The algorithm has only been properly tested on the X-band data measured with MECORT. The next step would be to analyse the Fynmeet data at 6.5 GHz. Lower PRF values were used for this data, but since the transmit frequency is lower, the data is not aliased. Figure 5.6 shows the Doppler spectrum data of a Bell 407 before velocity compensation measured by Fynmeet.

Due to the lower centre frequency, the maximum Doppler frequency at the tip of the blade is lower. Figure 5.6 furthermore shows that the return from the blade flashes as well as the sinusoids from the blade tips are very strong. It is therefore important to analyse the data measured at the lower RF frequency, since it might prove that the algorithm performs better at lower frequencies. This fact was addressed in the paper by Pouliguen *et al.* [8] where the results from a physical optics model of the return signal from a helicopter rotor showed that, for frequencies in the C-band, higher SNR levels for the sinusoids in the time-frequency data were seen.

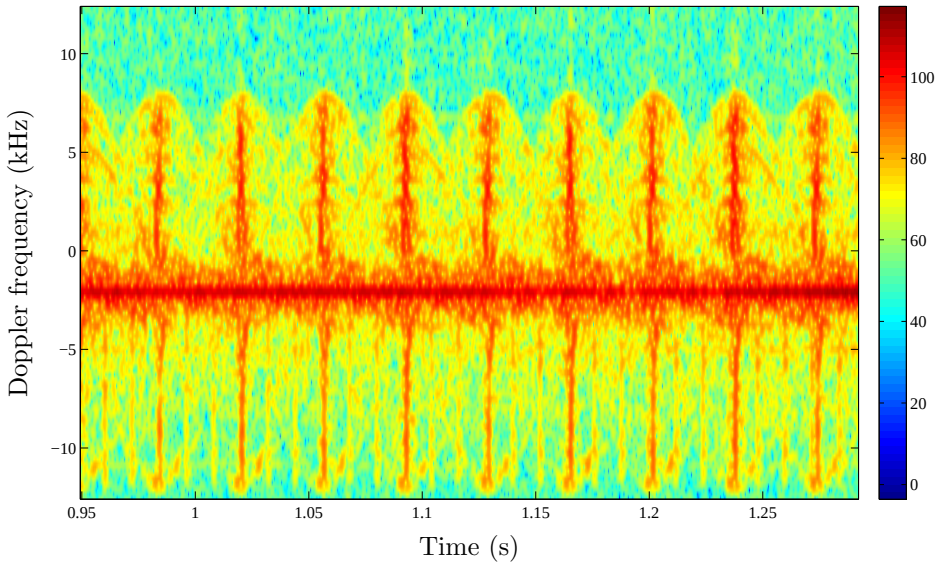

Figure 5.6: Doppler spectrum data before velocity compensation of the Bell 407 recorded by Fynmeet with f_c at 6.7 GHz, and a PRF of 25 kHz.

5.3.5 Polarization

In the paper by Pouliguen *et al.* [8] it is shown that, by using horizontal polarization (HH) the sinusoids in the Doppler spectrum data have a higher SNR than in the case of vertically polarized data. Since the two available radar facilities are vertically polarized, this question needs to be addressed by extending the point scatterer simulation model to account for both types of polarizations. It can therefore be predicted from Pouliguen *et al.* [8] that the performance of the algorithm would improve, given a horizontally polarized antenna. The paper specifically states that the weaker return signals from the receding blades will not be so much weaker than the signal of the approaching blades when using HH polarization.

5.3.6 Signal to noise ratio analysis

Although the probability of correct identification over increasing range has been calculated and presented in Chapter 4, one of the most important aspects to address in the future work is the performance of the algorithm against the SNR. The signal power of the sinusoids in the Doppler spectrum data needs to be determined, rather than the signal power of the blade flash, since the sinusoids are used in the IRT to form a focused 2-D image of the blade tips. One method that can be used to extract the sinusoids from the

Doppler spectrum data is to use the output of the IRT. Since the angular velocity of the blade is estimated by the IRT, this can be used to build a sinusoid that will match the sinusoids in the data. The phase of the sinusoid can also be determined from the IRT. It has been determined that zero phase is at the top part of the IRT image. The sinusoids can then be plotted onto the Doppler spectrum data and used to extract the data from the sinusoids, to estimate the signal power. Figure 5.7 shows this method implemented on Doppler spectrum data of the AS 350B and the three sinusoids are seen fitted onto the data.

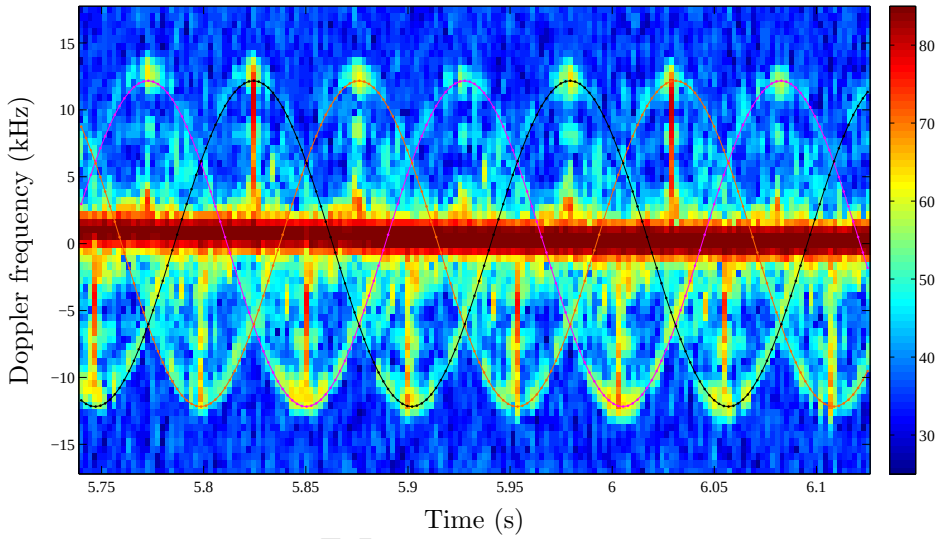

Figure 5.7: Doppler spectrum data of the AS 350B with sinusoids estimated from the IRT process fitted onto the data.

The amplitude of the sinusoids was estimated from the maximum Doppler frequency of the focused blade tip in the focused image of the blade tips. Figure 5.7 shows, however, that the scatterers from the blade tips appear to be not perfectly sinusoidal. While the top half of the sinusoids fits the data well, it appears that the bottom half does not fit the sinusoids. The sinusoids resulting from the tip scatterers appear to have a larger amplitude for the approaching blades, which might imply that the approaching blades turn slightly faster than the receding blades, resulting in a higher Doppler frequency at the blade tip.

The noise of the data in the Doppler spectrum can be determined by using the standard deviation of the Doppler bins at the top and bottom of the figure. The SNR of the input to the IRT can thus be determined. The estimated blade parameters should then be shown against the corresponding SNR.

An important question to address is whether a processing gain is achieved by using the IRT process. This can be determined by using either simulated data or measured helicopter data. For both methods the energy of the focused blade tip can be used to calculate the signal power at the output of the IRT. To calculate the noise by using measured data the areas next to the focused blade tips can be used to estimated the noise power by taking the standard deviation of the data. For simulated data the noise can be determined by taking the spectrogram for generated white Gaussian noise. This noise can be used as input to the IRT, and the standard deviation of the image can be used as an estimate for the noise.

By showing the estimated blade parameters against the SNR of Doppler spectrum data, a thorough understanding of the performance of the algorithm will be formed. These results can furthermore be used to predict the performance of the helicopter for ranges further than those measured during the trial, i.e. beyond 14 km.

5.3.7 Sensitivity analysis of the technique

In order to achieve optimal results from the technique the parameter set that will minimise the blade length estimation error should be investigated. By performing a sensitivity analysis on the parameters given in Equation 3.30 the expected size of the blade length estimation error can be determined given a certain set of parameters. By using such an analysis the optimal parameter set can be determined which will minimize the estimation error.

5.4 Summary

In this research a new method was developed to estimate three helicopter blade parameters from the radar return signal. The study showed that the number of main rotor blades, blade length and rotation rate of the main rotor can be used to aid in the positive identification of a helicopter. The objectives of this research study have been:

- To gain knowledge in the field of NCTR and to review the current work on blade modulation and the methods proposed in order to use this as an aid in identifying helicopters.

- To develop a simulation model that demonstrates the micro-Doppler phenomenon and to use this to gain more insight into the problem.
- To develop a technique for extracting information from the micro-Doppler return, and to determine whether these estimates would contribute to the identification of a target. This method can be verified by using the data generated from the simulation model as input to the algorithm.
- To use measured radar data of helicopters to verify the simulation results and to test the algorithm, and thereafter to extend the processing method as necessary to gain as much information as possible from the recorded data.
- To perform a statistical analysis of all the measured data to gain insight into the conditions in which the proposed algorithm would work on its own, and when other methods are needed to investigate it further.
- To document the method that was used, clearly showing both the advantages and disadvantages of using the method.

A thorough understanding of the problem were formed by a detailed discussion of the work presented in the literature to address the problem of helicopter identification. The developed simulation model showing the micro-Doppler effect for a helicopter was verified by means of the mathematical expression for both the blade flash and the sinusoidal blade tip scattering. The HBM algorithm that was developed to extract the information of the helicopter blade parameters was verified by means of the simulation model and this method was validated with measured data. A helicopter trial was conducted in which nine different helicopters were measured to validate the algorithm and to determine the performance of the algorithm under various conditions. Data from all the helicopters was analysed, showing the performance of the algorithm at different ranges. The limitations of the method were discussed, as were possible solutions to some of the limitations. The research questions for future work resulting from this study have also been addressed.

Appendix

A Waveform description

This Appendix contains a detailed description of the waveforms that were used during the inbound and outbound run measurements for the datasets discussed in Chapter 4. The two sections in the Appendix gives the parameters of the waveforms for the outbound and inbound runs respectively.

The parameters of the waveforms given in the tables include:

- Waveform number
- Number of HBM bursts in the waveform
- PRI of both the tracking and HBM bursts
- PRF of both the tracking and HBM bursts
- Number of pulses in both the tracking and HBM bursts
- Pulse width of both the tracking and HBM bursts
- Duty cycle of both the tracking and HBM bursts

A1 Waveforms used during the outbound run

The waveforms used during the outbound run of the data shown in Chapter 4 is described in Table A1.

Table A1: Different helicopters used for the helicopter experiment trial in August 2007 on the CSIR campus in Pretoria. Helicopters from three different classes were used, and the rotor and blade parameters are indicated in the table for the nine different helicopters.

Index number:	**Waveform number:**	**Number of HBM bursts**	**PRI (ns)**		**PRF (Hz)**		**Number of pulses:**		**Pulse width (ns)**		**Duty cycle (%)**	
			Track	**HBM**	**Track**	**HBM**	**Track**	**HBM**	**Track**	**HBM**	**Track**	**HBM**
1	750	1	1333	286	7501.9	34965	14	64	44	5	3.30	1.75
2	756	1	1333	323	7501.9	30959.8	14	64	44	5	3.30	1.55
3	768	1	1333	370	7501.9	27027	14	64	44	5	3.30	1.35
4	864	1	1000	400	10000	25000	14	64	44	8	4.40	2.00
5	754	1	1333	286	7501.9	34965	8	64	44	5	3.30	1.75
6	758	1	1333	303	7501.9	33003.3	8	64	44	5	3.30	1.65
7	762	1	1333	323	7501.9	30959.8	8	64	44	5	3.30	1.55
8	766	1	1333	345	7501.9	28985.5	8	64	44	5	3.30	1.45
9	770	1	1333	370	7501.9	27027	8	64	44	5	3.30	1.35
10	774	1	1333	400	7501.9	25000	8	64	44	8	3.30	2.00
11	778	1	1333	435	7501.9	22988.5	8	64	44	8	3.30	1.84
12	773	10	1333	370	7501.9	27027	8	64	44	5	3.30	1.35
13	761	6	1333	323	7501.9	30959.8	14	64	44	5	3.30	1.55
14	868	1	1000	303	10000	33003.3	14	64	44	5	4.40	1.65
15	757	10	1333	286	7501.9	34965	8	64	44	5	3.30	1.75
16	761	10	1333	303	7501.9	33003.3	8	64	44	5	3.30	1.65
17	765	10	1333	323	7501.9	30959.8	8	64	44	5	3.30	1.55
18	769	10	1333	345	7501.9	28985.5	8	64	44	5	3.30	1.45
19	777	10	1333	400	7501.9	25000	8	64	44	8	3.30	2.00
20	781	10	1333	435	7501.9	22988.5	8	64	44	8	3.30	1.84

A2 Waveforms used during the inbound run

The details of the waveforms used during the inbound run data set is shown in Table A2.

Table A2: Different helicopters used for the helicopter experiment trial in August 2007 on the CSIR campus in Pretoria. Helicopters from three different classes were used, and the rotor and blade parameters are indicated in the table for the nine different helicopters.

Index number:	**Waveform number:**	**Number of HBM bursts**		**PRI (ns)**		**PRF (Hz)**		**Number of pulses:**		**Pulse width (ns)**		**Duty cycle (%)**	
				Track	**HBM**	**Track**	**HBM**	**Track**	**HBM**	**Track**	**HBM**	**Track**	**HBM**
1	750	1		1333	286	7501.9	34965	14	64	44	5	3.30	1.75
2	756	1	6	1333	286	7501.9	34965	8	64	44	5	3.30	1.75
3	768	1	6	1333	345	7501.9	28985.5	8	64	44	5	3.30	1.45
4	754	1		1333	286	7501.9	34965	8	64	44	5	3.30	1.75
5	758	1		1333	303	7501.9	33003.3	8	64	44	5	3.30	1.65
6	762	1		1333	323	7501.9	30959.8	8	64	44	5	3.30	1.55
7	766	1	10	1333	345	7501.9	28985.5	14	64	44	5	3.30	1.45
8	770	1		1333	370	7501.9	27027	8	64	44	5	3.30	1.35
9	774	1		1333	400	7501.9	25000	8	64	44	8	3.30	2.00
10	778	1		1333	435	7501.9	22988.5	8	64	44	8	3.30	1.84
11	773	6	10	1333	370	7501.9	27027	14	64	44	5	3.30	1.35
12	761	6	10	1333	323	7501.9	30959.8	14	64	44	5	3.30	1.55
13	868	1		1000	303	10000	33003.3	14	64	44	5	4.40	1.65
14	757	10		1333	286	7501.9	34965	8	64	44	5	3.30	1.75
15	765	10		1333	323	7501.9	30959.8	8	64	44	5	3.30	1.55
16	769	10		1333	345	7501.9	28985.5	8	64	44	5	3.30	1.45
17	767	6		1333	345	7501.9	28985.5	14	64	44	5	3.30	1.45
18	755	2		1333	286	7501.9	34965	8	64	44	5	3.30	1.75
19	782	1		1333	476	7501.9	21008.4	8	64	44	8	3.30	1.68
20	760	6		1333	303	7501.9	33003.3	8	64	44	5	3.30	1.65
21	764	6		1333	323	7501.9	30959.8	8	64	44	5	3.30	1.55
22	772	6	10	1333	370	7501.9	27027	8	64	44	5	3.30	1.35

Bibliography

[1] P. Tait, *Introduction to Radar Target Recognition*. United Kingdom: The Institution of Electrical Engineers, 2005.

[2] "Radar Systems Panel of the IEEE Aerospace and Electronic Systems Society, USA, IEEE standard radar definitions" *IEEE Aerospace and Electronic Systems Society*, 1998.

[3] V. Chen, F. Li, S. Ho, and H. Wechsler, "Micro-Doppler effect in radar: phenomenon, model, and simulation study" *Aerospace and Electronic Systems, IEEE Transactions on*, vol. 42, no. 1, pp. 2–21, Jan. 2006.

[4] V. Chen, F. Li, S. Ho, and H. Wechsler, "Analysis of micro-Doppler signatures" *Radar, Sonar and Navigation, IEE Proceedings*, vol. 150, no. 4, pp. 271–6–, 1 Aug. 2003.

[5] S. Yoon, B. Kim, and Y. Kim, "Helicopter classification using time-frequency analysis" *Electronics Letters*, vol. 36, no. 22, pp. 1871–1872, 26 Oct 2000.

[6] J. Martin and B. Mulgrew, "Analysis of the theoretical radar return signal form aircraft propeller blades" *Radar Conference, 1990., Record of the IEEE 1990 International*, pp. 569–572, 7-10 May 1990.

[7] B. Bullard and P. Dowdy, "Pulse Doppler signature of a rotary-wing aircraft" *Aerospace and Electronic Systems Magazine, IEEE*, vol. 6, no. 5, pp. 28–30, May 1991.

[8] P. Pouliguen, L. Lucas, F. Muller, S. Quete, and C. Terret, "Calculation and analysis of electromagnetic scattering by helicopter rotating blades" *Antennas and Propagation, IEEE Transactions on*, vol. 50, no. 10, pp. 1396–1408, Oct 2002.

[9] M. Bell and R. Grubbs, "JEM modeling and measurement for radar target identification" *Aerospace and Electronic Systems, IEEE Transactions on*, vol. 29, no. 1, pp. 73–87, Jan 1993.

[10] J. Misiurewicz, K. Kulpa, and Z. Czekala, "Analysis of recorded helicopter echo" pp. 449–453, 14-16 Oct 1997.

[11] C. Rotander and H. V. Sydow, "Classification of helicopters by the l/n-quotient" *Radar 97 (Conf. Publ. No. 449)*, pp. 629–633, 14-16 Oct 1997.

[12] K. Kulpa, Z. Czekala, J. Misiurewicz, and J. Falkiewicz, "Parametric detection of the helicopter hub echo" *Radar Conference, 1999. The Record of the 1999 IEEE*, pp. 262–266, 1999.

[13] S. Qureshi, S. Mirza, and M. Arif, "Inverse radon transform-based image reconstruction using various frequency domain filters in parallel beam transmission tomography" *Engineering Sciences and Technology, 2005. SCONEST 2005. Student Conference on*, pp. 1–8, 27-27 Aug. 2005.

[14] J. Tikkinen, E. Helander, and A. Visa, "Joint utilization of incoherently and coherently integrated radar signal in helicopter categorization" in *IEEE International Radar Conference*, pp. 540– 545, 9-12 May 2005 2005.

[15] J. Allen, "Short term spectral analysis, synthesis, and modification by discrete fourier transform" *Acoustics, Speech and Signal Processing, IEEE Transactions on*, vol. 25, pp. 235–238, Jun 1977.

[16] H. Green, "Electromagnetic backscattering from a helicopter rotor in the decametric wave band regime" *Antennas and Propagation, IEEE Transactions on*, vol. 42, no. 4, pp. 501–509, Apr 1994.

[17] J. Misiurewicz, K. Kulpa, and Z. Czekala, "Analysis of radar echo from a helicopter rotor hub" vol. 3, pp. 866–870, 20-22 May 1998.

[18] D. Barton, *Modern Radar System Analysis*. Norwood, MA: Artech House, Inc, first edition ed., 1988.

[19] M. Skolnik, *Introduction to Radar Systems*. New York: McGraw-Hill Book Company, second edition ed., 1980.

[20] F. Zhang, G. Bi, and Y. Chen, "Tomography time-frequency transform" *Signal Processing, IEEE Transactions on [see also Acoustics, Speech, and Signal Processing, IEEE Transactions on]*, vol. 50, no. 6, pp. 1289–1297, Jun 2002.